Department Chemie
Fachgebiet Theoretische Chemie
Technische Universität München

A Relativistic Density Functional Study of Uranyl Hydrolysis and Complexation by Carboxylic Acids in Aqueous Solution

Rupashree Shyama Ray

Vollständiger Abdruck der von der Fakultät für Chemie der Technischen Universität München zur Erlangung des akademischen Grades eines

Doktors der Naturwissenschaften (Dr. rer. nat.)

genehmigten Dissertation.

Vorsitzender: Univ.-Prof. Dr. K.-O. Hinrichsen

Prüfer der Dissertation:

1. Univ.-Prof. Dr. N. Rösch
2. Univ.-Prof. Dr. A. Türler

Die Dissertation wurde am 15.01.2009 bei der Technischen Universität München eingereicht und durch die Fakultät für Chemie am 10.02.2009 angenommen.

Acknowledgement

It was a grand opportunity and great exposure for me to do a Ph.D. at TU München. During my Ph.D. I have worked w ith a great number of people whose contribution in assorted ways to the research and the making of the thesis deserve special mentioning. It is a pleasure to convey my gratitude to them all in my humble acknowledgment.

First of all, I would very much like to thank Prof. Dr. Notker Rösch for his supervision, guidance and advice throughout my Ph.D. career as well as for giving me an extraordinary exposure to the frontiers of science. His extraordinary scientific intuition and insight has made him a constant oasis of ideas and passions in science, which was a great source of inspiration for me. Above all his spirit and dedication always provided me unflinching encouragement in various ways.

I gratefully acknowledge Dr. Sven Krüger for his advice, supervision and crucial contribution, which made him a backbone of this research and thus to this thesis. His involvement with his originality has triggered and nourished my intellectual maturation, which will benefit me for a long time to come. I am greatly indebted to Sven for his extended help and support in academic and nonacademic issues.

I convey special acknowledgement to Prof. T. P. Radhakrishnan and Prof. K. D. Sen for their indispensable endorsement throughout my scientific career.

It is a pleasure to pay tribute to the actinide group past and present members Dr. F. Schlosser, Dr. L. Moskaleva, A. Kremleva, S. N. Derrar, and Dr. O. Zakharieva for stimulating discussions as well as for the pleasant work culture in the team. Collective and individual acknowledgements are also owed to my colleagues: Dr. A. Matveev, Dr. A. Genest, G. Dixit, G. Galstyan, R. Ramakrishnan, H. Alexandrov, D. Başaran, Dr. B. Martorell, S. Parker, Z. Zhao, E. Vladimirov, M. Metzner, M. H. Rotllant, G. Petrova, and those not mentioned here, whose presence was refreshing, helpful, and memorable. Very many thanks to the secretary Frau Mösch for her friendly gesture and help in administrational issues.

My parents deserve special mention for their inseparable love, care and blessings. Without their consistent support I would not be what I am today. Words fail to express my appreciation to my sister Baijayanti, brother Manmath and sister-in-law Chinmayee whose love, support and persistent confidence in me made my way much easier through ups and downs.

It is a pleasure to express my gratitude wholeheartedly to Jayanta, Vijay, Kali, Indrajit, Sushree and Snigdha for their indispensable friendship and support. My special acknowledgement to Kiran, Somnath, Gopal, Raghu, Divita and Siham for their cooperation and providing me an amiable atmosphere in a foreign land, miles away from home.

Finally, I would like to thank everybody who was important to the successful realization of this thesis.

"Knowledge has three degrees -- opinion, science, illumination. The means or instrument of the first is sense; of the second, dialectic; of the third, intuition."

---Plotinus

Dedicated to my family

Contents

List of Abbreviations

au	atomic units
BP	Becke-Perdew (exchange-correlation functional)
Calc.	calculated
CASPT2	complete active space with second-order perturbation theory
CCSD(T)	Coupled-cluster with Single and Double and perturbative Triple excitations (method)
CI	Configuration Interaction (method)
CN	Coordination number
COSMO	conductor-like screening model
DF	density functional
DFT	density functional theory
DHF	Dirac-Hartree-Fock (method)
DK	Douglas-Kroll (procedure)
DKH	Douglas-Kroll-Hess (procedure)
DKS	Dirac-Kohn-Sham (method, Hamiltonian)
ECP	effective core potential
EXAFS	extended x-ray absorption fine structure spectroscopy
Exp.	experimental
FC	frozen core
FF	fitting function
GGA	generalized gradient approximation (of xc functional)
HF	Hartree-Fock (method)
HOMO	Highest occupied molecular orbital
LUMO	Lowest unoccupied molecular orbital

KS	Kohn-Sham (method, Hamiltonian)
LCGTO	linear combination of Gaussian-type orbitals
LDA	local density approximation (of xc functional)
LDA/BP	BP single point on LDA geometry
MO	molecular orbital
MP2	second-order Møller-Plesset perturbation theory
NMR	nuclear magnetic resonance
PBEN	Perdew-Burke-Ernzerhof (exchange-correlation functional), modified according to Nørskov *et al*.
PCM	polarizable continuum model
PP	Pseudopotential
QM	quantum mechanics
RECP	relativistic effective core potential
SCF	self-consistent field (procedure)
SO	spin-orbit (interaction, method)
SR	scalar-relativistic
TRLFS	Time-resolved laser-induced fluorescence spectroscopy
UAHF	united atom – Hartree-Fock
vdW	van der Waals (radius)
VWN	Vosko-Wilk-Nusair (exchange-correlation functional)
XANES	x-ray absorption near edge spectroscopy
XAS	x-ray absorption spectroscopy
xc	exchange-correlation (functional, potential, energy)
XRD	x-ray diffraction
ZORA	zeroth-order regular approximation (method)

1 Introduction

1.1 Actinide compounds and their computational modeling

The environment is one of the most intricate systems from a chemist's perspective. A very large number of chemically active compounds and minerals reside within the earth's crust. The interaction of water with rocks and minerals at the atomic level is a poorly understood phenomenon exhibiting its own chemical processes. Similarly, from a chemist's point of view, the actinides are complex elements, which make the chemical interactions of actinides in the environment multifarious. Predicting the chemistry and the migration of actinides in the environment requires the analysis of all local conditions. Additionally quantitative knowledge of the competing geochemical processes affecting the actinides behavior is crucial. Precipitation and dissolution of actinides limit the concentration of actinides in solution, while complexation and redox reactions determine the distribution and stability of the species. The interaction of a dissolved species with mineral and rock surfaces and/or colloids determines their migration rates. Understanding this dynamic interplay between the actinides and the environment is crucial for an accurate assessment of the feasibility of storing nuclear waste in geologic repositories. One has to determine the chemical species involved and to study their interaction with the surrounding media under environmental conditions.

With the Manhattan project in 1945, the "actinide concept" was introduced into the periodic table, opening a new horizon to heavy element chemistry. However, the study of the phenomenon of radioactivity had already begun with the discovery of uranium ores by Henri Becquerel in 1896,[1] and was followed by the work of Pierre and Marie Curie on radium. In middle of the 20th century, research mainly focused on nuclear properties and the development for nuclear weapons. Since the first nuclear test explosion in New Mexico in 1945, a large amount of high-level radioactive wastes are accumulating in different countries, owing to the military and civil usage of nuclear power. Radionuclides also are released to the environment from mining and milling operations (uranium ores), nuclear

fuel fabrication processes, nuclear waste recovery, nuclear weapon production, transportation of nuclear material etc. Also the use of depleted uranium munitions in the Gulf war of 1991 and the Kosovo war in 1999 elevates the concentration of uranium in the environment. This is a major concern to the common people. Therefore, nuclear waste becomes a serious issue and studies are being carried out to understand the chemical behavior and forms of actinides under environmental conditions.[2–9]

Recent years have witnessed a dramatic rise in interest within the chemistry community for investigating actinide compounds. Most of the actinide elements are artificial (with the exception of Th, Pa, U, Np, Pu, and Am). Some of them are synthesized by neutron irradiation of uranium;[10] others are produced in atom amounts by bombardment with heavy ions.[10] The actinide elements occupy their unique position in the periodic table owing to the presence of 5*f* electrons in their valence shell. Incomplete *f* and *d* sub shells and a large number of stable and meta stable oxidation states result in a complicated chemistry for the early actinides.[11] It has been particularly difficult to reconcile a description of the fascinating structural and electronic behavior of f-series metals and their compounds. Thus, actinides provide many challenges for chemical research.

Two major reasons underline the scarcity of fundamental experimental data for actinide compounds. The first is the complexity of the problem, in certain cases experimental observations are difficult to interpret and do not provide direct insight as the interpretation has to rely on model assumptions.[12] The second reason is the inherent danger and expense of handling actinide species, which are mostly radioactive and highly toxic. Solution chemistry of actinides is very important in determining the constitution and equilibrium constants of complexes including the identification of isomers, i.e. chemical analysis to determine their structure and to discuss chemical bonding and reactivity. The experimental conditions relevant to environmental chemistry of aqueous solution, such as pH, concentration, ionic strength and the presence of complexing ligands usually allow a variety of coexisting species, leading to a high intricacy in to the system. In addition, experiments that are extremely sensitive to air require extra caution. Therefore, one is confronted with a difficult task when determining experimentally the properties of a specific actinide compound. Thus, simulation is an attractive and relatively cheap alternative to provide detailed information complementary to experiment. Ideally, one would like to use theoretical chemistry as an instrument to generate reliable predictions of the properties of the molecular complexes that one is interested in. While the computational approach is increasingly popular in transition metal coordination chemistry, it still presents a scientific challenge in actinide chemistry due to the complicated electronic structure of the actinides. Until recently, the methods available were not very

suitable for application to the realistic (large) model systems. This situation is changing because the available computational power keeps increasing. Parallel programs such as PARAGAUSS[13,14] scale well with the size of the molecule as well as with the number of processors. Recent developments of quantum chemistry methods[15–25] rendered reliable relativistic electronic structure calculations possible even for large complexes of heavy elements and opened a computational route, complementing experimental efforts, to many properties of these complexes.

Quantum chemistry faces particular challenges when describing the actinides.[15] Today, the challenge remains, in spite of considerable progress in last few decades; actinide chemistry is still far from being an area for routine applications of quantum chemistry, except for small closed-shell systems. Several problems have to be solved. First, the actinide elements comprise the heaviest elements of the periodic table besides the new transactinide elements synthesized only in amounts of a few atoms.[26] Consequently, many electrons have to be dealt with, most of them occupying inert core shells. Second, scalar and often spin-orbit relativistic effects have to be included for even a qualitative understanding of the actinide chemistry.[27] Third, correlation effects resulting from the interaction between the electrons are at least equally important. Finally, the 5f, 6d, and 7s orbitals are comparatively close in energy and spatial extent and can all participate in bonding.[28] The correct description of these dynamic and static electron correlation effects is extremely important and difficult in these cases.[18] Various methods for the inclusion of relativistic effects in electronic structure calculations have been discussed early and briefly by Pepper and Bursten[15] and in detail by Balasubramanian.[29] Such methods include the frozen-core (FC) approximation,[30,31] relativistic effective core potentials (RECP) or pseudopotentials[32,33] and scalar relativistic methods such as the Douglas-Kroll-Hess (DKH) approach[17,34,35] or the zeroth-order regular approximation (ZORA).[36–38] The Dirac-Kohn-Sham (DKS) Hamiltonian[39] is too demanding for extensive studies of large actinide species due to four-component nature of the wave function.

Solution chemistry of actinides is a vital part of environmental and applied actinide chemistry. Thus, it is essential to consider solvent effects while dealing with actinide systems in the environment, owing to the significant effect of solvent molecules on various molecular properties under study.[40] Effective solvent models in quantum chemistry may generally be divided into two main categories, (i) the polarizable continuum (PCM) models and (ii) the discrete solvation models.[41–45] With the inclusion of solvent effects, studies of actinide compounds under environmental conditions become accessible. This widens the application of theoretical chemistry and makes it extremely useful for studying computationally species that are difficult to isolate experimentally. In this way, besides to

primary structural aspects, hydration number,[21,45–48] solvation energies,[22,47,49] hydrolysis species,[50,51] redox behavior,[20,49] and ligand exchange mechanisms[19,44,52–54] are investigated using quantum mechanical tools. However, the complexity and size of real chemical systems limits theoretical studies to model systems. Proper description of solvent effects as well as accurate evaluation of thermodynamic data is rather demanding. In fact, they present major challenges for present-day quantum chemistry.

1.2 Motivation and overview

The chemistry of actinide elements, such as actinide hydrolysis, complexation, and condensation to polynuclear species, colloid formation, and interaction with the surrounding geologic media is a research topic of increasing importance. In this context, this thesis aims to contribute information about uranium(VI) complexation in an aqueous environment. The main concern is uranium complexation with natural organic compounds like humic acids. The focus of this work is on uranyl complexation with carboxylate ligands, serving as model systems of humic acids at low pH as well as at environmental conditions. In addition, the first hydrolysis product of uranyl, $[UO_2OH]^+$ is discussed in detail, which is an important reference species for uranyl complexation at slightly acidic to neutral pH (3-7).

Uranium is by far the most widely studied and best understood of the actinide elements. For the high oxidation state (VI), the uranyl ion UO_2^{2+} is the predominant species at low pH values. Hydrolysis of actinides is an important phenomenon in the environment. The hydrolysis of the uranyl dication, UO_2^{2+} has been studied more intensely[55] than that of any other actinide cation, partially because the relatively low level of radioactivity of natural uranium, compared to other actinides, facilitates experiments. Though a large amount of data on hydrolysis of uranium is available in literature,[10,11] some aspects still remain controversial. Characterization and energetic aspects of hydrolytic species are rather difficult; some of these species are well defined, but not all.[56,57] The hydrolysis of uranyl(VI) begins at about pH 3, leading to the formation of both mono- and polynuclear hydrolysis products $[(UO_2)_m(OH)_n]^{2m-n}$. The first hydrolysis product of uranyl(VI), $[UO_2OH]^+$, is addressed in this work.[58] Previous studies revealed different structures for the species; the computational determination of the formation energy of uranyl monohydroxide is also under debate.[22,45] Thus, the structure of uranyl(VI) monohydroxide is examined, taking into account coordination numbers varying from four to six. In addition, the hydrolysis free energy referring to the formation of uranyl

monohydroxide is determined.

The investigation and understanding of the interaction of actinide species with humic substances is an integral topic of environmental chemistry and safety analysis for radioactive waste management, including long-term storage.[5,6] Thermodynamic and kinetic studies on the formation of actinide complexes provide data for speciation calculations. Based on these data, it might be possible to predict actinide transport behavior in the environment. With the help of these models, strategies may be developed to retard the release of actinides and to reduce their migration rates.[3,11] Hence, understanding the interplay between actinides and humic substances is essential. Carboxylic groups are considered as the main functional groups of humic substances that are mainly responsible for the complexation of metal ions at low pH values due to their strong actinide complexing ability.[2,11,59] Phenolic, enolic, and aliphatic OH groups, amino sites, and possibly other functional groups might also be relevant.[60] Due to their complex nature and varying composition as well as depending on their origin, humic substances are not well-defined substances; rather they allow only an averaged experimental characterization. On the other hand, from the computational point of view, such rather large molecules are too demanding to be treated as complete systems. Therefore, it is common as in experimental studies, to investigate the properties and interactions of humic substances with the help of small complexes by analogy. The effect of the main functional groups thus is modeled by corresponding small organic compounds.[61]

In this thesis, previous work[62] on the complexation of uranyl by aliphatic carboxylate ligands at low pH is extended. This includes uranyl complexes with various aromatic carboxylic ligands. Aromatic groups contribute a large proportion (25-80 C mass %) to humic acids.[63] Aromatic carboxylic acids such as benzoate and its methyl and hydroxyl derivatives are chosen as models to simulate the interaction of actinides with corresponding groups of humic acids. The impact of structural and chemical changes on the actinyl complexation is investigated on these molecules to characterize the varying properties of functional groups present in humic substances. In addition, the goal is to contribute to the discrimination of different coordination modes of the carboxylic ligands i.e. monodentate, bidentate, or chelate.

Complexation of actinide ions with carboxylic groups at low pH is rather interesting owing to their strong complexating ability as well as the simplicity of the process compared to the situation at elevated pH. At neutral and high pH, various processes such as precipitation, hydrolysis and formation of polynuclear complexes and colloid formation make the interaction of actinides with humic substances more complicated. Even at moderate pH (4-6), hydrolysis is already important as a competing process to

complexation. Thus, in order to investigate actinide interaction with natural organic matter at environmental conditions, the study of ternary systems of actinides-humic acid, and hydroxide is necessary. Formation of complex hydrolysis products for some actinides makes this system rather complicated and explains the scarcity of experimental as well as theoretical work in that area. The current work presents a first step towards understanding complicated ternary systems of uranyl-hydroxo-humate at moderately acidic conditions, by investigating hydroxide complexes of uranyl-acetate, which serve as models of humic acid carboxylic groups.

This thesis is divided into the following parts.

Chapter 2 briefly summarizes the relevant general aspects of actinide chemistry and then focuses on actinide environmental chemistry. Experimental results on hydrolysis, actinide complexation by carboxylic acids, and humic substances are presented to establish a background for the subsequent discussion. Additionally, a short survey of typical experimental methods, such as extended x-ray absorption fine spectroscopy (EXAFS), and Time-resolved laser-induced fluorescence spectroscopy (TRLFS), used for identification and characterization of actinide species, will be given with respect to the information that can be obtained from these methods.

Chapter 3 describes the computational method used in this work and the relevant features of the parallel quantum chemistry code PARAGAUSS employed. First, the most relevant basics of the applied density functional approach are presented focusing on relativistic effects. Then, the treatment of solvent effects, essential for an adequate modeling of actinide species in aqueous solution, will be introduced. At the end of this chapter, computational parameters and procedures will be summarized.

Chapter 4 presents the computational results including a comparison to available experimental data. In the beginning, the mononuclear hydrolysis product of UO_2^{2+}, $[UO_2OH]^+$, will be discussed (Section 4.1). The second part deals with actinide complexation by carboxylate ligands. First of all the coordination number for uranyl-acetate will be discussed with respect to implications for the complexation of actinides by humic substances followed by the uranyl complexation of aromatic carboxylic acids in comparison to earlier results for aliphatic ones (Section 4.2). In the end, the ternary uranyl-hydroxo-acetate are discussed, as models of uranyl humate complexation at ambient condition (Section 4.3). A summary of the results and an outlook on future work of interest and open questions will form the last chapter of this thesis.

2 Actinide chemistry introduction

After a short introduction to basic aspects of actinide chemistry, this chapter presents some topics of uranium chemistry relevant for the studies of this thesis, like complexation in aqueous solution, hydrolysis and complexation with natural organic compounds.

2.1 General actinide chemistry

The actinide series comprises of 15 consecutive chemical elements from actinium to lawrencium (atomic numbers 89-103), in which the 5f shell is being filled. The general electronic configuration of actinides is [Rn] $5f^m$ $6d^n$ $7s^2$, where Rn stands for the radon core, *m* varies from 1 to 14 and *n* can be 1 or 2. All actinide elements are unstable toward radioactive decay; the reason that actinium, thorium, protactinium, and uranium are found in nature at all is because some of their isotopes are unusually stable and others are being formed constantly by decay of the long-lived isotopes. Based on natural occurrence, artificial creation, and long half-lives, six of the 14 elements i.e. thorium, uranium, neptunium, plutonium, americium, and curium, are of long-term environmental concern.[64]

Oxidation states of actinides are the most characteristic property that affects their chemical behavior like precipitation, complexation, sorption, and colloid formation.[65] In contrast to the lanthanides, in which the oxidation state usually is +3,[11] both in aqueous solution and in solid compounds, the early actinides, up to and including americium, exhibit a variety of oxidation states. The common oxidation states of americium and the higher actinides in aqueous solution is +3; nobelium (Z = 102) forms the sole exception owing to the stability of its dication in aqueous solution. In the earlier part of the actinide, series the higher oxidation states indicate, at least qualitatively, that the fourth and higher ionization potentials for these elements must be rather small. Table 2.1 gives an overview over known oxidation states of early actinides. Actinyls, AnO_2^+ and AnO_2^{2+} are the common oxygenated species of actinides (An = Pa–Am) in higher oxidation states +V and

Table 2.1. Oxidation states[a] of light actinide elements Ac to Cm. Most stable (bold), unstable (in parenthesis), and claimed (?) oxidation states are indicated.

Ac	Th	Pa	U	Np	Pu	Am	Cm
III	(III)	(III)	III	III	III	**III**	**III**
	IV	IV	IV	IV	**IV**	IV	IV
		V	V	**V**	V	V	V ?
			VI	VI	VI	VI	VI ?
				VII	(VII)	VII ?	

[a] Ref. 6.

+VI.[65] They exhibit bond orders larger than 2 e.g. for uranyl.[66] Actinyl ions AnO_2^{m+} are known to be linear.[67] As an exception however, the ThO_2 molecule, isoelectronic to UO_2^{2+}, is distinctly bent (122º).[66] Differences between bent ThO_2 and linear UO_2^{2+} have been assigned to changes in relative stabilities of the atomic *d* and *f* orbitals.[68,69] In most actinides the *d* orbitals are energetically below the *f* orbitals and a linear conformation is preferred.

The ionic radii of actinide elements decrease gradually as one moves along the actinide series. This steady decrease in the ionic radii with increase in nuclear charge, called actinide contraction, is analogous to the lanthanide contraction.[66] The cause of the actinide contraction is the imperfect shielding by the 5*f* electrons.

Actinides have stronger complexing ability than lanthanides,[70] owing to the wider spatial extension of 5*f* orbitals, relative to 7*s* and 7*p* orbitals, than the corresponding 4*f* orbitals relative to the 6*s* and 6*p* orbitals in lanthanides. Thus, 5*f* orbitals of the actinides can be involved in covalent hybrid bonding.[65] In addition to this, the energies of the *5f*, *6d*, *7s*, and *7p* orbitals are comparable over a range of atoms (especially U to Am).[70] Since these orbitals overlap spatially, bonding can involve any of them. The ground state configuration of uranium is $5f^3\ 6d^1\ 7s^2$.

As the actinide, ions are characteristically non-polarizable and their bonding is strongly ionic they are classified as “hard” acids. Thus, they form strong complexes with hard bases such as carbonate, hydroxide, or oxygen of water molecules.[9,65] Owing to the wide variety of ligands forming actinide complexes, and the large number of different oxidation states, the stereochemistry found in complexes and compounds of actinides is extraordinary.[65]

2.1.1 Uranium

Uranium is a naturally occurring element found in low concentrations within all rocks, soil, and water. This is the highest-numbered element to be found naturally in significant quantities on earth. Even though uranium is a rare earth element, it gained importance because of its application to nuclear power and nuclear weapons since mid 20^{th} century, posing a great danger to the environment. Since the discovery of nuclear fission by Hahn and Strassman in 1938, the chemistry, materials science, and nuclear properties of uranium have occupied a central position in the field of nuclear science. ^{238}U is the most abundant isotope of uranium found in the nature with a half-life of $4.5x10^9$ years.

2.1.2 Complexation and stability constant

Uranium is a strongly electropositive element and its compounds are thus difficult to reduce to metal. Correspondingly, uranium is very reactive; it combines more or less readily with all the elements. The most stable oxidation states of uranium in natural environment are +4 and +6. The tetravalent state is dominant in reducing waters and hexavalent in oxidizing waters. Compounds containing tetravalent uranium are insoluble at mildly acidic to alkaline conditions, whereas those containing uranium(VI) are highly soluble and mobile.[11] The pentapositive state of uranium is the least stable oxidation state of uranium in solution. The hexavalent uranium ion is unstable in aqueous solutions owing to its high charge: it is stabilized by the formation of uranyl UO_2^{2+}. It is generally agreed that the uranium(VI) ion exists in the form of uranyl UO_2^{2+}.[65] Although the uranyl dication is involved extensively in uranium complexes, the bare UO_2^{2+} dication in gas phase was not detected experimentally until 1996.[71] In aqueous solution in contact with air, UO_2^{2+} forms soluble complexes with carbonate, and hydroxide; UO_2^{2+} is also highly susceptible to adsorption by organic compounds. The hydrolytic behavior and stereochemistry of UO_2^{2+} in aqueous solutions have been extensively studied and can vary considerably.[65] The overall pattern comprises the (linear) axial O-U-O uranyl moiety that is surrounded by 4, 5, or 6 ligands in or close to its equatorial plane. This yields a tetragonal, pentagonal, or hexagonal bipyramidal coordination, respectively.[70] For uranyl the pentagonal coordination is found to be preferred in general in various experimental[48,72–74] and computational studies.[22,45,47] Dioxouranium(VI), UO_2^{2+}, exhibits characteristic bond distances of about 175 to 183 pm in solution, distinctly shorter than corresponding distances to equatorial ligands such as water (237 to 253 pm).[45,47,75,76] The discussion whether 5*f* orbitals are involved in the formation of complexes involving UO_2^{2+} can be summarized as follows.[65,68,69] The HOMO of UO_2^{2+} is a σ_u orbital with largely O-2*p* character; its LUMO

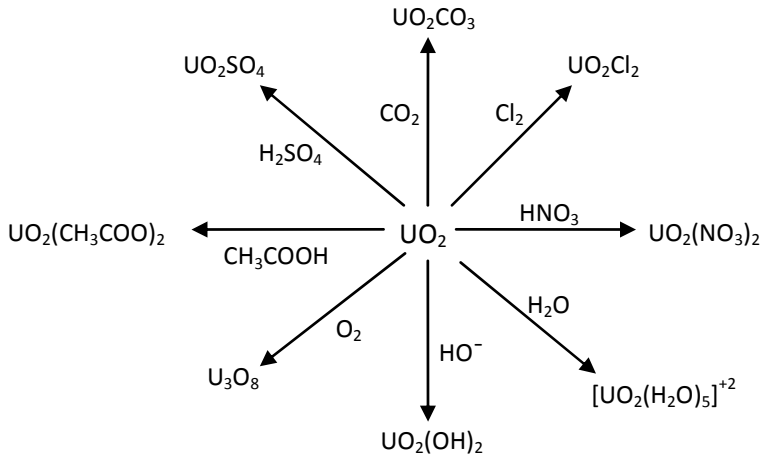

Figure 2.1. Exemplary uranyl complexation with various ligands. (Adapted from Ref. 75).

is formed by an empty $5f_{\varphi}$ orbital. Additionally, the effect of equatorial ligands is secondary compared to that of axial ones.[18,49,55] The constraints imposed by the presence of the two oxo groups in the linear moiety UO_2^{2+} provide an inherent steric hindrance on the number of ligands that can bind to uranyl. In absence of steric factors, uranyl primarily binds ligands via electrostatic interactions. Increase in the effective charge density of the equatorial ligand favor strong bonds.

A very large number of organic and inorganic anions form complexes with UO_2^{2+} (Fig. 2.1). There are some systematic studies showing the complexation of UO_2^{2+} with carbonate, nitrate, sulfate, oxalate, acetate and hydroxyl.[65,70] Uranyl-acetate complexes are important because they allow one to selectively extract the uranyl from mixtures in solution.[10]

Complexation can occur with more than one ligand or actinide ion; therefore, several species may be associated with a given ligand.

A solvated metal ion (An) or actinyl may react with one or more potentially anionic ligands (L) to form complexes of type An_aL_b, where L has substituted one or more of the coordinated solvent molecules:

$$a\ An^{x+} + b\ L^{y-} \rightarrow (An_aL_b)^{ax-by} \quad (2.1)$$

The stability of this complex is defined by its stability constant

$$\beta_{ab} = [(An_aL_b)^{ax-by}]/[An^{x+}]^a[L^{y-}]^b \quad (2.2)$$

where the quantities in brackets represent concentrations for equilibrium quotients or activities for equilibrium constants. Stability/equilibrium constants are an effective measure of the affinity of a ligand for a metal ion in solution and a quantitative indication

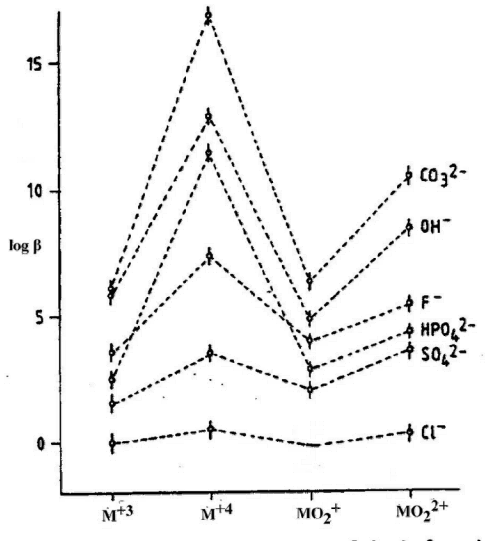

Figure 2.2. Average stability constants β for the formation of 1:1 complexes of the actinide ions M^{3+}, M^{4+}, MO_2^+ and MO_2^{2+} with various anions. Adapted from Ref. 7.

of the strength of ligand binding in different oxidation states.[77] This is directly related to the Gibbs free energy of the system via

$$\Delta G = -RT\ln\beta \tag{2.3}$$

For a given oxidation state the values of the constants tend to fall into three groups. The trend in strengths of complexation of various ligands with actinides (Fig 2.2) is[11]

$$OH^-, CO_3^{2-} > F^-, CH_3COO^-, HPO_4^{2-}, SO_4^{2-} > Cl^-, NO_3^-.$$

Acetate complexes uranyl stronger than a sulfate ligand, but weaker than fluoride and phosphate. The strength of complexation of a given ligand to actinides in different oxidation states (Fig 2.2) varies as

$$An^{4+} > AnO_2^{2+} \geq An^{3+} > AnO_2^{1+}$$

The stability constant can also be described in terms of undissociated acid (bronsted acids):

$$a\ An^{x+} + b\ LH^y \rightarrow (An_aL_b)^{ax-by} + bH^+ \tag{2.4}$$

The stability of this complex is then defined by the alternative stability constant

$$\beta_{ab}^* = [(An_aL_b)^{ax-by}][H^+]^b/[An^{x+}]^a[LH]^b \tag{2.5}$$

The quantitative difference between the two sets of stability constant is the dissociation constant of the acid:

$$\log \beta_{ab} = \log \beta_{ab}^* + pK_a \tag{2.6}$$

Thus, the dissociation of the acid (in the frame of bronsted acid) is included in the alternative constants β_{ab}^*.

It is often difficult to measure the chemical activity of the actinide ions, ligands as well as complexes, thus concentrations are used commonly instead of activities. Such stability constants are valid only for a limited range of conditions owing to their dependence on the ionic strength of the solution. Determining formation constants of complexes formed by a divalent cation and a very simple low molecular weight ligand, such as the acetate anion, is apparently a simple task, but when dealing with UO_2^{2+} complexes in aqueous solution, some factors render the problem more complicated: (a) the tendency of dioxouranium(VI) to form several stable hydrolytic species, also at low pH which interferes seriously with the formation of complex species and (b) the tendency of this cation to saturate the coordination sphere by forming several binary and ternary species. Thus, under common conditions, usually several complexes may coexist in solution. Only at rather high or low pH, and concentrations with high or low actinide to ligand ratio, a simple well-defined species may be obtained.

2.1.3 Hydrolysis

Hydrolysis of actinides in aqueous solution is an interesting phenomenon due to a plethora of species involved. The importance for understanding technical applications only in part explains the large number of studies on the hydrolysis of actinides in aqueous solution.[55] During the last forty years, hydrolysis of actinides has been reviewed several times.[78–83] Hydrated actinide ions act as cationic acids and form hydroxide complexes by splitting off protons. In acidic solution complexation of actinides is more important than hydrolysis. Hydrolysis reactions start in acidic to alkaline solutions for the common oxidation states (3+, 4+, and 6+) and often dominate over other complexation reactions in neutral and basic solutions.[83] For most of the actinides hydrolysis strongly depends on pH and the oxidation state. Thus, hydrolysis reactions are important for all actinides ions at pH values found in natural waters, with the exception of pentavalent actinyl ions AnO_2^+ owing to their low charge of +1.

As with the formation of complexes, the propensity to form hydrolysis complexes decreases in the order An(IV) > An(III) > AnO_2^{2+} > AnO_2^+.[84] Actinide (IV) ions, An^{4+} have large charge-to-radius ratios and form hydrolysis products even in acidic solution, as low as pH = 0.[65] The trivalent ions An^{3+} and the hexavalent actinyl ions AnO_2^{2+} start to hydrolyze at room temperature at about pH = 4. Actinyl(V) species $[AnO_2]^+$ do not readily hydrolyze until pH = 9. For tetra and hexavalent cations, hydrolysis can lead to the formation of oligomers and polymers.[11] However, polymers of AnO_2^{2+} species are more readily decomposed by simple acidification of the solutions. Hydroxide-bridged

polynuclear complexes have been observed for several actinide cations[100–103] and the tendency towards polymer formation is a function of charge density of the actinide ion.[103] Substitution of the hydroxide ions can suppress hydrolysis. Under strongly basic conditions, formation of precipitates of hydroxides, oxides, and basic salts or formation of colloids is possible, depending on the actinide element and its oxidation state.[6,66,85]

Uranium hydrolysis

The hydrolysis of the uranyl dication, UO_2^{2+}, which is also a topic of this thesis, has been studied more intensely than that of any other actinide cation.[55] The composition and stability of the various hydroxo-uranyl complexes have been explored under various conditions of pH,[86] temperature[87] and uranyl concentration by different experimental techniques such as potentiometry,[88,89] spectrophotometry,[90] solvent extraction,[91] chromatography[92] and solubility.[93,94] The hydrolysis of uranyl(VI) begins at about pH = 3. It leads to the formation of both mono- and polynuclear hydrolysis products (Fig 2.3), i.e. $[(UO_2)_m(OH)_n]^{2m-n}$, labeled by the indices (m.n)

$$m\,[UO_2]^{2+} + n\,H_2O \rightarrow [(UO_2)_m(OH)_n]^{2m-n} + n\,H^+. \qquad (2.7)$$

Number and identity of the chemical species present in solution vary with the concentration of both UO_2^{2+} (aq) and OH^-(aq) along with the pH of the solution. The most

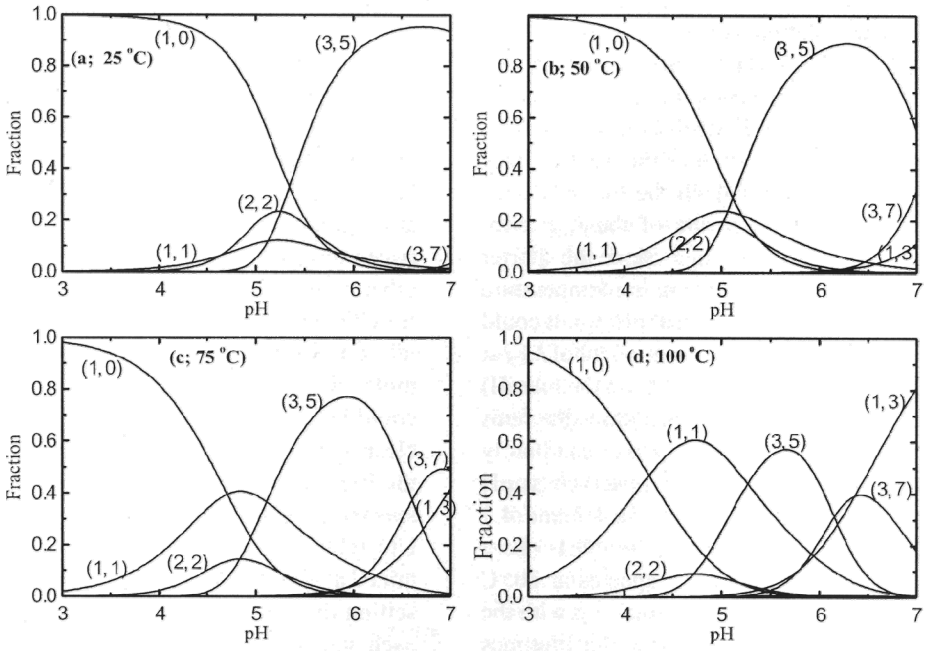

Figure 2.3. Speciation diagram (taken from Ref.112) of uranyl(VI) hydrolysis at different temperatures as a function of pH from speciation calculations for $5x10^{-5}$ mol/L U(VI) concentrations, (a) 25°C (b) 50°C (c) 75°C (d) 100°C (*m*,*n*) designates corresponding uranyl hydroxide species $[(UO_2)_m(OH)_n]^{2m-n}$.

prevalent species are monomeric, dimeric, and trimeric ions, with the latter two being favored for higher UO_2^{2+} concentrations (> 10^{-4} M). Within a wide range of values of pH and concentration, the predominant complex is the dimer $[(UO_2)_2(OH)_2]^+$, in all the solution media studied.[65] The dimer does not dissociate very readily in the solution, so the monomer $[UO_2OH]^+$ is formed in appreciable amounts only in very dilute solution and at elevated temperatures. In concentrated solutions above 10^{-3} M U(VI), oligomeric hydrolytic species are formed. Examples of such species include $[(UO_2)_2(OH)_2]^{2+}$, $[(UO_2)_3(OH)_4]^{2+}$, $[(UO_2)_3(OH)_5]^+$, $[(UO_2)_3(OH)_7]^-$, $[(UO_2)_3(OH)_8]^{2-}$, $[(UO_2)_3(OH)_{10}]^{4-}$ (Fig. 2.3).[81,85] At higher pH, hydrous uranyl hydroxide precipitates.[85] Precipitation can be prohibited by adding countercations[95] to yield monomeric hydroxide species $[UO_2(OH)_n]^{2-n}$ (n = 3, 4, 5).[96,97]

Although the composition of some of the hydrolytic species is known, most of the scarce structural information for the polynuclear species in solution is obtained from corresponding crystal structures.[98–101] The interpretation of solution data[78,102] is complicated by the simultaneous presence of various species. For example, polynuclear species with bridging H_2O, O, Cl and OH, suggested in several studies, are still under discussion.[99,103] Bridging by two hydroxide groups is generally assumed for the dimeric species $[(UO_2)_2(OH)_2]^{2+}$ and was confirmed in recent theoretical studies.[99,104] The structure of trimeric species is largely unknown.

Hydrolysis of tetravalent uranium, U^{4+}, is of concern only in reducing solution, as UO_2^{2+} is predominant in oxic waters. The hydrolysis of U(IV) increases with increasing ionic strength and temperature. Polynuclear hydrolytic species form readily and are likely to be formed in weakly acidic solutions or at very low concentrations of U(IV).[65] Mononuclear species have been studied in acidic solutions and they start to appear at uranium concentration less than 0.1 mol/L:[105]

$$U^{4+} + n\,H_2O \rightarrow [U(OH)_n]^{4-n} + n\,H^+ \qquad (2.8)$$

Qualitatively the hydrolysis of U(IV) is rather similar to that of Th(IV), although conclusive identification of individual species is lacking.[105] The study of U(IV) is quite complicated due to the precipitation of insoluble hydroxides and oxides. There is reasonable experimental evidence confirming the formation of $[U(OH)]^{3+}$, in contrast to other hydrolysis products such as $[U(OH)_2]^{2+}$ and $[U(OH)_3]^+$.[10,103] Although a large amount of data is consistent with the neutral species $U(OH)_4$ or $(UO_2 \cdot 2H_2O)$, it is rather unclear whether this species is mono- or polymeric.[8,105] The hydrolysis of UO_2^+ of low net charge is quite weak.[83] UO_2^+ has a tendency of disproportionate to U^{+4} and UO_2^{2+} which limits hydrolyzing capability.[10] The hydrolysis constant for U(V) is believed to be similar to that

of NpO_2^+ and PuO_2^+.[106]

To illustrate the similarity of actinide hydrolysis for the species of same oxidation state but different elements, Np(V) and Np(VI) may be taken as example. NpO_2^+ is the preferred Np oxidation state, however, and is the most studied actinyl(V) species. Neptune(V) does not hydrolyze readily below pH = 9.[107] At higher pH values, the hydrolysis species $NpO_2(OH)$ and $[NpO_2(OH)_2]^-$ have been observed.[108,109] Hydrolysis of Neptune(VI) starts at pH 3–4.[85,110] There are indications for polynuclear hydrolysis species similar to U(VI). The dimeric species $[(NpO_2)_2(OH)_2]^{2+}$ and the trimeric species $[(NpO_2)_3(OH)_5]^+$ have been reported.[110,111]

Although a large amount of data on hydrolysis of uranium is available in the literature, the hydrolytic behavior of these actinides still remains controversial in some aspects. The precise number and composition of oligomeric species actually formed is not yet clear.[55,57,65] With a few exceptions, quantitative hydrolysis measurements of actinide ions are complicated due to the insolubility and strong sorption ability of actinide hydroxides. Additionally, the problem of polymerization of the mononuclear or polynuclear complexes in higher pH medium arises. There have been extensive efforts to determine hydrolysis constants of uranyl. Results on uranium(VI) at elevated temperatures suggest[87,112] that at elevated temperature, hydrolysis is enhanced owing to the increase of the degree of ionization of water, which in turn increases the concentration of hydroxide ions, by two orders of magnitude. Interestingly, uranyl monohydroxide becomes more important at higher temperature due to the decrease in the dielectric constant of water.[113] Several studies provide information on uranyl hydrolysis constants determined by various methods and at different ionic strengths.[56,57,80,81] Grenthe *et al*.[105] provide rather accurate hydrolysis constant for uranyl at zero ionic strength.

This thesis contributes a study on the monomeric hydrolysis product $[UO_2OH]^+$ of dioxouranium(VI). Several computational studies yielded different structures and coordination numbers of uranyl monohydroxide.[22,45,114] Also the computational determination of the hydrolysis free energy of the uranyl-aqua complex is under debate.[22,45]

2.2 Actinide environmental chemistry

To gain a better understanding of the interaction of actinides in the environment (Fig. 2.4), one needs detailed information on their chemical speciation in natural waters in association with natural mineral phases. Quantitative knowledge of competing processes that affect the actinides distribution and speciation is crucial.

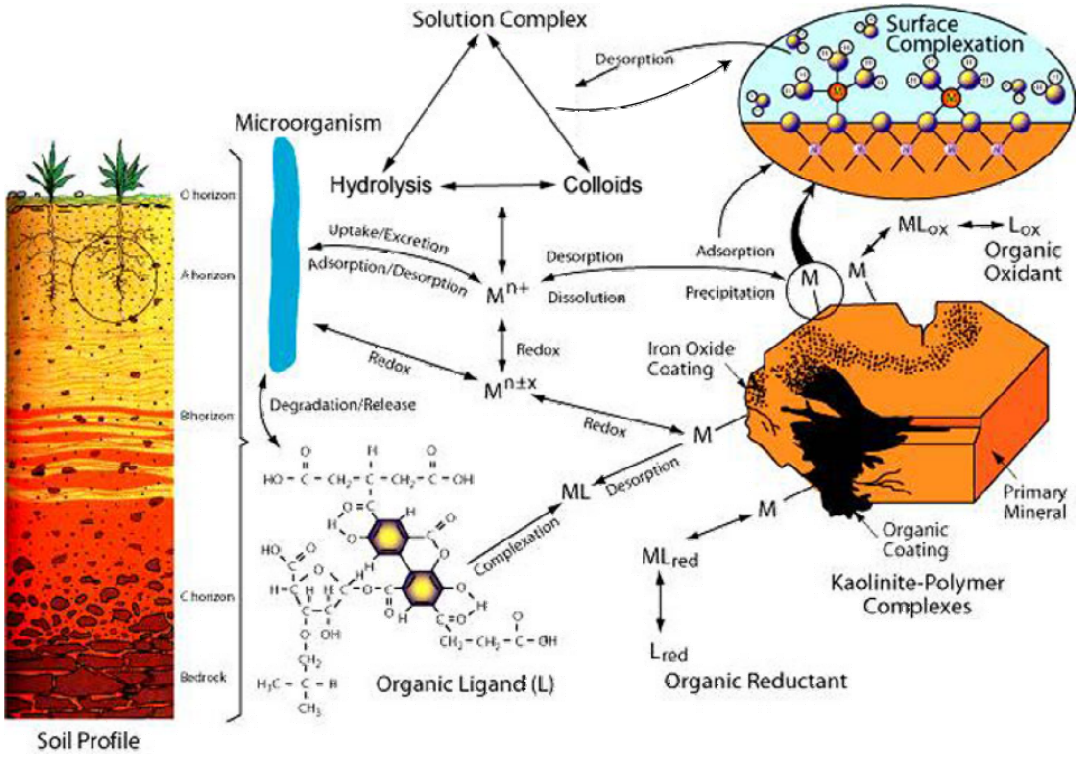

Figure 2.4. Schematic respresentation of actinide interaction in the environment. Adapted from Surface and Aqueous Geochemistry Group, Stanford, USA.

As a rule of thumb, U(VI), Np(V), Pu(IV), Am(III), and Cm(III) are the prevalent oxidation states in most ocean or groundwater environments at general conditions (Section 2.1). Thus, the actinide elements exhibit a distinctly different chemical behavior mainly owing to their different stable oxidation states. Additional chemical processes occurring in solution are likely to affect the stability of the actinide's oxidation state.[10,65] Important processes in the environment involving actinides are (1) precipitation, (2) complexation, (3) sorption, and (4) colloid formation (Fig 2.4). Precipitation can occur if there is sufficient concentration of the actinide in solution to exceed the solubility product constant for the formation of a solid phase. Besides the prevalent Pu(IV), under some conditions Pu(V) can be dominant;[83] in natural waters containing carbonate, Pu(V) complexates with the carbonate ligands, in very low concentration, less than about 10^{-6} M. The solubility of an actinide is limited primarily by two properties: the stability of the actinide-bearing solid (the solubility-controlling solid) and the stability of the complexes forming in solution. The existence of U(V) and U(VI) in environmental waters under reducing conditions would provide a mechanism for the release of uranium due to the enhanced mobility of penta and hexavalent species in comparison with tetravalent hydroxide. This could be of importance under conditions when one of the oxidation states V or VI dominates entirely over IV. U(IV) forms insoluble, polymeric, mixed hydroxides and carbonates in anoxic waters, but

is oxidized to U(VI) under oxic conditions. The latter species can be soluble, allowing migration.[9]

The chemistry of actinides in environmental aqueous systems is dominated by hydroxide and carbonate complexation, considering inorganic systems only. The behavior of actinide elements in waters of geological systems is strongly influenced by hydrolysis since it may limit solubility, lead to sorption, compete with complexation by other ligands and/or change the redox potentials of redox couples.[115] Other ligands, such as phosphate, sulfate, and fluoride, can lower the actinide concentration (because of the low solubility of the corresponding solid phase), but their concentrations in natural waters are generally low. Complexation with organic substances increases the amount of the actinide in solution and thus tends to increase the rates for release and migration.[3,7] In addition to the inorganic ligands in ground water, there are naturally occurring organic ligands that can complex the actinides rather strongly and could effect actinide transport. The most important natural ligands are humic and fulvic acids.[116] This topic, which is of concern of this thesis, will be discussed in detail in the next section.

The role of colloids in facilitating actinide transport is far from clear;[6] however, greatly enhanced transport of actinides has also been observed.[6,7] Among the two mechanisms proposed to explain colloid formation, "intrinsic" or "eigen" colloids are expected to be formed by condensation of actinides by hydrolytic or precipitation processes. A second mechanism of actinide incorporation into colloids is the formation of "associative" or "pseudo" colloids.[6] The solubility of actinides depends on complex formation and colloid formation that itself is influenced by actinide concentration. The diversity of these effects obviously can make experimental research quite complicated. In the next sections selected topics of actinide environmental chemistry, that are relevant to

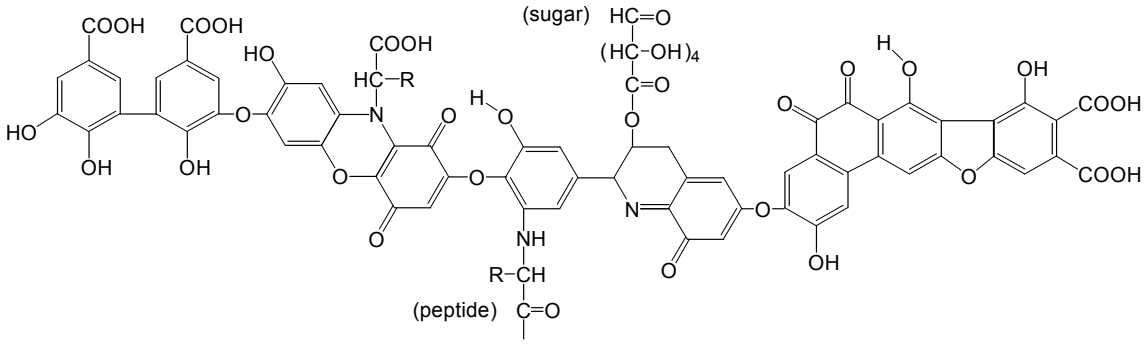

Figure 2.5. Model structure of a humic acid. Adapted from Ref. 60.

the actinide species investigated in this thesis, will be introduced in more detail. Thus, the focus will be on uranium interaction with humic substances and the formation of ternary complexes of uranyl-humate with hydroxides.

2.2.1 Actinide interaction with humic substances

Complexation of actinides by humic substances plays an imperative role in the migration and the retardation of actinides in the environment and therefore is an important ingredient of safety analysis for radioactive waste management, including long-term storage.[2,3] The migration of actinides is also influenced by colloid formation in solution. Humic acids themselves form colloids.[7] The binding of metal ions to humic acids leads to the formation of compact and less hydrophilic structures, which result in molecular aggregation and/or coagulation.[3] The aggregates may remain suspended in solution as colloids owing to their small size (e.g. < 45 mm). Actinide ions can be incorporated directly as bound metal ions or the humic acid can serve as a host to the sorption of hydrolyzed actinide ions onto the colloid surface forming the so called "pseudocolloids".[117]

Humic substances are ubiquitous in the environment. They are one of the dominant components of soil organic matter and responsible for their dark brown color. Their concentrations depend on many factors such as climate, pH, substrate material, topography, and time. Humic acids and related substances are among the most widely distributed organic materials in nature. They are found not only in soils but in natural waters, sewage, compost heaps, marine and lake sediments, peat bogs, lignites, brown coals, rocks, and miscellaneous other deposits.

Humic acids are the fraction of humic substances that is not soluble in water under

Table 2.2. Fractions of functional groups in samples of humic (HA) and fulvic (FA) acids (in percentage of oxygen).

		COOH	Acidic OH	Alcoholic OH	C=O	OCH_3	Other
HA	A	34–50	7–14	1–8	15–30	2–4	5–29
	B	39–46	9–11	0–13	4–11	– [b]	26–39
	C	31	12	24	19	2	12
FA	A	57–75	1–10	9–20	11–17	3–5	0–10
	B	39–64	5–9	24–35	4–10	– [b]	0–11
	C	64	8	14	14	2	0

A = Ref. 122, B = Ref. 123, C = Ref. 124. [b] Not determined

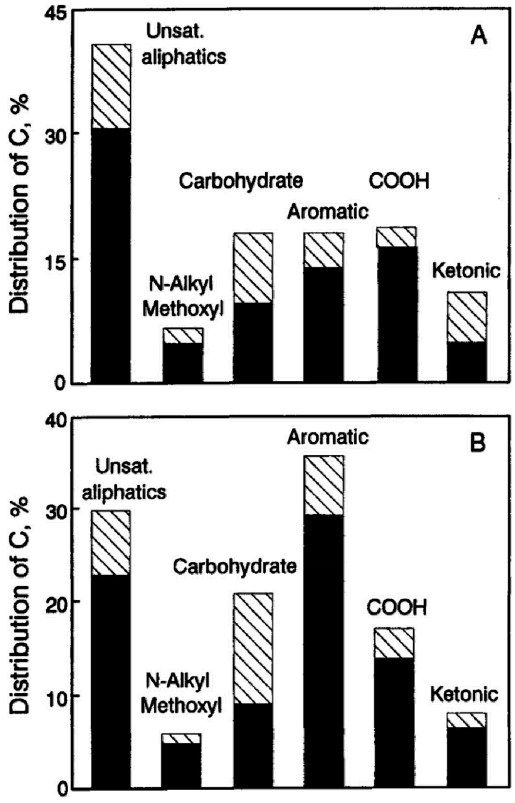

Figure 2.6. Composition of organic carbon (C) in stream and ground water fulvic (A) and humic acids (B) from four different sources. The hatched portion of the bars indicates the range of values obtained. From Ref. 60.

strongly acidic conditions (pH < 2) but is soluble at higher pH values. In soils the humic content varies from 0 to 10%,[3] it can be extracted using various reagents. Fulvic acids make up the light yellow fraction of humic substances, which is soluble in water under all pH conditions. They remain in solution after removal of humic acid by acidification. In general, the structures of humic acids have more aromatic and less aliphatic character than fulvic acids.[3] Fulvic acids are characterized by lower molecular weights 300 to 2000 amu, while 1000 to 50000 amu is typical for aquatic humic acids and 50000 to 100000 amu for soil humic acids.[60]

A large number of studies of the complexation of radionuclides, such as uranium, with humic substances have been performed.[12,59,61] However, due to the chemical and structural heterogeneity of humic substances, the nature of metal complexation sites in humic substances is still uncertain.[60] Humic substances may be described as a coiled hydrocarbon backbone with various functional groups such as carboxylic, phenolic or aliphatic OH, carbonyl, and amino substituents, that are discussed as complexing sites for metal ions (Fig. 2.6).[60,118–120]

A substantial fraction of the mass of the humic and fulvic acids is contributed by

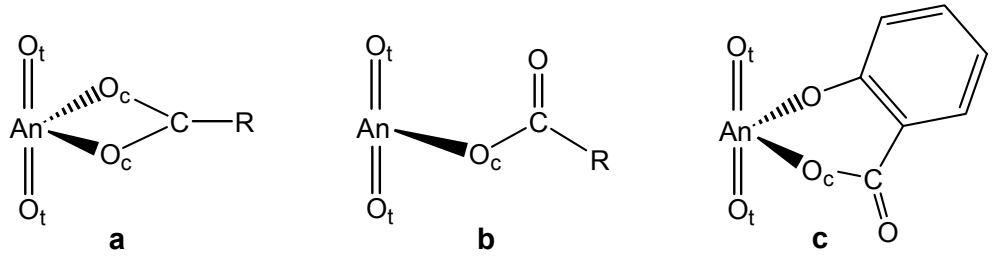

Figure 2.7. Possible coordination modes of carboxylate groups at actinyls: bidentate (a), monodentate (b), and chelate (c) coordination.

carboxylic acid functional groups, which endow these molecules with the ability to complexate positively charged multivalent ions at low pH values.[3,11,59] Table 2.2 lists the distribution of oxygen donor sites for samples of humic and fulvic acids.[60] The complexation of ions is probably the most important role of humic acids in the biosphere. This facilitates the uptake of these ions by several mechanisms, one of which is prevention of precipitation; another seems to be a direct and positive influence on their bioavailability.[6]

Humic acids also have a smaller fraction of phenolic functional groups, which can be detected by various chemical methods.[60] The influence of phenolic OH groups on the complexation properties of humic acids is under investigation.[121–125] The ratio of the carboxylate capacity to that of phenolate is higher in fulvic acids than in humic acids (Table 2.2).[126] pK_a values for carboxylate groups of 3.6±0.1 and 4.8±0.2 have been found for fulvic and humic acids, respectively;[60] pK_a values of ~9.7±0.2 have been reported for phenolic groups.[127] These data indicate that in most natural waters carboxylate groups will be almost ionized whereas phenolic groups remain protonated.

The content of aliphatic or aromatic acid groups in humic acids is difficult to quantify[60] (Fig 2.6). The fraction of aromatic carbon varies strongly, from ~25 to 80 mass percent.[60] Terrestrial humic acids tend to be more "aromatic" in nature (having more benzene and phenol like components) while marine humic acids exhibit a prevailing contribution of aliphatic carbon. Fig 2.6 illustrates the variation of the composition of organic carbon in stream and ground water fulvic and humic acids. The distributions are qualitatively similar, with the exception of the aromatic content which is higher for humic than for fulvic acids. Aromatic carboxylic acids tend to have lower pK_a values than aliphatic acids,[128] which lead to the assumption that also carboxylic groups attached to an aromatic framework are more easily deprotonated at lower pH. However, the character of humic substances depends strongly on their source, which complicates the characterization of interactions of actinides and humic acids. Besides the identification of complexation

sites, another major issue is to understand the complexation mechanisms in order to model, may be even influence the migration or the retardation of actinides.

The interaction of humic acids with actinides is mainly mediated by carboxylic groups of humic substances as active sites of complexation. Such complexes have been experimentally investigated by x-ray diffraction (XRD) and EXAFS spectroscopy, to determine structures, and coordination modes and coordination numbers of complexes.[129–139] With respect to this thesis, especially the coordination chemistry of uranyl(VI) species is of concern. A carboxylate group can coordinate to an actinyl in bidentate (Fig 2.7 a) or monodentate fashion (Fig. 2.7 b); pseudo-bridging coordination, i.e. monodentate coordination accompanied by a strong hydrogen bond between the free carboxylate oxygen and an aqua ligand of the uranyl, has also been suggested.[104] In addition, chelate coordination via adjacent hydroxyl groups, e.g. in salicylate or α–hydroxyl benzoate, is discussed (Fig. 2.7 c).[140] Another coordination mode, where the two oxygen centers of the carboxylate form a bridge between two neighboring uranyl moieties, is found in many crystal structures.[103] Analysis of various crystal structures indicates preference for bidentate coordination for uranyl ions.[141] Tris(carboxylato) complexes such as $M[UO_2(OOCCH_3)_3]$ (M = monovalent cation) where three carboxylates act as bidentate ligand, exhibit a higher stability, thus corroborating the above result.[103] Bidentate coordination has also been suggested for the complex $[UO_2(OOCCH_3)_3]^-$ in solution.[142]

EXAFS results on the complexation of uranyl by humic acids, from solids and in solution, are interpreted to show monodentate coordination.[61,121,132,143] However, it is not clear why only monodentate complexation of uranyl should occur, considering the complex structure of humic substances and the predominance of carboxylic groups as complexing sites. To investigate coordination types, different modes have been studied in this thesis, using model complexes of uranyl with various simple aromatic carboxylates as ligands (see Section 4.2). Due to their complex and heterogeneous nature, a thermodynamically based description of humic-substances complexation with metal ions is difficult. The kind and number of complexating functional groups is uncertain. There are different models to formulate the complexation of humic substances allowing an approximation explanation of the complexation behavior, e.g. see Refs. 11,144,145. However, complexation data that were determined under various experimental conditions and evaluated by different models are not comparable with each other.[12]

2.2.2 Ternary complexes

The formation of ternary actinide complexes, i.e. with three different types of ligands, in

aquatic solution has been of interest in various research fields such as synergistic extraction[146] solubility[147,148] and sorption[149,150] of actinides in the environment. However, many studies on the complexation of actinides focused on the simpler question of how binary complexes form. Thus, although the pH of the natural water varies between 6-10,[7] most of the studies are carried out at low pH,[12,59,61,78] because processes are simpler, avoiding competing phenomena such as hydrolysis, precipitation etc. that occur at elevated pH. Nevertheless, the formation of ternary complexes at around neutral pH is quite probable and cannot be excluded. Thus, it is essential to explore this topic to understand the environmental phenomena.

Mixed hydroxyl complexes, $An(OH)_qL_p$ have been proposed a long time ago.[151] They form the largest class of ternary complexes in aqueous solution. For some species, they are readily encountered even in weakly acidic solutions.[83] Systematic studies of the rate and mechanisms of intermolecular and intramolecular exchange reactions of ternary U(VI)-fluoride-carboxylate ligand complexes have been done.[152–154] The most extensively studied ternary actinide complexes remain the hydroxyl-carbonates.[83] In the recent literature, also the formation of a ternary U(VI)-hydroxo-acetate complex, $[UO_2(CH_3COO)_3OH]^{2-}$, is discussed;[133,155] however, stability constants are not available. In near-neutral ground water stable ternary actinide complexes can be formed by various ligands, such as hydroxide and carbonate, together with natural organic compounds, such as humic and fulvic acids.

There are only a few detailed experimental studies on ternary actinide complexation that involve humic acids. Ternary lanthanide complexes with organic ligands have been reported to be more stable than binary lanthanide complexes.[156] Zeh *et al.*[157] studied the sorption of UO_2^{2+} ion into humic colloids in Gorleben ground water by ultra filtration and anion exchange under controlled CO_2 pressure between pH 1 and 10; they analyzed their data assuming the formation of uranyl-hydroxo-humate UO_2(OH)HA(I). Pashalidis *et al.*[158] explored the formation of ternary uranyl-humate complexes at pH 7.5 to 7.9 with the solubility enhancement method. The resulting stability constant for the formation of the ternary complex UO_2(OH)HA(I) is slightly higher than that for the formation of uranyl-humate UO_2HA(II).[158] Sachs *et al.*[159] suggested the formation of an UO_2(OH)HA(I) complex from $[UO_2OH]^+$ and HA at pH 7, based on laser-induced fluorescence spectroscopy experiments; the corresponding stability constant is 6.58 ± 0.24. Using the equilibrium dialysis-ligand exchange technique, Glaus *et al.*[160] studied the formation of a mixed uranyl-carbonato-fulvate complexes at pH 7.

Considering the polyfunctional nature of humic substances, it is a general believed that the complexing capacities are sensitive to the pH value. These features have been

observed in an acidic to neutral pH range (3–7),[117,145] but above pH 7 the formation constant of actinide-humate complexes remain uncertain. Stability constants of uranyl-humate and ternary uranyl-hydroxo-humate complexes are found to be comparable.[158,159] However, invoking simple electrostatic arguments, one would expect the humate complexation constant for the uranyl monohydroxide complex to be weaker than that of the non-hydrolyzed uranyl-humate complex. To contribute to the understanding of uranyl-humic interaction at ambient conditions, the ternary complexation of uranyl(VI) with carboxylate and hydroxide ligands is investigated in this thesis.

2.3 Experimental identification and characterization

As discussed in the preceding section, the chemical behavior of actinides is significantly influenced by the oxidation state, coordinated ligands, and experimental conditions. Thus, proper characterization of the involved species under environmental conditions is vital for understanding complex processes. In this context various experimental methods such as potentiometric titrations,[161] infrared (IR),[162] Raman,[86,163] and nuclear magnetic resonance (NMR) spectroscopy,[154] X-ray diffraction,[141] and X-ray absorption fine spectroscopy (XAFS)[164,165] have been applied to gain chemical and structural information. Equilibrium constants for the complexation process involved can be quantified by laser spectroscopy (TRLFS).[166]

XAFS is a spectroscopic technique that uses X-rays to probe the physical and chemical structure of matter at an atomic scale.[164,165] The absorption spectrum is divided into two parts: X-ray absorption near edge structure spectroscopy (XANES) at energies close to a specific X-ray absorption edge and the extended X-ray absorption fine structure (EXAFS) at higher energies. XANES provides useful information about the oxidation state, the molecular symmetry, and the local structure of an actinide compound. Extended X-ray absorption fine structure spectroscopy yields information on certain geometry parameters, such as bond lengths to first, second and even more distant atomic neighbor shells and the corresponding coordination numbers.[164,165] Usually parameters (with estimated error bars in parentheses) obtained from analysis of such spectra related to a specific absorbing atom are distances R (±2 pm), coordination numbers (±15 to 20 %), Debye-Waller factors (±0.5 pm^2), and the nuclear charge Z of neighboring atoms (±4).[167] These parameters are especially relevant for the description of An-ligand distances in the equatorial actinyl plane where often only average distances can be determined; note that atomic shells, which are separated by less than 10 pm, are hard to resolve. EXAFS results are an average over samples, thus under environmental conditions the coexistence of

various complexes is not distinguished in EXAFS studies, at variance with the direct evidence from vibrational spectroscopy.

In contrast to the above spectroscopic methods, x-ray crystal structure data add detailed information on structural aspects, such as bond lengths, bond angles as well as the coordination modes of the ligands. However, this method is limited to crystalline compounds only. For disordered systems like the chemistry of actinides under environmental conditions, optical absorption and scattering spectroscopic methods are considered to be some of the most reliable techniques for detection and characterization.[168] In addition X-ray absorption spectroscopy (XPS) is a powerful tool to study the speciation of actinides at relatively low actinide concentration in the environment.[169] Core level shifts determined by XPS provide vital information regarding charge and oxidation state of the actinides.[170–172] Solubility measurement, colorimetry, polarography and spectrophotometric methods are used to determine the stability constants with reasonable accuracy.[83] Potentiometry is one of the most convenient and successful techniques employed for metal complex equilibrium measurements.[161] However, no structural information gained from this study is limited, only the charge of species present is obtained.

Raman scattering and infrared (IR) absorption spectroscopy provide explicit information on the structure as well as the composition of the actinyl species via characteristic vibrational modes, e.g. the characteristic symmetric (ν_{sym}) and antisymmetric (ν_{asym}) stretching frequencies of the actinyl moiety.[162] A major advantage of these methods is the possibility to identify the individual species in a solution containing various compounds. Raman spectroscopic studies determined a linear relationship between symmetric uranyl stretching frequency (ν_{sym}) and the number of equatorially coordinated ligands such as hydroxide or carbonate.[86,163]

Time-resolved laser-induced fluorescence spectroscopy (TRLFS) is a powerful speciation technique,[166] usually applied to samples containing more than a single component where each component may be detected by its specific peak and luminescence decay time. It is often used in actinide chemistry for direct speciation of luminescent metals such as UO_2^{2+}.[166] Advantages of TRLFS are (i) its high sensitivity that enables studies at submicromolar concentrations and (ii) emission, excitation, and lifetime resolutions, which are characteristic of the metal ion and its chemical environment. TRLFS has been used for identification and determination of the stability constant of various actinide complexes.[166]

3 Computational method

A scalar relativistic (SR) extension of the linear combination of Gaussian-type orbitals density-functional (LCGTO-DF)[173] method as implemented in the parallel code PARAGAUSS[13,14] was used to carry out all calculations. PARAGAUSS has certain distinguishing features, such as the consequent parallel implementation of all demanding tasks, an efficient relativistic treatment of heavy atoms, and various approaches for describing interactions of a system with its surrounding.[47,174-177]

In the following sections, some computational details relevant for the calculations performed in this thesis are presented. Relativistic effects are discussed briefly (Section 3.1). The treatment of solvent effects in terms of a polarizable continuum model (PCM model) is sketched in Section 3.2. In Section 3.3, the basis sets will be described. Then some technical details for the calculation of vibrational frequencies will be discussed in Section 3.5. Section 3.6 contains a brief description of thermodynamic corrections in energetics.

3.1 Density functional methods

Ab initio methods and methods based on density functional theory (DFT) are most powerful and sophisticated tools of quantum chemistry for determining the electronic structure of molecular systems. The *ab initio* methods include Hartree-Fock Self-Consistent Field (HF-SCF) and post-HF methods like Møller-Plesset perturbation theory (MP2) and configuration interaction (CI).[15,178–180] Highly accurate multiconfigurational methods such as complete active space approach (CASSCF, CASPT2) and coupled-cluster with single and double and perturbative triple excitations (CCSD(T)) are the more accurate methods available today.[181,182] However, the most reliable *ab initio* methods, which account accurately electron correlation, are still limited to rather small systems due to high computational costs.[20] More recently, DFT methods became particularly attractive because

of the inclusion of correlation in a very efficient manner.[13,14] For many chemical problems, DFT methods furnish a sufficiently accurate, yet computationally efficient description of molecular structures and energetics.[183] DFT forms the basis and framework of all research that is presented in this thesis.

The basis of DFT is the Hohenberg-Kohn[184] theorem, stating that the ground state energy of a many-electron system is a functional of the electron density ρ. In other words, the density ρ uniquely defines the potential of the system, which parameterizes the Hamiltonian and thus the wave function. It follows that the many-body wave function is a functional of the density, and hence all properties of the system can be expressed as a functionals of the electron density.[184] The exact ground-state density minimizes the ground-state total energy functional.[185]

The corresponding variational procedure is usually carried out by solving the Kohn-Sham (KS) equation, leading to an effective one-electron problem. The effective potential v_{eff} governing the one-electron problem comprises the (external) nuclear potential v_{nuc}, the classical Coulomb or Hartree potential v_{coul}, and the exchange-correlation (xc) potential v_{xc}.[184,186] Formally, the exchange-correlation potential is given as the functional derivative of the corresponding exchange-correlation energy E_{xc} with respect to the density ρ. However, the exact form of the exchange-correlation potential v_{xc} of KS theory is not known and approximations have to be used instead.[13,14] Different approximations are available for a proper description of v_{xc}.[183,187,188,194] The local density approximation (LDA) is based on the assumption that v_{xc} is a simple function of the density ρ. The generalized gradient approximation (GGA) represents an improvement by taking into account the gradient of the local electron density. Other alternatives are the hybrid functionals, where the exchange part of a GGA is mixed explicitly with the exact non-local exchange energy of the KS determinant, using a fixed ratio.

3.1.1 Evaluation of exchange-correlation methods

In this thesis, three different exchange-correlation functionals were applied to determine various properties of actinide complexes: the LDA functional as parameterized by Vosko, Wilk, and Nusair (VWN),[189] and the GGA functionals suggested by Becke and Perdew (BP)[190,191] as well as the revised version of the Perdew-Burke-Ernzerhof functional of Nørskov *et al*. (PBEN).[192]

LDA often yields more accurate results for molecular geometries and vibrational frequencies.[193,194] Gradient-corrected functionals (generalized gradient approximation,

GGA) are known to perform better for energy parameters.[193,194] Therefore, using the structures obtained at the LDA level, the energetics was subsequently determined in a single-point fashion (LDA/GGA procedure), for most cases with the GGA functional suggested by Becke and Perdew (BP).[190,191] The additional advantage of this strategy is reduced computational effort during the optimization due to the simpler LDA functionals. However, the LDA minimum is different from the GGA minimum; thus, the "single-point" energetic GGA evaluation is somewhat inconsistent.

To adopt a more consistent treatment, GGA functionals are also used for the optimizations being aware of the fact that GGA functionals overestimate the bond distances slightly. The differences between these two strategies are usually small and depend on the systems investigated. This strategy was tested earlier for some actinide system such as actinide hexafluorides AnF_6 (An = U, Np).[195] The well-known trend[193,194] that LDA distances are more accurate (±3 pm) and GGA tends to slightly overestimate distances (+4 pm) is confirmed. Solvated actinyl complexes $[AnO_2(H_2O)_5]^{2+/+}$ as well as uranyl dimer complexes $[(UO_2)_2(OH)_2(H_2O)_n]^{2+}$ (n = 0, 6) show elongated bond distances for the GGA functionals BP and PBEN.[62] However, the calculations also revealed the typical overestimation of binding energies by LDA (up to ~130 kJ mol^{-1} per F in AnF_6) which renders this functional inadequate for discussions of energetic properties.

To quantify the energetic aspects, the LDA/BP and BP procedures have been compared for $UO_2(H_2O)_5^{2+}$. The difference in the total electronic energy between LDA/BP and BP is 12 kJ mol^{-1}, which is rather small keeping in mind the accuracy of present day computational methods. Therefore, a combined approximate LDA-BP approach seems justified by its specific advantages. Thus, the LDA (VWN) functional was chosen for all geometry optimizations to benefit from the overall more accurate geometric parameters. However, for uranyl-monohydroxide (Section 4.1), the GGA functionals (BP and PBEN) were adopted in addition, to provide a better representation of weak interactions as well as to exclude possible methodological artifacts due to the known overestimation of weak nonbonding interactions by LDA functionals. The distance between oxygen centers of a water dimer are somewhat better described by the BP functional (282 pm) than by VWN (270 pm); the experimental value is 297 pm.[196]

Due to their complex form, exchange-correlation potentials and energies cannot be evaluated analytically. The grid for the numeric integration of the exchange-correlation functional was chosen as a superposition of atom-centered spherical grids.[197] The grid consisted of 70 radial shells and integrated exactly angular momentum components up l =19. For typical complexes these grids comprise about 26000, 8500, 10000, 11000, and

9000 points for U, F, O, C, and H centers, respectively.

3.1.2 Relativistic density functional method

A relativistic description of electrons in molecules that contain one or more heavy atoms is essential for accurate calculations of the electronic structure of such molecules.[27,29] Relativistic effects can be considered as a consequence of the speed of light being finite, resulting in significant changes of the electron structure and the corresponding properties.[27] In quantum chemistry, this effect is related to differences introduced by substituting the non-relativistic Schrödinger equation by the relativistic Dirac equation. Relativistic effects on the valence electrons are in general expected to be chemically important only for higher values of the nuclear charge. Thus, they are rather relevant for actinides ($Z \geq 89$).[27–29] In molecular systems, the relativistic contraction (direct relativistic effect of s orbitals), the relativistic self-consistent expansion (indirect relativistic effect of d and f orbitals) and spin-orbit interaction are the major effects.[198,199]

Solving the relativistic analogue of the Kohn-Sham problem, namely the Dirac Kohn-Sham (DKS) equation, requires a large computational effort owing to the complexity involved in the four component form of the one-electron wave functions. Thus, often a simplified form of the theory is used which is restricted to the two components that describe the electron degrees of freedom. The reduction of relativistic quantum chemistry to a two-component form can be achieved by unitary transformations, which decouple the Hamiltonian, which in fact helps in cutting down the computational cost. The Douglas-Kroll (DK) transformation is one very successful and well-established procedure[200] for molecular systems, in particular in the Douglas-Kroll-Hess (DKH) approach.[35] The DKH formalism generates a scalar-relativistic (SR) variant if one neglects spin-orbit (SO) interaction; otherwise, one arrives at a SO variant of the method.[201] As implemented in PARAGAUSS, the second-order Douglas-Kroll transformation incorporates relativistic effects and decouples electronic and positronic degrees of freedom of the Dirac-Kohn-Sham equation.[16,34] In this work the scalar-relativistic variant of the DKH approach is applied throughout. Spin-orbit effects are neglected because all species treated have a closed-shell electronic structure, where spin orbit effects are rather small.[230]

Besides the very popular DKH approach, there are several other methods and approaches available to account for relativistic effects on the electronic structure. The use of effective core potential (ECP) methods is an alternative approximate method, providing sufficiently high accuracy and low computational cost for systems containing heavy

elements.[32,33,202–204] This approach is most often used as it avoids an explicit relativistic treatment of the molecular valence electronic structure whereas the effect of the core electrons is represented by an appropriate potential operator. Another alternative is indirect inclusion of relativistic effect via the frozen core approximation.[30,31] Another efficient two-component method is the zeroth-order regular approximation (ZORA)[36–38] which is also available as scalar relativistic variant.

3.2 Modeling of solvation effects

3.2.1 Solvent effects in quantum chemistry

As discussed in the previous chapter, it is often mandatory to model solvent effects in chemistry. Especially properties of molecular ions are strongly affected by solvent interactions. Stabilization of charged species in solution, compared to their gas phase structure, is the most important of these consequences. Additionally, solvent interaction can significantly affect structures and energetic of such species.[40,205,206] The computational modeling of conditions in solution demands in principle a high-level quantum mechanical approach because it is crucial to describe with reasonable accuracy charge transfer between solute and solvent, hydrogen bonding as well as coordination numbers and bond breakings that occur when the solute interacts with the solvent.

Effective solvent models in quantum chemistry may generally be divided into two main categories, (i) the polarizable continuum (PCM) models[41–44] and (ii) the discrete solvation models.[41,44,45] In the first approach, the solvent is modeled as a macroscopic dielectric continuum characterized by a dielectric constant.[205]

Even though solvent continuum models were introduced more than a century ago, their merging with a quantum mechanical model of the solute began more than 30 years

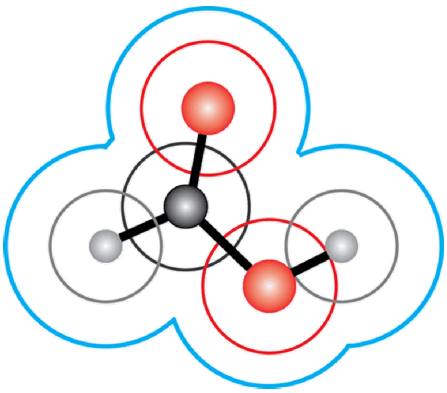

Figure 3.1. Schematic representation of the cavity constructed around a solute molecule in a polarizable continuum model (PCM). Adapted from Ref. 62.

ago by Tomasi, Claverie, Rivail and Tapia.[207–210] Since those pioneering works[211] it has become customary to represent long-range solvent effects in quantum chemistry calculations with the help of a polarizable continuum model (PCM),[205,211] where the solute is placed in a cavity of a polarizable dielectric medium. Among many variants, the conductor-like screening model (COSMO)[212] has become very popular due to its economy.[213–215]

In the second approach, the solvent is treated explicitly as a collection of discrete molecules. To achieve an effective method, the solvent molecules, or at least the major part of them, may be treated classically by means of force fields. This leads to combined quantum mechanics/ molecular mechanics (QM/MM) methods.[216–218]

A quantitative description of solvent effects cannot be achieved easily with polarizable continuum models for several reasons. Especially short-range solvent effects due to coordinated aqua ligands or due to directed hydrogen bonds are not described by PCM models. For numerous actinide species in solution it has been shown that these short-range effects especially of the first solvation shell can be rather strong and notably affect molecular structures, vibrational frequencies, and solvation energies.[19,21,22,41,43–47,104,219] In addition, for uranyl-carboxylate complexes, the effect of short-range solvent effects is emphasized and a brief comparison to the corresponding long-range effect is provided.[219] Thus in the PCM models, for an accurate calculation of the solvation energy, such aqua ligands have to be taken into account explicitly in the quantum chemistry models.[47,220] Therefore, a combined strategy that considers both explicit coordination of aqua ligands from at least the first coordination sphere and treats the remaining solvent as a polarizable continuum is recommendable.[220]

3.2.2 The conductor like screening model (COSMO)

In the COSMO approach,[212] the solute is represented by a charge distribution in a cavity of the solvent, simulated by a continuous polarizable medium with a dielectric constant ε. In this model, the surface charge density due to the discontinuity of the dielectric constant at the cavity surface is determined by a conductor-like boundary condition,[212] i.e. the total Coulomb potential is taken to vanish on the cavity surface. By partitioning the cavity surface into small patches, so-called tesserae, the surface charge is approximated by a set of point charges. Point charges are placed at representative points of each tesserae that can be determined in different ways.[47]

The COSMO variant implemented in the program PARAGAUSS was employed in

this thesis (see Section 3.2.2).[47] The dielectric constant ε = 78.39 for solvent water. Furthermore, in the program PARAGAUSS a tessalation scheme has been chosen that allows a symmetry-adaptation of the COSMO approach; it leads to a distribution of surface grid points, which complies, with the symmetry of the molecule.

In addition to the original COSMO model, the PARAGAUSS solvent module also accounts for short-range nonbonding solvent effects via a force field.[47] For reasons of economy, it is customary to treat dispersion and repulsion interactions by means of a pair potential approach.[221]

The choice of shape and dimension of the solute cavity represents one of the most delicate steps in defining a continuum solvation model.[222] In the majority of the PCM models, the solute cavity is built with a set of interlocking spheres usually centered on the atoms or atomic groups of the solute (Fig. 3.1). Several studies show that standard van der Waals (vdW) radii provide a reasonable cavity size,[205] although a number of improvements have been suggested. A cavity scaling factor is usually introduced to enlarge the basic atom or group radii before the individual spheres are defined. In PARAGAUSS, the default vdW radii of these spheres are scaled by a factor 1.2, except for H where the radius is not scaled.[223] Note that PCM results are known to depend crucially on the sphere radii.[215] Furthermore, the cavity shape is smoothened by introducing additional spheres according to the GEPOL algorithm to avoid cusps or narrow niches in the cavity.[62,224] Several studies showed that the cavity size is very important for determining accurate solvation energy.[205,206,215,221–226] For neutral solutes, the mean deviations with respect to experimental data as low as 2 kJ mol^{-1} can be obtained with a limited number of parameters; however, the situation is rather demanding for ionic species, where the errors are usually larger than 8 kJ mol^{-1}. The definition of cavities based on chemical considerations (basically hybridization, formal charge, and first neighbor inductive effect) that are presented in a united-atom topological model (UA0) is known to provide better solvation energies compared to a model embedded in a cavity constructed by van der Waals radii.[215,227] In the UA0 approach, each heavy atom of the solute is surrounded by a sphere; hydrogen atoms are enclosed in the sphere of the atom to which they are bonded. UA0 radii have been developed in a semi-empirical fashion by optimizing a set of parameters in such a way that the solvation energies based on HF-SCF calculations fit a sizeable experimental data set involving various compounds.[214,227] These radii are empirically adapted to the effective charge of the corresponding atomic centers. The solvation energies of small molecules such as H_2O, NH_3, F^-, and OH^-, as determined with UA0 radii as well as vdW radii show that the UA0 approach yields better agreement with the experiment.[47] For anions, the average deviation from experiment decreases to 5 kJ mol^{-1} with the UA0 approach

compared to 13 kJ mol^{-1} calculated with the standard method using a cavity derived from interlocking spheres with vdW radii.[47] For the calculation of the acidity of substituted benzoic acids (Section 4.2.1), UA0 radii are used in this thesis to compare the trends in the free energy of deprotonation with corresponding pK_a values. Neither method, with vdW or UA0 radii, provides a correct trend for the differences of free energies of deprotonation of various substituted benzoic acids as will be seen in Section 4.2. As these differences caused by substitution are rather small (< 5 kJ mol^{-1}) due to very similar pK_a values of these acids, this issue provides a rather challenging test for solvation methods.

3.3 Basis sets

Basis sets and related computational parameters are chosen as in earlier and related studies[62,125,230] to allow easy comparison and are reviewed shortly in this section. The Kohn-Sham orbitals (see Section 3.1) were represented by flexible Gaussian-type basis sets, contracted in a generalized fashion using appropriate atomic eigenvectors from spin-averaged atomic calculation in I_h symmetry. The size of the primitive basis sets and the corresponding contracted basis is given in the notation (n_0s, n_1p, n_2d, n_3f) and [N_0s, N_1p, N_2d, N_3f], respectively. n_l and N_l denote the number of orbital exponents and contracted functions, respectively, which are associated with an angular momentum *l*. For U, the basis set of the size (24s, 19p, 16d, 11f),[228] contracted to [10s, 7p, 7d, 4f] was used. The light atoms were described by standard basis sets:[229] (9s, 5p, 1d) → [5s, 4p, 1d] for F,[229a] (9s, 5p, 1d) → [5s, 4p, 1d] for C and O[229b,c] and (6s, 1p) → [4s, 1p] for H.[229b,d] Exponents of all basis sets are collected in Appendix A.

In the LCGTO-FF-DF method, the classical Coulomb contribution to the electron-electron interaction is evaluated via an approximate representation of the electron density, using an auxiliary basis set.[173] In this way computationally demanding four-center integrals can be efficiently avoided; only three-center integrals have to be evaluated. The size of the auxiliary basis sets is specified by the notation (n_0s, n_1r^2, m_1p, m_2d, m_3f). The exponents of the corresponding s- and r^2-type "fitting functions" were constructed from the s- and p-functions of the orbital basis and scaled by a factor of 2.[173] For U only every second p-exponent was used, to avoid numerical instability due to near linear dependency of the set because of strong overlap of s- and r^2-type functions. In addition, five p, d, and f type "polarization exponents" were added, each as geometric series with a progression of 2.5, starting with 0.1, 0.2, and 0.3 au, respectively (see Appendix A). Thus, the auxiliary charge density basis sets were (24s, $9r^2$, 5p, 5d, 5f) for U (12s, $9r^2$, 5p, 5d) for F, (9s, $5r^2$, 5p, 5d) for C and O, (6s, $1r^2$, 5p) for H. Comparison with results of other DF calculations

confirmed the accuracy of the current FF approach for actinide complexes.[195]

The uranium basis sets suggested by Minami and Matsuoka (24s, 19p, 16d, 11f)[228] together with the enlarged variant (24s, 19p, 16d, 13f, 2g), had previously been tested on the six- to four-valent actinyls UO_2^{2+}, UO_2^{+}, and UO_2 and the hexahalogenides UF_6 and UCl_6.[230] With the standard basis, bond lengths were well reproduced with very small changes in distances, 0.2 to 0.9 pm (0.1–0.5%) compared to the enlarged basis. In addition, the difference in vibrational frequencies was relatively small, 3 to 11 cm^{-1}, i.e. less than 1% except for UF_6 (1.5%). However, a significant variation in binding energies was noticed,[230] up to 30 kJ mol^{-1} or 4%, but in the present context this was not considered significant to warrant the extra cost of the larger basis sets.

The effect of the contraction scheme was tested for two flexible sets; (24s, 19p, 16d, 11f) → [10s, 7p, 7d, 4f] and [9s, 7p, 6d, 4f].[230] The more flexible contraction yielded results of comparable accuracy as the contracted basis sets: bond distances deviate by ~0.5 pm and energies by 5 kJ mol^{-1}.[230]

Extension of the auxiliary basis of U by a set of five g exponents, constructed according to the procedure given above, confirmed the accuracy of the selected auxiliary basis set. For instance, with additional g exponents, bond lengths of uranyl monoformate in monodentate coordination changed by less than 20 pm and the total energy changed less than 4 kJ mol^{-1}.[62] Overall, these results corroborated the quality of the contracted standard basis sets for U that is employed for all calculations of this thesis.

3.4 Structure optimization

Molecular structures were optimized with the quasi-Newton method, employing an update scheme like BFGS.[231] In the geometry optimizations, the total energy and elements of the density matrix are required to converge to high precision, 10^{-8} au; for the largest component of the displacement gradient vector and the update step length, the convergence criteria were set at 10^{-6} au.

3.5 Vibrational frequencies

As discussed previously, vibrational frequencies for actinide complexes are very important indicators for characterization and structure analysis. However, full frequency calculations are rather demanding for complexes of the size studied in this thesis because in the PARAGAUSS version used in most of the calculations, only first-order derivatives are

available.[13] Additionally, infrared and Raman spectroscopic measurements of actinyl complexes usually focus on the characteristic symmetric (ν_{sym}) and antisymmetric (ν_{asym}) actinyl stretching frequencies. Therefore, one possibility is to determine only these frequencies via numeric second derivatives using a step size of 0.1 a. u., by neglecting the coupling to other frequencies while the other degrees of freedom were kept frozen. This strategy generally yields reliable results for stretching frequencies; however, bending modes are known to be more affected and not easy to calculate accurately by a restricted approach.[195] In addition, small force constants determined as finite differences of energy gradients may be susceptible to numeric inaccuracies and parameters such as the chosen displacement.

Previous calculations on uranyl and the dimeric uranyl species $[(UO_2)_2(OH)_2]^{2+}$ in the gas phase (GP) and in solution (PCM) yielded only minor differences for ν_{sym}, i.e. at most 0.2 and 2 cm^{-1} employing this approach compared to a full frequency calculation.[232] These differences are negligible when comparing to experimental values of uranyl stretching frequencies that are typically in the range of 850-870 cm^{-1} for the symmetric mode ν_{sym} and about 960 cm^{-1} for the antisymmetric mode ν_{asym}.[162,233,234]

Test calculations on uranyl $[UO_2(H_2O)_n]^{2+}$ (n = 0, 5) and bidentate (n = 0, 3) and monodentate (n = 4) uranyl monocarboxylate complexes $[UO_2(OOCR)(H_2O)_n]^{+}$ (R = H, CH_3, CH_2CH_3) in the gas phase were discussed earlier.[62] The symmetric uranyl stretching frequency ν_{sym} is quite stable with respect to the applied approximations and differs by at most 0-4 cm^{-1} in gas the phase and 10 cm^{-1} in solution, [62] i.e. only by about 1% of its absolute value. Variations for the antisymmetric stretching frequency ν_{asym} is slightly larger, up to 20 cm^{-1}.[62]

In version 3.1 of PARAGAUSS,[235] newly developed analytical second derivatives have become available. This new option was used for some calculation of this work. Such analytical force constants provide a numerically stable and efficient way to compute harmonic vibrational frequencies of many-atomic systems. Test calculations on some

Table 3.1. Comparison of characteristic vibrational frequencies of H_2O, CH_3COO^-, $[UO_2OH(H_2O)_4]^+$ with numerical as well as analytical second derivatives. Δ indicates differences of analytical and numerical frequencies.

System	Numerical	Analytical	Δ
H_2O	1534, 3716, 3839	1536, 3716, 3842	2, 0, 3
H_3CCOO^-	1706, 2907	1705, 2906	-1, -1
$[UO_2(H_2O)_4OH]^+$	856, 937	855, 936	-1, -1

simple systems such as H_2O, CH_3COO^-, $[UO_2(H_2O)_4OH]^+$ have been performed to check the reliability of the method. For comparison, the numerical frequencies were calculated (see above). In the gas phase, the numerical frequencies are in better agreement with analytical ones. Table 3.1 compares characteristic vibrational frequencies of the above species determined in numerical and analytical way. Differences are negligible in all cases, at most 3 cm^{-1}. This accuracy in calculating frequencies with numerical second derivatives is quite good and comparable to that of analytical ones. However, calculating normal modes with analytical second derivatives is more economic than the numerical procedure.

3.6 Thermodynamic corrections

Thermodynamic corrections are taken into account to achieve a more realistic description for comparison with experiments at standard temperature and pressure. For systems calculated in quantum chemical methods, the total electronic energy corresponds to zero temperature and zero pressure conditions. However, generally experimental conditions are taken at a standard pressure of 1 atm and standard temperature of 25°C. Thus, to close the gap to actual experimental conditions, thermodynamic corrections are applied to the electronic energy to obtain reaction enthalpies and Gibbs free energies, ΔG, obtained via vibrational and rotational partition functions. The Gibbs free energy in solution is determined by a thermodynamic cycle, employing the free energy of the corresponding reaction in the gas phase and solvation free energies of all species involved (Eq. 3.1), since the vibrational spectrum of the solvent is not available in molecular calculations.

Thus, ΔG for the reaction A+B → C + D is determined as:

$$\Delta G_{aq} = \Delta G_g + \Delta G_{sol}(C) + \Delta G_{sol}(D) - \Delta G_{sol}(A) - \Delta G_{sol}(B) \qquad (3.1)$$

Gas phase free energies are calculated based on geometries optimized without symmetry constraints and the corresponding results of a vibrational normal mode analysis. Solvation

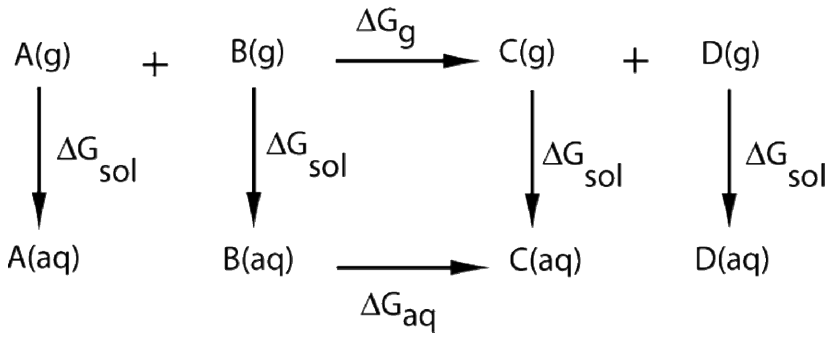

Figure 3.2. Schematic representation of the thermodynamic cycle for estimating the free energy ΔG_{aq}.

energies are determined by $\Delta G_{sol} = G_{aq} - G_g$.

In the gas phase, standard conditions imply a pressure of 1 atm; in solution standard conditions refer to a one-molar concentration which corresponds to 24.45 atm. For consistency, all species should be referenced to same pressure. Therefore, a correction term of 8 kJ mol^{-1} for each species involved in the reaction has been accounted for, to convert standard state results for the gas phase (1 atm) to results in solution with standard state of 24.45 atm. For each water molecule, a special correction of 18 kJ mol^{-1} is applied to reflect the conventional standard state of water, 1354 atm.

4 Results and discussion

This chapter is divided in three sections.

Section 4.1 presents results for the monomeric hydrolysis product, $[UO_2OH]^+$ of uranyl. Structure and coordination number of uranyl monohydroxide and the free energy of hydrolysis of uranyl will be discussed as obtained from calculations using different exchange-correlation functionals. The results of this study represent valuable reference material for the subsequent investigation of uranyl complexation at about neutral pH.

Section 4.2 focuses on uranyl complexation by carboxylate ligands. The first section is devoted to an investigation of the coordination number of uranyl monoacetate $[UO_2(OOCCH_3)]^+$. This section mainly focuses on uranyl complexation with aromatic acids. Structures and energetics were characterized and differentiation of various coordination modes of the carboxylic group (bidentate, monodentate, or chelate) was investigated. Additionally the stability constants of uranyl-monocarboxylate complexes are examined. Finally, the implications of these results on uranyl complexation by humic acids will be considered.

The last, Section 4.3 collects results on ternary complexes of uranyl-acetate with hydroxide. The discussion focuses on structure, energetics as well as stability constants of the ternary system. As for the uranyl-carboxylate system, different coordination modes have been investigated. The chapter concludes with a discussion of the implications of the presented results on actinide complexation by humic acids at slightly acidic to neutral pH.

4.1 Uranyl monohydroxide

As discussed previously in Section 2.1.3, hydrolysis of uranium plays a pertinent role in understanding the complexation behavior of this element in aqueous media. The smallest hydrolysis product $[UO_2OH]^+$ occurs in dilute solutions with pH 4-6 that contain less than 10^{-4} mol/L uranium.[65] The work to be discussed in the following will deal mainly with this compound. Uranyl monohydroxide with coordination numbers four to six was studied in detail to provide more insight into the structural aspects as well as to determine the thermochemistry and hydrolysis free energy of the uranyl-aqua complex, which corresponds to the formation of $[UO_2(H_2O)_4OH]^{1+}$. In the literature no detailed computational study on uranyl monohydroxide is available. Limited results have been obtained for complexes in the gas phase and in solution, but without considering possible isomers.

Uranyl monohydroxide has been computationally studied by means of force field based molecular dynamics,[236] quantum chemical Car-Parrinello simulation,[237] pseudopotential DF approaches with GGA functionals ((PBE and BP86)[238] and a hybrid DFT method (B3LYP)[22,45,239]) as well as the frozen core (FC) ZORA approach to relativistic DFT.[238] Either gas phase[239] or solution simulations based on PCM models (COSMO,[22,238] COSMO-PCM (CPCM)[238] a COSMO variant with different parameters and BSJ[45]) have been performed.

Ingram *et al.*[238] reported only one isomer of $[UO_2(H_2O)_4OH]^{1+}$. It exhibits a structure with one aqua ligand oriented with its molecular plane in the equatorial plane of uranyl and four water ligands perpendicular to that plane. Hay *et al.*[45] found a linear U-O-H fragment in the complex $[UO_2(H_2O)_4OH]^{1+}$, in contrast to the expectation of a bent structure of this moiety and to the structures of di- and tetrahydroxo complexes, $[UO_2(OH)_2]$ and $[UO_2(OH)_4]^{2-}$, where bent U-O-H fragments were predicted[48,240] computationally. In conclusion, the structure of uranyl monohydroxide is not well established.

The hydrolysis free energy ΔG_{hyd} of the uranyl-penta aqua complex was calculated by Hay *et al.*[45] at 55 kJ mol^{-1} by means of a hybrid DF approach whereas Tsushima *et al.*[22] determined the same quantity as -1.3 kJ mol^{-1}. A DF Car-Parrinello MD simulation[237] reports 40 kJ mol^{-1} for ΔG_{hyd}. Thus, the results for the free energy of hydrolysis depend notably on the procedure used.

The structural features of uranyl monohydroxide are rather difficult to study experimentally because the compound a stable and predominant species only at rather low

uranium concentration, in a narrow pH window. Therefore a detailed computational study on structure and energetic is worthwhile.

4.1.1 Models

Uranyl monohydroxide was optimized without any symmetry restrictions applying three exchange-correlation functionals, one LDA (VWN) and two GGA (BP, PBEN) variants. Along with penta-coordination, tetra- and hexa-coordination of uranyl monohydroxide was considered. Various isomers of $[UO_2(H_2O)_4OH]^{1+}$ have been generated by deprotonating different hydrogen atoms of the aqua ligands of $[UO_2(H_2O)_5]^{2+}$. Interestingly seven isomers of uranyl monohydroxide, close lying in energy were determined. Although three more starting structures were examined, the optimizations lead to structures identical to those of other isomers. Isomer structures were regarded as identical if the following criteria were fulfilled: similar ligand orientation, differences in bond lengths less than 0.5 pm, difference of bond angles below 3° and difference in total electronic energy < 1 kJ mol^{-1}. Nevertheless, these rather strict criteria still allow hydrogen bonds O···H to differ by up to 10 pm. In the following, only interligand contacts shorter than 300 pm are arbitrarily regarded as hydrogen bonds to simplify the discussion. The isomers obtained can be regarded as representative set of models structures. Second-shell solvation effects will modify these model structures.

For each such structure, a normal mode analysis without any symmetry constraints was carried out in the gas phase and in solution to confirm its character of a local minimum. The frequencies obtained are used to determine the free energy terms in the gas phase. Various low frequency modes, corresponding to the intermolecular hydrogen bonding and bending modes of water molecules have been identified. The lowest frequency values, which might imply numerical artifacts, were checked with a larger integration grid and tight convergence criteria for optimization. However, the frequency values hardly changed (by less than 2 cm^{-1}). This finding illustrates the accuracy of the computational approach applied.

4.1.2 Geometry

LDA structures

Morphologically, the various isomers differ mainly with respect to the orientation of the aqua ligands in the first coordination shell. Aqua ligands with different orientations lead

Table 4.1 Calculated structural parameters of various isomers (LDA, distances in pm) and symmetric and antisymmetric uranyl stretching frequencies ν_{sym} (in cm^{-1}) of uranyl-aqua and uranyl monohydroxide complexes $[UO_2(H_2O)_nOH]^{1+}$ with n = 3, 4 and 5. Given are the results from gas phase (GP) and solvation (PCM) calculations.

Complex	isomer	CN	$U{=}O_t$[a]	$U\text{-}O_h$	$U\text{-}O_w$	$U\text{-}O_{eq}$	ν_{sym}	ν_{asym}
GP								
$UO_2(H_2O)_5^{2+}$		5	176.6	-	239/239/239/242/243	240	897	990
$[UO_2(H_2O)_3OH]^{1+}$		4	179.2	206	241/241/242	232	853	934
$[UO_2(H_2O)_4OH]^{1+}$	1	4	178.4	215	230/241/242/347	232	866	954
	2	5	178.7	214	240/242/244/262	241	855	936
	3	5	179.0	209	243/244/250/254	240	848	930
	4	5	178.9	211	244/245/248/250	239	854	939
	5	5	178.9	211	243/245/247/253	240	849	933
	6	5	178.3	221	242/242/245/245	239	874	954
	7	5	178.8	208	247/248/249/251	241	854	939
PCM								
$UO_2(H_2O)_5^{2+}$		5	177.7	-	234/234/237/240/241	237	869	918
$[UO_2(H_2O)_3OH]^{1+}$		4	179.8	209	236/236/236	229		
$[UO_2(H_2O)_4OH]^{1+}$	1	4	179.3	217	231/236/236/356	230	841	901
	2	5	180.2	212	237/245/245/247	237	830	884
	3	5	180.3	211	238/242/248/249	238	827	883
	4	5	180.3	212	240/242/245/249	237	878	962
	5	5	180.2	210	242/243/244/249	238	831	886
	6	5	180.3	210	243/244/245/246	237	829	883
	7	5	180.0	210	243/245/247/247	239	834	889
$[UO_2(H_2O)_5OH]^{1+}$[b]		5	179.4	220	238/239/243/246	237		
Exp.								
$UO_2(H_2O)_5^{2+}$			177(12)		241	241	870[c]	961
$[UO_2(H_2O)_4OH]^{1+}$							849[d]	

[a] average values, [b] most stable isomer, [c] Ref. 162 [d] Ref. 86

to hydrogen bonds of variable strength. Geometry parameters of various isomers in the gas phase and in solution are collected in Table 4.1. Isomers are numbered in the order of increasing length of the hydrogen bonds around the OH ligand of the species in solution (Fig. 4.2). Isomer 1 is a four-coordinated complex, with one aqua ligand hydrogen bonded to the hydroxide group and an adjacent water molecule. All other isomers, 2 to 7, show uranyl to be five-coordinated. Compared to isomer 1, four-coordinated uranyl monohydroxide modeled as $[UO_2(H_2O)_3OH]^{1+}$ (Fig. 4.1) exhibits significant differences of the geometry parameters in the gas phase: the strong hydrogen bond to the hydroxide group in $[UO_2(H_2O)_4OH]^{1+}$ elongates the $U\text{-}O_h$ bond to 215 pm whereas $U\text{-}O_h$ amounts to

only 206 pm in $[UO_2(H_2O)_3OH]^{1+}$. As a result of the strong U-O_h bond, a longer U=O_t bond of 178.7 pm and average bonds of uranyl to aqua ligands U-O_w, of 241 pm are calculated for $[UO_2(H_2O)_3OH]^{1+}$ compared to isomer 1 of $[UO_2(H_2O)_4OH]^{1+}$ (U=O_t = 178.4 pm, U-O_w = 238 pm). Nevertheless, the average equatorial U-O bond, U-O_{eq} is the same for the above two complexes, 232 pm. As for various other uranyl complexes U-O_{eq} is mainly determined by the coordination number of uranyl; for further details on this topic, see the discussion of uranyl monocarboxylate in Section 4.2.

In the gas phase, the structural features of the penta-coordinated isomers differ from those of four-coordinated isomer 1. In isomer 1, U=O_t and U-O_w distances are shorter due to fewer competing ligands in the equatorial shell. The hydrogen bond of the aqua ligand in the second coordination shell (O···H = 160 pm) to hydroxide ligand leads to a relatively long U-O_h bond of 215 pm (Table 4.1). Terminal uranyl bonds of penta-coordinated isomers are up to 0.6 pm than those of the four-coordinated isomer 1. This is consistent with a weak red shift of 10–20 cm^{-1} for the symmetric and antisymmetric uranyl stretching frequencies (Table 4.1). One of the U-O bonds to the aqua ligands in isomer 1 with 230 pm length is the shortest calculated for all isomers (Table 4.1), while the others (241 pm) are only slightly shorter than the typical U-O_w bond length of five-coordinated isomers (240-250 pm).[45,48,62,220]

Among the penta-coordinated isomers, the variation in geometry is small in the gas phase, with the exception of isomer 6 (Table 4.1). U=O_t varies by 0.3 pm and the average uranyl-aqua ligand bond U-O_w differs by 3 pm. For various isomers, the hydroxide bond to uranium varies by 4 pm in the series. This relatively large difference in U-O_h roughly follows the strength of the hydrogen bonds between the aqua ligands and the OH group. The average U-O distance in the equatorial plane, U-O_{eq}, is rather stable and amounts to

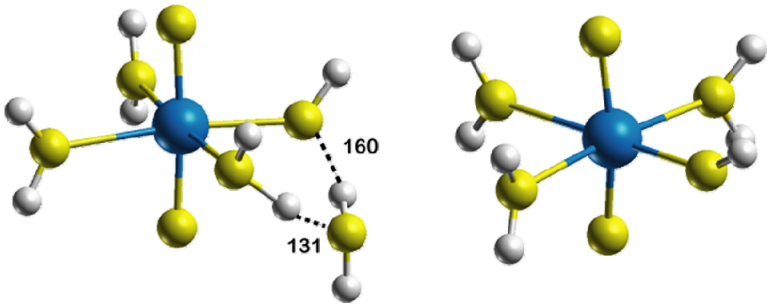

Figure 4.1 Optimized structure of four-coordinated uranyl monohydroxide $[UO_2(H_2O)_4OH]^{1+}$ isomer 1 and $[UO_2(H_2O)_3OH]^{1+}$ in the gas phase at the LDA level. Also shown are calculated O···H distances (in pm) of hydrogen bonds that are formed within the ligand sphere.

240±1 pm for all penta-coordinated isomers. Isomer 6 contains two strong hydrogen bonds to the hydroxide group with O···H distances of 179 pm and 181 pm. Therefore, its geometry parameters are different from those of other penta-coordinated isomers; U=O_t with 178.3 pm is relatively short and the U-O_h bond of 221 pm is the longest of all the isomers studied. A relatively long U-O_h bond of 214 pm was calculated also for isomer 2, which features a rather short (strong) interligand hydrogen bond of 172 pm to OH group. Compared to other five-coordinated isomers, isomer 3 and 7 show strong U-O_h bonds of about 209 pm, concomitant to the long and weak hydrogen bond to the OH group in isomer 3 (O···H = 221 pm) and the absence of hydrogen bonds in isomer 7.

Some isomers show the same structures in the gas phase and in solution, for others a slight rearrangement in the network of the hydrogen bonds are obtained due to solvent effects. With inclusion of solvent effects, a general trend to slightly longer hydrogen bonds involving the OH groups was calculated, with the exception of isomer 1. Solvent

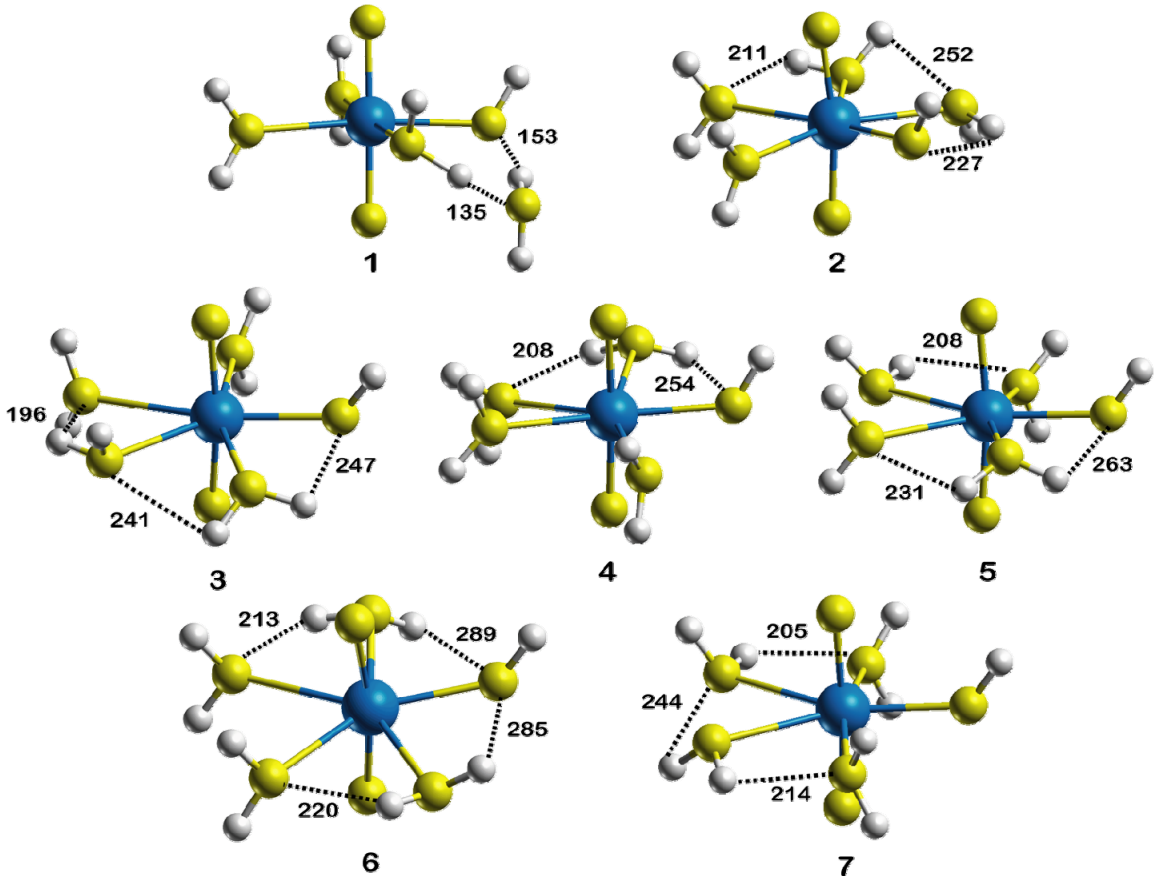

Figure 4.2 Optimized structures of isomers of uranyl monohydroxide $[UO_2(H_2O)_4OH]^{1+}$ in solution (LDA functional). Also shown are calculated O···H distances (in pm) of hydrogen bonds that are formed within the ligand sphere.

effects elongate terminal U=O_t bonds by about 1 pm, while the average distance U-O_w shrinks by 2–6 pm. In general, for solvent models including a molecular shaped cavity, polar bonds were calculated longer than in the gas phase.[261] The polar bond U-O_h is elongated by 1–2 pm in some cases, except for isomers 2, 5 and 6. Thus, the main trends of solvent effects on geometry parameters are in line with earlier studies on uranyl-carboxylates[62,58] as well as other theoretical studies.[22,45,238] The exceptions noticed for the U-OH bond will be discussed below.

At least two hydrogen bonds are present in each isomer, and the various isomers are mainly distinguished by the position of these bonds (Fig. 4.2). Except in isomer 7, aqua ligands form hydrogen bonds with the hydroxide group; O···H distances vary from 135 to 289 pm. The number of hydrogen bonds either remains the same or increases when one goes from the gas phase to aqueous solution.

Structures in solution have been obtained by optimization starting from the gas phase structures. To ensure the structural correspondence between gas phase and solution structures, the above isomers were optimized once again in the gas phase again starting from structures obtained in solution with restricted optimization step length. In all cases, the gas phase structures optimized independently could be confirmed. There is a slight change in the orientation of aqua ligands for these isomers yielding new hydrogen bonding patterns in solution (Fig. 4.3).

During geometry optimization with a solvent model, isomers 4 and 6 change from

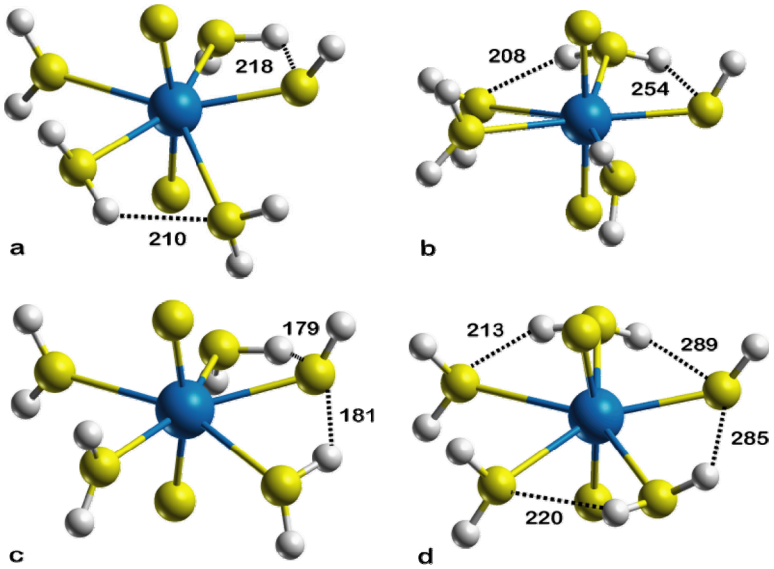

Figure 4.3 Optimized structures of isomers 4 and 6 of uranyl monohydroxide $[UO_2(H_2O)_4OH]^{1+}$ in the gas phase and in solution: isomer 4 in the gas phase (a) and in solution (b), isomer 6 in the gas phase (c) and in solution (d).

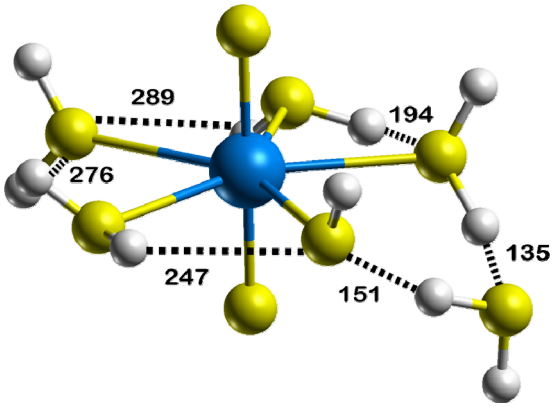

Figure 4.4. Optimized structure of an exemplary isomer of hexa-coordinated uranyl monohydroxide $[UO_2(H_2O)_5OH]^{1+}$ in solution.

their gas phase structures. In isomer 4, the hydrogen bond of an aqua ligand to the hydroxide group is considerably weaker as shown by the increase of the O···H contact from 218 to 254 pm (Fig. 4.3 a, b). This allows the aqua ligand to form a second hydrogen bond of length 210 pm (Fig. 4.3 b). A similar effect is observed for isomer 6, where hydrogen bonds to OH are also lengthened due to solvation; the aqua ligands involved each form an additional hydrogen bond (Fig. 4.3 c, d). As a result, the hydrogen-bonding network of isomer 6 rearranges and the U-O_h bond contracts considerably, by 11 pm. Similar effects are observed for isomers 2 and 5. Thus, the weakening of the hydrogen bonds counteracts the screening effect of the solvent environment, which leads to longer polar bonds. As a result, counteracting solvent effects on the U-O_h bond are calculated (Table 4.1).

Hexa-coordinated uranyl monohydroxide (Fig. 4.4) was also considered to examine the coordination number of uranyl in uranyl monohydroxide. Starting from the structure of the hexa-coordinated uranyl-aqua complex, optimizations in solution yielded always penta-coordinated uranyl-hydroxide with one aqua ligand moved to the second coordinating shell. Intermolecular hydrogen bonding at distances of 151 pm and 135 pm (Fig. 4.4) were calculated for the most stable isomer. Compared to the geometry parameters (average) of penta coordinated isomers of $[UO_2(H_2O)_4OH]^{1+}$, the uranyl-hydroxide bond of the complex $[UO_2(H_2O)_5OH]^{1+}$ is notably elongated, by about 8 pm, which in turn leads to a shortening of the terminal bonds of uranyl, by about 1 pm, and of the uranyl-aqua bonds, by 2 pm (Table 4.1).

The symmetric uranyl stretching frequency was calculated at 841 cm^{-1} for the four-coordinated isomer 1 and at 832 cm^{-1} on an average (for all five-coordinated isomers, except isomer 4). The corresponding experimental frequency is 848.5 cm^{-1}.[86] This

experimental value was estimated from Raman measurements of polynuclear hydrolytic species of uranyl where the symmetric uranyl stretching frequency has been found to scale with the number of OH groups coordinated.[86] The current results show rather good agreement and confirm this experimental estimate.

GGA structures

It is well known that LDA functionals do not properly describe nonbonding interactions as they tend to overestimate them.[183] For this reason, in this study also gradient corrected BP and PBEN functionals were used to optimize $[UO_2(H_2O)_4OH]^{1+}$ to check the LDA results. A brief comparison of main structural features of uranyl monohydroxide complexes with different functionals is provided in Table 4.2. The structure of all isomers are similar to those calculated with the local density approximation in almost all cases, with the only exception of isomer 1. In the PBEN optimization (Fig. 4.6) isomer 1 adopts a structure that differs significantly from the LDA and BP results (Fig. 4.5). While with

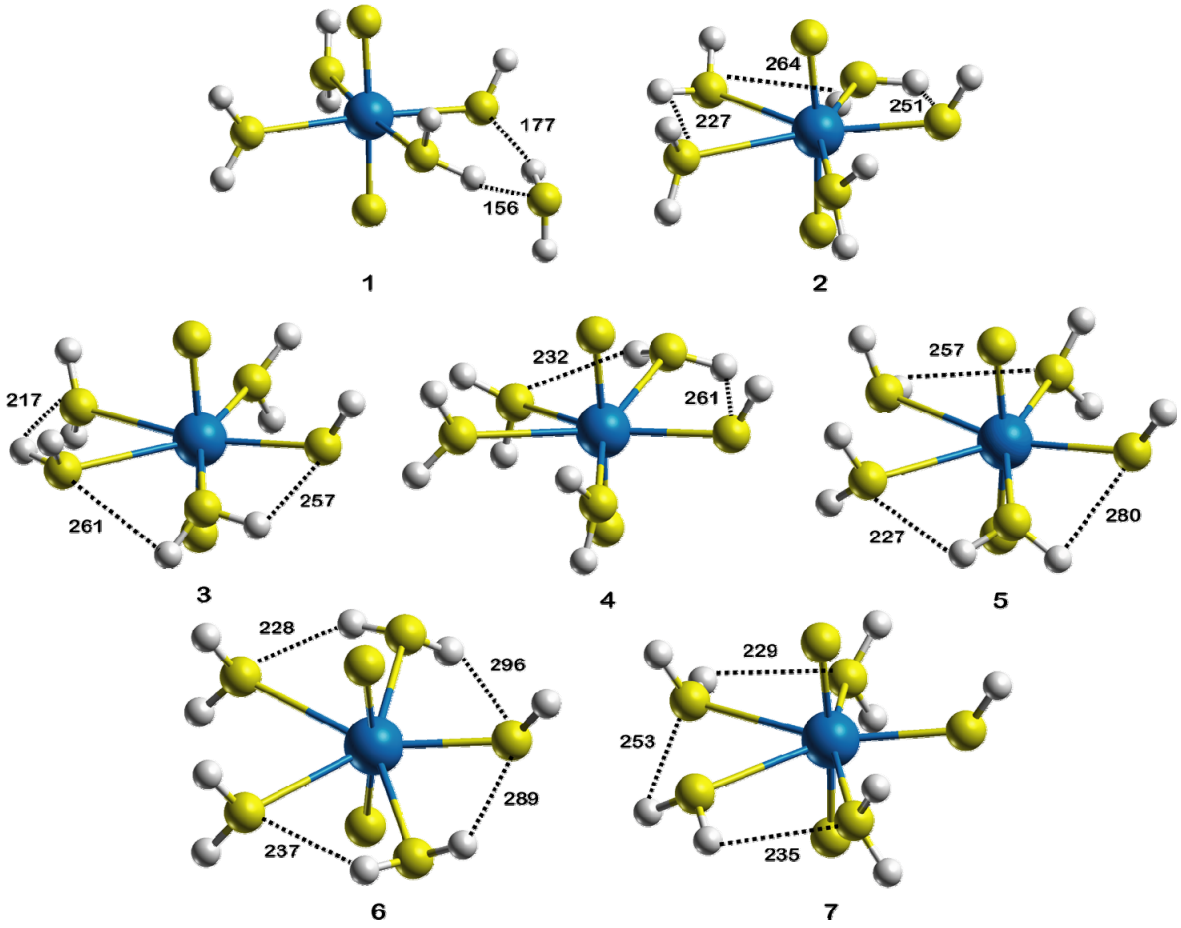

Figure 4.5. Optimized structures of isomers of uranyl monohydroxide $[UO_2(H_2O)_4OH]^{1+}$ in solution (BP functional). Also shown are calculated O···H distances (in pm) of hydrogen bonds that are formed within the ligand sphere.

the BP functional, the hydrogen bonds of the aqua ligand in the second shell are weakened, one of these contacts is lost applying the PBEN functional. Instead, that water ligand is connected to the complex by only a single hydrogen bond of length 159 pm. This leads to a shortening of the U-O_h bond by 3 pm, compared to the LDA and BP structures. Due to these strongly deviating structures, isomer 1 will be excluded from the following discussion.

The isomers optimized with the GGA functionals contain the same number of hydrogen bonds as obtained at the LDA level (Fig. 4.4, Fig. 4.5). Slight changes of the orientation of aqua ligands are noted. In general, the GGA optimizations yield elongated bond distances as well as hydrogen bonds. The PBEN functional furnishes slightly longer bonds than the BP functional (Table 4.2).[183] While the strong uranyl bond is only moderately affected (up to 2 pm longer compared to LDA), the equatorial U-O distances to the aqua ligands U-O_w are calculated distinctly longer at the GGA level, by 8 to 15 pm,

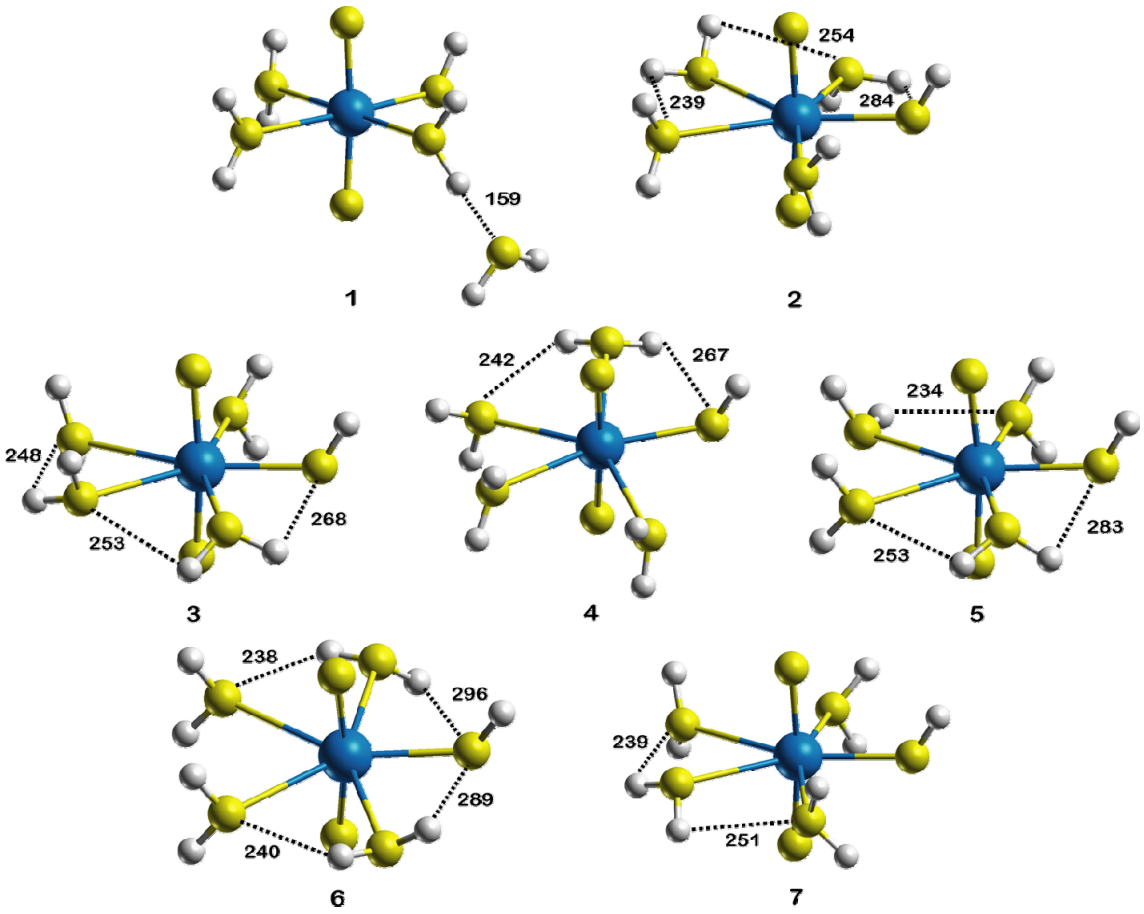

Figure 4.6. Optimized structure of isomers of uranyl monohydroxides $[UO_2(H_2O)_4OH]^{1+}$ in solution (PBEN functional). Also shown are calculated O···H distances (in pm) of hydrogen bonds that are formed within the ligand sphere.

Table 4.2. Calculated structural parameters (LDA, BP, PBEN; average distances in pm) as well as symmetric and antisymmetric uranyl stretching frequency ν_{sym} and ν_{asym} (in cm^{-1}) of uranyl monohydroxide complexes $[UO_2(H_2O)_4OH]^{1+}$ in comparison to other theoretical results. Results from calculations on gas phase (GP) models and solvation (PCM) calculations.

	Method		CN	U=O_t[a]	U-O_w[a]	U-O_h	ν_{sym}	ν_{asym}
GP	DKH	LDA	4	178.4	238	215	866	954
			5	178.9	248	210	852	936
		BP	4	179.9	247	214	850	934
			5	180.4	257	212	824	909
		PBEN	4	180.4	252	211	839	921
			5	180.4	262	212	827	911
	ZORA, ADF[b]	PBE	5	179.7	260	211	865	948
		BP	5	180.0	259	212	859	941
	PP, G03[b]	PBE	5	179.4	256	211	841	921
	PP, G03[c]	B3LYP	5	178.6	258	215	818	
	PP, G03[d]	B3LYP	5	178.3		216		
PCM	DKH	LDA	4	179.3	234	217	841	901
			5	180.2	244	211	844	906
		BP	4	181.0	243	217		
			5	181.7	253	214		
		PBEN	4	181.0	247	217		
			5	181.6	257	215		
	ZORA, ADF[b]	PBE	5	179.8	258	212	861	942
		BP	5	180.1	259	212	856	931
	PP, G03[b]	PBE	5	180.7	252	212	807	862
Exp.[e]							849	

[a] average values [b] Ref. 238, [c] Ref. 239, [d] Ref. 45, [e] Ref. 86

and the U-O_h elongates by 3-6 pm. The trend of geometry parameters from gas phase to solution is consistent for all functionals studied: the U=O_t bond elongates by 1 pm, U-O_w bonds shorten by 3–5 pm and U–O_h bonds are slightly elongated, by 1 to 3 pm, for the five-coordinated structures. For all isomers, the symmetric uranyl stretching frequencies ν_{sym}, calculated with GGA functionals in the gas phase (Table 4.2), show red shifts compared to the LDA results, in agreement with the elongation of the terminal uranyl bonds. The close similarity of LDA and GGA results confirms that the well-known tendency of LDA[183] to overbinding, but in this case it does not lead to structural artifacts.

Comparison to other theoretical studies

Few calculations have been published, which provide structural details of uranyl monohydroxide. Penta-coordinated uranyl monohydroxide was reported from DF[45,238] and force field calculations.[236] Interestingly, none of these earlier studies inspected the coordination number of uranyl monohydroxide in solution or reported on different isomers.

Oda *et al.*[239] studied the symmetric Raman active frequency of uranyl monohydroxide for models with four- to six-coordination in the gas phase with B3LYP DF calculations applying a large-core pseudopotential. Agreement to the experimental symmetric uranyl stretching frequency[86] of 849 cm^{-1} is better for four- and five-coordination, but is underestimated in the six-coordinated complex. For penta-coordinated uranyl monohydroxide, the calculated symmetric uranyl stretching frequency is 847.5 cm^{-1}, corrected with a scaling factor of 1.036.[239] The unscaled B3LYP result of 818 cm^{-1} compares favorably with the gas phase results obtained in the present work with GGA functionals for five-coordinated species (BP: 824 cm^{-1} and PBEN: 827 cm^{-1}, Table 4.2). Interestingly, a relatively short uranyl bond of 178.6 pm was obtained in that study,[239] going along with the rather long U-O_h bond of 215 pm. GGA results of the present and other studies in the gas phase[238] yielded U=O_t by about 1 pm longer and U-O_h by 3–4 pm shorter (Table 4.2). Very similar results had been obtained in another study that applied large-core pseudo potentials.[45] The six-coordinated complex $[(UO_2(H_2O)_5OH]^{1+}$ was optimized only with LDA in this study and the corresponding structure contains an aqua ligand in the second shell. At the B3LYP level, Oda *et al.*[239] also did not obtain any structures with six aqua ligands in the first coordination shell.

Ingram *et al.*[238] calculated the monohydroxide of uranyl using two exchange-correlation functional, PBE and BP86, both in the gas phase and in solution, using a pseudopotential as well as the FC ZORA approach. They used the solvation models CPCM and COSMO to describe long-range solvent effects. They reported only a single isomer. The proposed structure of $[UO_2(H_2O)_4OH]^{1+}$ shows three upright aqua ligands and one ligand oriented parallel to the equatorial plane of uranyl, similar to isomer 4 (Fig. 4.2). The GGA results of that study in overall are agree well with the present findings using the BP and PBEN functionals for five-coordinate species in the gas phase (Table 4.2). As exception, the vibrational frequencies were calculated ~20 cm^{-1} higher with the FC ZORA approach.

Comparison of results for five-coordinate species in solution obtained with GGA functionals shows that slightly longer bonds were obtained the in the present study: U=O_t

bond by ~1 pm, U-O_h bond by 2–3 pm. This differences are larger than in the gas phase; they partially can be traced back to differences in solvation effects. Inspection of Table 4.2 shows that solvation effects of this study and those of the pseudopotential PBE approach using the CPCM solvation model[238] are similar: U=O_t elongates by a little more than 1 pm, U-O_w decreases by 4–5 pm, while U-O_h increases by 3 pm. At variance with these results, the FC ZORA approach, applying the COSMO solvation model,[238] yields much smaller solvation effects: U=O_t increases by only 0.1 pm and U-O_w decreases by up to 2 pm while U-O_h is stable. However, Shamov *et al*.[247] using an all-electron ZORA-COSMO approach with the PBE functional, determined a strong effect of solvation on the geometry parameters of $UO_2(H_2O)_5^{2+}$. U-O_w shrinks by 7 pm compared to the gas phase result, in agreement with the present results where ΔU-O_w = 6 pm for $UO_2(H_2O)_5^{2+}$ due to solvation. In addition one should notice that in Ref. 238 a slightly larger radius, 200 pm, for U has been used when constructing the solute cavity. That parameter was 186 pm in the present work and 170 pm in Ref. 247.

In a theoretical study[45] using a large-core pseudopotential approach with the B3LYP functional, a linear U-O-H arrangement for $[UO_2(H_2O)_4OH]^{1+}$ was calculated in the gas phase while in the present study the U-O-H angle amounts to 125°. To check a possible linearity of the U-O-H fragment in uranyl monohydroxide, the rather simple model $[UO_2OH]^+$ was studied. Without symmetry constraints, both in the gas phase and in solution, the bent U-O-H structure is preferred. The angle U-O-H is calculated at 165° in the gas phase and at 128° in solution. Bent hydroxide ligands are better π-donors as pointed out by Bursten *et al*.[241] Thus, a bent U-O-H moiety should always be preferred.

Comparison to $[UO_2(H_2O)_5]^{2+}$

To study the structural effect of the hydroxide group on the uranyl-aqua complex in the gas phase and in solution, geometry and vibrational frequencies were compared to the characteristics calculated for a uranyl complex with just five aqua ligands. Due to the strong binding of the hydroxide ligand, the terminal uranyl bond is 2 pm longer and the average uranyl-aqua distance is ~5 pm longer, both in gas phase and in solution (Table 4.1). In the gas phase the change in U=O_t is reflected also in the stretching frequencies of the uranyl moiety; ν_{sym} decreases by 37 cm^{-1} and ν_{asym} by 51 cm^{-1} on average for all the isomers. In solution, the red shift of the uranyl symmetric vibrational mode amounts to about 25 cm^{-1} for four- as well as five-coordinate species. This value agrees very well with the experimental difference of 21 cm^{-1} (Table 4.1).

Table 4.3. Pertinent atomic populations (in %) of molecular orbitals of $[UO_2OH]^+$ related to the OH group. Orbital numbers and orbital energies (in eV) are given for the calculations on the model in the gas phase.

Orbital	ε	O_t	U			O_h		H
		sp	p	d	f	s	p	sp
45a	-32.7	4	56			36	1	2
48a	-28.3	6	36	2		41	6	9
50a	-18.2	6	4	9	7	3	54	15
51a	-15.9	60		23			16	
54a	-15.2	60	1	2	26		10	
55a	-14.7	56	3	2	23	1	13	1
56a	-14.6	41	5	1	30		22	1
57a	-14.4		1	6	10		72	10
58a	-12.9	24	6		31		39	

Electronic structure and bonding

The interaction of the hydroxide ligand with uranium changes only slightly the effective configuration of uranium. The d and f populations of the uranium center of uranyl monohydroxide increase weakly, by 0.1 e, compared to the effective configuration in the uranyl-aqua complex with the effective configuration $7s^{0.1}$ $6p^{-0.1}$ $6d^{1.9}$ $5f^{2.7}$ of uranium. The valence sp orbitals of the OH moiety can act as σ- and π-donor orbitals in the U-OH bond.[241] The U 5f and 6d orbitals compete to act as acceptor orbitals in the ligand bonding.[242] The dominant equatorial ligand donation is expected to involve U 6d orbitals, except when symmetry permits only 5f orbitals to be involved.[242] To analyze the U-OH bonding and possible π contributions, a Mulliken analysis of OH-related molecular orbitals (MOs) was carried out for the small model system $[UO_2OH]^+$ in the gas phase; Table 4.3 shows all valence orbitals with contributions from the OH group of more than 10%. The MOs at lowest energies, -32.7 eV (45a) and -28.3 eV (48a), represent the σ and σ* contributions to the U-OH bond and involve mainly U 6p contributions. MOs 51a, 54a and 55a are orbitals of uranyl (π_g, π_u with admixture of σ type) with small O 2p contributions of the OH group (Table 4.3). The HOMO 58a as well as the two MOs below, 56a and 57a, contain relatively large O_h 2p contributions and reflect the π interaction of the OH group with uranyl (Fig. 4.7). MO 57a essentially is an O_h lone pair (2p) with small π-bonding f and d admixtures of uranium. The second lone pair of OH^- is oriented parallel to the axis of uranyl; therefore it easily mixes and is distribute over several MOs. Also, MO 56a shows a weak π-bonding character with respect to the U-OH bond and MO 58a represents the corresponding antibonding partner. From the O_h (2p)

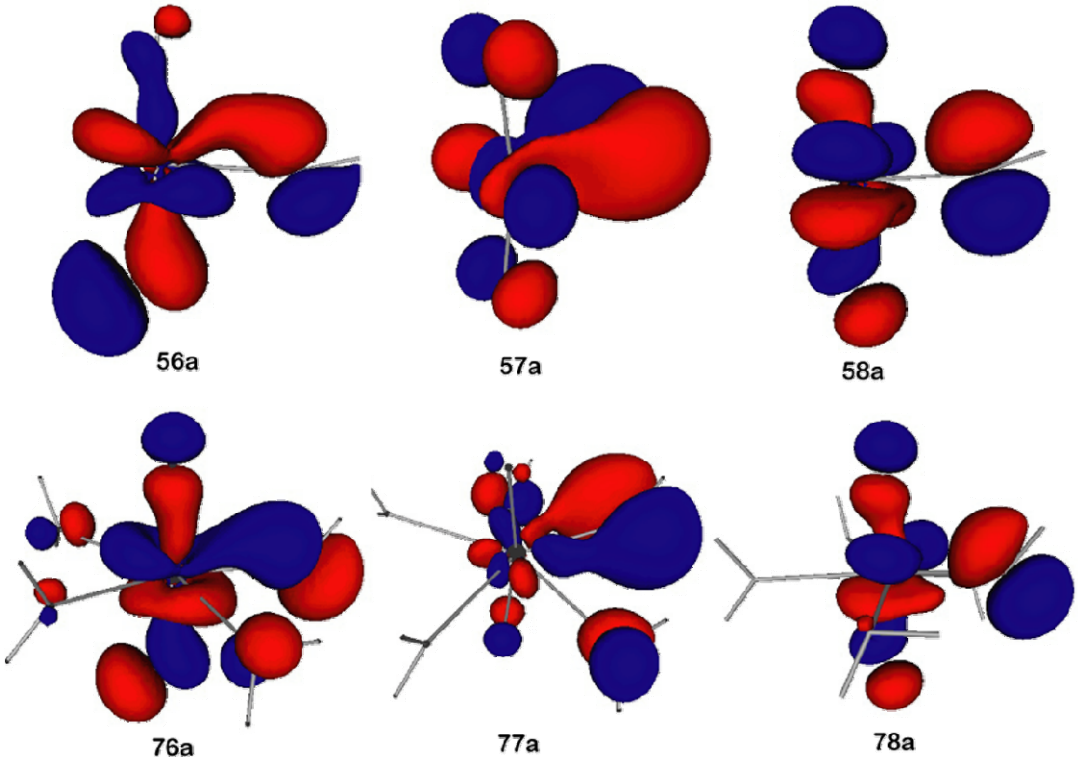

Figure 4.7. Sketches of those molecular orbitals involving the OH group that participate in the π-interaction of $[UO_2OH]^+$ (top row) and $[UO_2(H_2O)_4OH]^{1+}$ (bottom row) between U 5f-orbitals and 2p orbitals of the O_h center (in the equatorial plane).

related orbitals it is obvious that essentially U 5f contributes to the π-interaction with the OH group. Fig. 4.7 shows that pertinent MOs of the small model $[UO_2OH]^+$ and of isomer 4 of $[UO_2(H_2O)_4OH]^{1+}$ are rather similar, even though the latter comprises several aqua ligands. From this MO analysis, one is lead to conclude that the elongation of the terminal uranyl bond is caused by electrostatic interactions and the competition in π bonding between the hydroxide and the terminal oxygen centers.

4.1.3 Energetics

Table 4.4 compares energies (both electronic and Gibbs free energy) of the various isomers determined with different functionals. Energy differences relative to isomer 1 are given both for the gas phase and in solution. The discussion will begin with the energies calculated with the BP functional in single-point fashion using LDA structures (LDA/BP). Isomer 1 was taken as reference, as it the most stable isomer in almost all cases. However, the trend changed slightly in solution, where some isomers are as stable as isomer 1. The energy differences between isomer 1 and isomers 5 and 6 are negligible

Table 4.4. Relative energies of various isomers of $[UO_2(H_2O)_4OH]^{1+}$ with respect to isomer 1. Electronic energy ΔE_{abs} and Gibbs free energy ΔG_{abs} (in kJ mol^{-1}) from gas phase (GP) calculations and solvation models (PCM), determined with LDA, BP single-point on LDA geometries (LDA/BP), BP and PBEN exchange-correlation functionals.

	isomer	GP				PCM			
		LDA	LDA/BP	BP	PBEN	LDA	LDA/BP	BP	PBEN
ΔE_{abs}	2	-14	-10	-11	-11	-16	-4	-7	-5
	3	-21	-8	-10	-9	-11	-3	-6	-5
	4	-26	-10	-10	-10	-18	-7	-11	-10
	5	-20	-6	-9	-9	-12	-1	-6	-3
	6	-18	-15	-10	-10	-12	-1	-5	-4
	7	-26	-11	-13	-13	-15	-5	-9	-7
	avg	-21	-10	-11	-10	-14	-5	-7	-6
ΔG_{abs}	2	-18	-15	-12	-20	-20	-9	-9	-13
	3	-24	-12	-14	-24	-15	-6	-9	-19
	4	-24	-8	-14	-21	-16	-5	-15	-21
	5	-19	-5	-12	-19	-11	1	-9	-13
	6	-19	-15	-12	-17	-12	-1	-6	-11
	7	-22	-7	-16	-23	-11	-1	-11	-17
	avg	-21	-10	-13	-21	-14	-5	-10	-16

~1 kJ mol^{-1}, for both electronic and free energies. This could be an artifact of the approximations involved in the LDA/BP approach. To get more insight, electronic and Gibbs free energies were calculated also with GGA functionals. Isomer 1 was also found to be most stable, using either the BP or the PBEN functional. However, the trend in relative stability of the isomers does not remain the same with different functionals. This difference in Gibbs free energies in solution of four- to five-coordinate species amount to 6–21 kJ mol^{-1} for LDA and GGA functionals. On average, five-coordinated isomers are less stable than isomer 1, by 10–20 kJ mol^{-1} in the gas phase and by 10–15 kJ mol^{-1} in solution. Thus, these energy separations are well above a thermal energy and clearly show the stability of four-coordinated complex in solution.

The relative stability of four- and five-coordinated uranyl monohydroxide, can be examined by the following reaction which entails the binding energy of an aqua ligand:

$$[UO_2(H_2O)_4OH]^{1+} \rightarrow [UO_2(H_2O)_3OH]^{1+} + H_2O \qquad (4.1)$$

These ligand abstraction energies ΔE_{abs} corresponding to Eq. 4.1 are collected in Table 4.5. Inspection of the electronic energies shows that the abstraction of a single water ligand from $[UO_2(H_2O)_4OH]^{1+}$ is endothermic for all isomers. With entropy corrections, the reaction energy becomes exothermic for GGA functionals, due to the increase in

Table 4.5. Energy (electronic, ΔE_{abs}, and Gibbs free energy, ΔG_{abs}, in kJ mol^{-1}, in solution) for abstracting the first aqua ligand from various isomers of $[UO_2(H_2O)_4OH]^{1+}$ (Eq. 4.1), determined with LDA, BP single-point on LDA geometries (LDA/BP), BP, and PBEN exchange-correlation functionals. Gibbs free energy values with standard state are corrections presented in parenthesis.

isomer	LDA		LDA/BP		BP		PBEN	
	ΔE_{abs}	ΔG_{abs}	ΔE_{abs}	ΔG_{abs}	ΔE_{abs}	ΔG_{abs}	ΔE_{abs}	ΔG_{abs}
1	94	42(60)	34	-18 (0.4)	41	-5 (13)	31	-7 (11)
2	79	22(40)	30	-26 (-8)	34	-14 (4)	27	-21 (-3)
3	83	28(45)	32	-24 (-6)	36	-15 (3)	28	-26 (-8)
4	77	26(44)	27	-25 (-5)	31	-20 (-2)	23	-27(-10)
5	82	32(50)	33	-17 (1)	36	-14 (4)	29	-20 (-2)
6	82	30(48)	33	-18 (-1)	37	-11 (6)	29	-18 (0)
7	79	31(49)	29	-19 (-1)	33	-16 (1)	26	-24 (-6)

entropy on the right hand side of Eq. 4.1. However, in the local density approach, due to considerably overbinding, the entropy effect does not overcome the energy difference and ΔG_{abs} is still endothermic. For isomer 1, the exothermicity in ΔG_{abs} is large (-18 kJ mol^{-1}) for the LDA/BP approach and rather small at the BP and PBEN levels (~ -6 kJ mol^{-1}). ΔG_{abs} of isomer 1 corresponds to the Gibbs free energy of hydrogen bonding of one aqua ligand in the second solvent shell. The slight exothermicity of ΔG_{abs} for isomer 1 shows that water ligands in the second solvent shell are unstable and prefer to stay at "infinite" separation. This could be an artifact of the PCM model used, which does not occur in the gas phase (where ΔG_{abs} = 78 kJ mol^{-1}) or when standard state corrections are applied (Table 4.5). The stand state correction of about 18 kJ mol^{-1} improved ΔG_{abs} for isomer 1; an endothermicity of ~12 kJ mol^{-1} was obtained for GGA functionals. For penta-coordinated isomers, the resultant energies fluctuate more or less around zero and the energy difference among them is rather small, at most 10 kJ mol^{-1}. Overall, the less exothermic water abstraction energies demonstrate again the preference for four-coordinate species.

4.1.4 Free energy of hydrolysis

The hydrolysis constant was determined from the free energy of the hydrolysis reaction of a uranyl penta-aqua complex:

$$[UO_2(H_2O)_5]^{2+} + H_2O \rightarrow [UO_2(H_2O)_4OH]^{1+} + H_3O^+ \qquad (4.2)$$

Table 4.6. Gibbs free energy $\Delta G_{hyd,}$ of uranyl hydrolysis (Eq. 4.2), both in the gas phase (GP) and in solution (PCM) as well as the corresponding solvation energy (Solv.), given in kJ mol^{-1}. ΔG_{hyd}(PCM) correspond to a Boltzmann average according to the Gibbs free energies of the isomers in solution. Energies in parentheses correspond to isomer 1. Comparison to other theoretical studies is also provided.

		ΔG_{hyd}		
		GP	Solv.	PCM
Calc.	B3LYP[a]	-106	+105	-1.0
	B3LYP[b]	-122	+177	+55
	BLYP[c]			+40
	BP[c]			+27
	LDA/BP	-138	+175	+38 (37)
	BP	-176	+193	+18 (17)
	PBEN	-148	+164	+16 (16)
Exp.[d]				+30±1

[a)] Ref. 22, [b)] Ref. 45, [c)] Ref. 237 (CPMD), [d)] Ref. 81, 87, 105.

A recent review recommended the equilibrium constant log β* = -5.25±0.24 for reaction Eq. 4.2, [81,105] from which a free energy of ΔG^0 = 29.9±1.4 kJ mol^{-1} can be inferred at 298 K. A similar value, 30.8±1.4 kJ mol^{-1} was obtained in a recent variable-temperature study of uranyl hydrolysis.[87] The hydrolysis constant varies with ionic strength, solution medium as well as with temperature. The stability constant of dimeric species increases with increasing ionic strength. Thus, monomeric species are difficult to detect in experiment.[79]

Results of previous DF studies for the hydrolysis energy ΔG_{hyd} of $[UO_2(H_2O)_5]^{2+}$ shall be compared, before the results of this study are presented. Tsushima *et al*.[22] using a large-core pseudopotential approach with the B3LYP exchange-correlation functional and a PCM solvation model determined a free energy change of only -1 kJ mol^{-1}. Although Hay *et al*.[45] used a quite similar method, they determined the vastly different value of 55 kJ mol^{-1}; they overestimated somewhat the experimental hydrolysis energy of about +30±1 kJ mol^{-1}.[81,87,105] A possible reason for this difference might be the application of PCM in a single-point fashion using structures optimized for the gas phase. In Car-Parrinello molecular dynamics simulations[237] ΔG_{hyd} was determined from thermodynamic integration, yielding 40 kJ mol^{-1} at the BLYP level and 27 kJ mol^{-1} at the BP level.

The present calculations show good agreement with the experimental hydrolysis energy for all variants of GGA functionals applied. The Boltzmann average of

ΔG_{hyd}(PCM) over all the isomers of uranyl monohydroxide was determined at 38 kJ mol^{-1} with the LDA/BP approach; this value differs by 8 kJ mol^{-1} from the experimental result. With the more accurate approach where the BP or the PBEN functionals were self-consistently applied, the hydrolysis energy was determined to 18 and 16 kJ mol^{-1}, respectively, underestimating the experimental value by 12 kJ mol^{-1} and 14 kJ mol^{-1}, respectively (Table 4.6). The Boltzmann average in these two GGA calculations, BP or PBEN, exhibit a major contribution from the four-coordinated complex (isomer 1, > 85%); however, in the LDA/BP approach, the population is divided between isomer 1 (45%) and isomer 4 (51%), owing their similar free energy values (Table 4.6). When standard state corrections (10 kJ mol^{-1}) are applied to the Gibbs free energy, the agreement with experiment is very good for the LDA/BP approach, but not with any of the two GGA functionals.

If one describes in Eq. 4.2 the solvated proton by the species $H_5O_2^+$, the solvation energy of proton can be more accurately determined. The solvation energies of $H_5O_2^+$ and H_3O^+ are -1080 kJ mol^{-1} and -1037 kJ mol^{-1}, respectively. The former value compares favorably with experiment in aqueous solution, -1111 kJ mol^{-1}.[243] Using $H_5O_2^+$ as model solvated proton, the resulting ΔG_{hyd} value is -6 kJ mol^{-1} with the LDA/BP approach. Therefore, compared to the experimental free energy of hydrolysis, the model reaction with $H_5O_2^+$ underestimates ΔG_{hyd} considerably. The experimental values for the solvation energy of uranyl corresponds to the interval of -1329 to -1827 kJ mol^{-1},[244] and the energy determined in the present work corresponds to -1526 kJ mol^{-1}, which falls within that interval. In an earlier work using a very similar computational approach, a solvation energy of -1546 kJ mol^{-1} had been obtained.[49] The difference to the present result is due to the previous use of C_s symmetry constraints as well as a variant of the GEPOL algorithm (GEPOL 87) for constructing the solute cavity of the PCM model. The uncertainty for the solvation energy of uranyl is rather large compared to the deviation of the solvation energy of a proton, 74 kJ mol^{-1} for H_3O^+ and 31 kJ mol^{-1} for $H_5O_2^+$. Thus, error cancellation is favorable when H_3O^+ is used as solvated proton in Eq. 4.2 instead of $H_5O_2^+$. As is well known from previous studies,[245–247] the bulk solvent effect is quite important for uranyl ions. Solvent effects of the second coordination shell were neglected in this study because of their high computational cost and optimization problems. Thus, further study with additional aqua ligands in the second shell may be worthwhile to reach an improved model of the thermochemistry.

4.1.5 Conclusion

In this study, for the first time various isomers of $[UO_2(H_2O)_4OH]^{1+}$ in solution were examined. In contrast to previous studies, a four-coordinated species was found to be preferred. Six further isomers of uranyl monohydroxide, all of them five-coordinated, were also determined. These isomers differ with respect to the position and orientation of inter-ligand hydrogen bonds. Electronic as well as free energies were calculated for all isomers using various exchange-correlation functionals. The four-coordinated isomer was found to be the most stable structure among the seven isomers using gas phase and solution models, independent of the exchange-correlation functional applied. Nevertheless, the energy difference to five-coordinated isomers is small, only up to 20 kJ mol^{-1} for all exchange-correlation functionals studied. This was confirmed by the reaction free energy for subtracting one aqua ligand from $[UO_2(H_2O)_4OH]^{1+}$, which was endothermic for the four-coordinated isomer, but fluctuates around zero for penta-coordinated species. The formation energy of $[UO_2(H_2O)_4OH]^{1+}$ by hydrolysis of the uranyl penta-aqua complex was calculated and compared to results of other studies. The results of this thesis agree rather well with the experimental energy at the LDA/BP level; BP and PBEN results slightly underestimate the experimental value. Comparison of different models for the solvated proton in the hydrolysis equation shows that this agreement is mainly due to favorable cancellation of errors in the solvation free energies of the cations involved.

4.2 Uranyl complexation by carboxylate ligands

Carboxylic moieties are the dominating functional groups of humic substances. Their importance derives from the fact that carboxylic groups exhibit a strong propensity to complexate uranyl at low pH values (Section 2.2.2).[3,11] Modeling of humic and fulvic acids as a whole with accurate quantum mechanical methods is impossible due to their variable structure as well as size. Thus, complexation of uranyl by humic acid is commonly addressed via simple model systems.[133,162,248] Active sites of humic acids are modeled and characterized by various small carboxylic acids (aliphatic and aromatic), which represent corresponding groups of humic substances. The chemical environment of a carboxylic group will affect its chemical properties. Thus, different carboxylic acids were examined to account for the variability of active groups in humic and fulvic acids. The same approach has also been successfully applied for alcoholic groups.[59,121,125]

The focus of this chapter will be on uranyl complexation with various aromatic carboxylate ligands, as extension of an earlier study on aliphatic carboxylate ligands.[62,219] To investigate the variability of carboxylate groups of humic substances, the influence of structural and chemical variations of the carboxylic acids on uranyl complexation was analyzed first. For this purpose, the aromatic residues of the carboxylate ligand with various substituents in different positions were examined to analyze steric as well as electronic variations. The main interest lies on the structure and energetics of different carboxylate coordination modes (bidentate, monodentate, or chelate via an adjacent hydroxyl group) as well as on their differentiation. Additionally the stability constants of uranyl-carboxylate species will be discussed. In the introductory section 4.2.1, a previous investigation on uranyl-acetate complexes will be extended by a refined analysis of the coordination number by means of more accurate model suite.

4.2.1 Monoacetate complexes

Uranyl complexation with various aliphatic acids such as formate, acetate, and propionate was studied earlier.[62] Coordination of carboxylate groups to uranyl in bidentate, monodentate and pseudo-bridging fashion (monodentate coordination accompanied by a hydrogen bond between the free carboxylate oxygen and an aqua ligand of the uranyl) was discussed.[62] Structural and energetic aspects were addressed for penta-coordinated uranyl carboxylate species, $[UO_2(OOCR)(H_2O)_{3/4}]^+$ with R = H, CH_3, CH_3CH_2 because coordination number N = 5 is the most common one for uranyl complexes.[134,137]

Table 4.7. Calculated interatomic distances (in pm) and symmetric uranyl stretching frequency ν_{sym} (in cm^{-1}) of $[UO_2(OOCCH_3)(H_2O)_n]^+$ exhibiting bidentate (bi) and monodentate (mono) carboxylate coordination for different equatorial uranyl coordination numbers N (N = 5, 6). N= 5+1 denotes models with one aqua ligand in the second coordination shell (Fig 4.9 c, d).

Complex	*n*	N	U=O_t[a]	U-O_c	U-C	U-O_w[a]	U-O_{eq}	ν_{sym}
bi	3	5	178.7	237[a]	277	236	237	853
	4	5+1	179.1	238[a]	278	235	236	831
	4	6	178.7	240[a]	278	246	244	846
mono	4	5	178.9	229	335	238	236	822
	5	5+1	179.2	230	335	238	236	817
	5	6	179.0	236	339	246	245	838

[a] average values

Bidentate coordination was found to be preferred when thermodynamic corrections are accounted for.[62]

However, there were relative large discrepancies between calculated and experimental findings on uranyl monoacetate:[62] uranyl carboxylate U-O_c distances were calculated too short by about 10 pm for both mono- and bidentate complexes. Calculated U-C distances underestimate the experimental ones by 10–15 pm for bi- and monodentate coordination modes. On the other hand, uranyl bonds U=O_t as well as the average uranyl-aqua distance U-O_w agree well with experiment.[62] Yet, the averaged distance, U-O_{eq}, between U and ligand O atoms in the equatorial plane satisfactorily matches experiment only for monodentate complexes. For complexes, which are experimentally assigned as bidentate coordination, the calculations underestimate this quantity by ~5 pm. A detailed discussion of various possible reasons for these uncommonly large deviations between experiment and density functional calculations is given in Reference 62. Due to the uncertainty of 15–25%, in determining the coordination number N experimentally, the existence of six-coordinate complexes has been investigated as one possible reason. Although N = 5 was found to be preferred in various experimental[48,72] and theoretical studies;[45,46] a first coordination shell with 4 or 6 equatorial ligands has also been discussed in the literature.[48,133,248] Coordination numbers (five or six) of uranyl monoacetate $[UO_2(OOCCH_3)(H_2O)_n]^+$ were investigated without any symmetry constraints, considering both bidentate and pseudo bridging coordination modes.[62] The effect of an additional aqua ligand in the first coordination shell on the structure, vibrational frequencies and energies of uranyl(VI) monoacetate was discussed.[62] The

investigation of the relative stability of five- and six-coordinate complexes had been restricted to a comparison of energies only. In the following, this aspect will be extended two-fold: thermodynamic corrections are calculated to allow a more accurate examination of relative stabilities. Secondly, also a refined model is studied, where six-coordinate complexes are compared to five-coordinate ones with an additional aqua ligand in the second solvation shell.

As a main difference to the penta-coordinate species, the hexa-coordinated uranyl monoacetate complexes are stabilized by a hydrogen-bonding network between the equatorial ligands (Fig. 4.8). The axial uranyl distances are almost invariant to these changes (Table 4.7). Also, aqua ligands move significantly out of the equatorial plane to

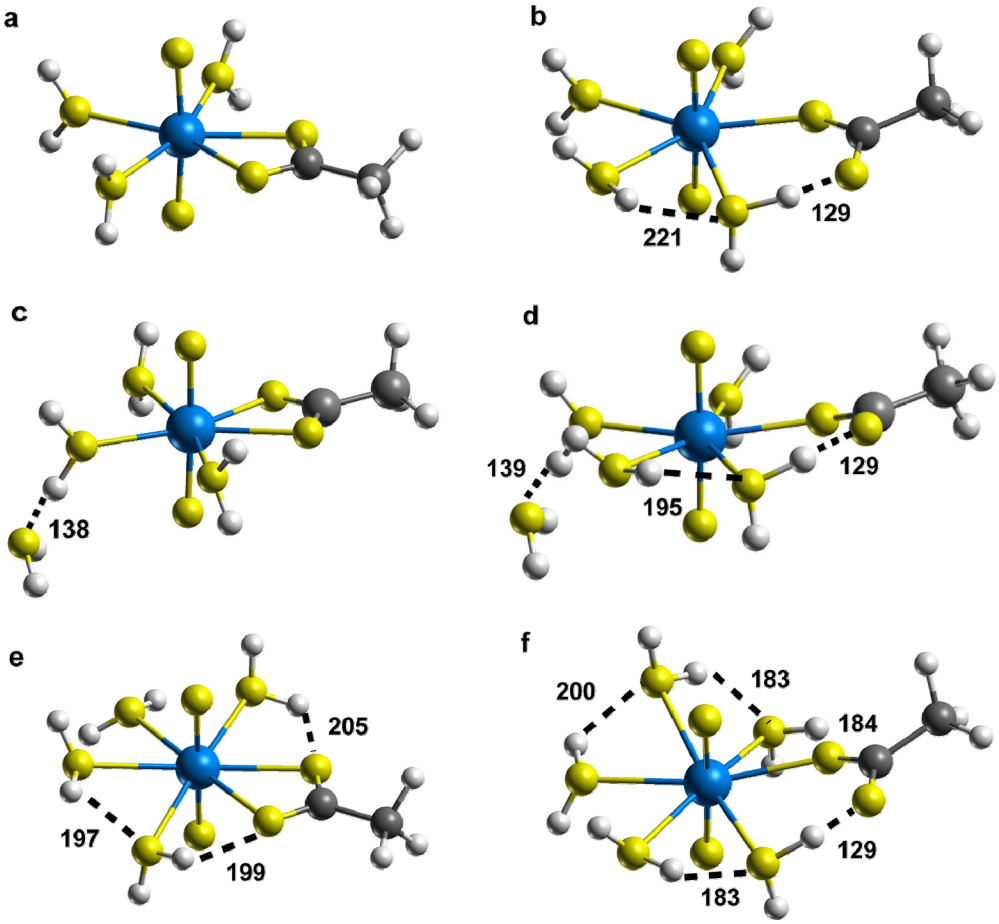

Figure 4.8. Optimized structures of uranyl monoacetate $[UO_2(OOCCH_3)(H_2O)_n]^+$ exhibiting bidentate and monodentate carboxylate coordination for different equatorial coordination numbers N = a+b, where a and b are the number of aqua ligands in the first and second coordination shell respectively (a) N = 5+0, bi (b) N = 5+0, mono (c) N = 5+1, bi (d) N = 5+1, mono (e) N = 6+0, bi (f) N = 6+0, mono. Also calculated O···H distances (in pm) of hydrogen bonds that are formed within the ligand sphere are shown.

Table 4.8. Binding energies ΔE and Gibbs free energies ΔG (in kJ mol^{-1}) of the addition of an aqua ligand to the penta-coordinate complexes $[UO_2(OOCCH_3)(H_2O)_n]^+$ in the first coordination sphere, (Eq. 4.3) and in the second solvent shell, (Eq. 4.4) and for the movement of an aqua ligand from the second to first coordination shell, (Eq. 4.5) for bidentate (bi, n = 3) and monodentate (mono, n = 4) coordination. The numbers in parenthesis correspond to Gibbs free energies including standard state corrections.

Eq.	Complex	ΔE		ΔG	
		GP	PCM	GP	PCM
4.3	bi	-66	-25	-4	36 (18)
	mono	-59	-9	-0.3	50 (32)
4.4	bi	-75	-38	-26	12 (-6)
	mono	-71	-34	-20	16 (-2)
4.5	bi	10	13	21	24 (24)
	mono	12	25	21	34 (34)

minimize the steric repulsion, resulting in significant elongations in U-O_w: 10 pm in bidentate and 8 pm in monodentate coordination (Table 4.7).

In order to discuss the energetic difference between coordination N = 5 and N = 6, the following equation was used:

$$[UO_2(OOCR)(H_2O)_n]^+ + H_2O \rightarrow [UO_2(OOCR)(H_2O)_{n+1}]^+ \quad (4.3)$$

In aqueous solution, the addition of one aqua ligand corresponding to Eq. (4.3) is calculated slightly exothermic both for bidentate (-25 kJ mol^{-1}) and monodentate (-9 kJ mol^{-1}) complexes (Table 4.8).[62] The bidentate hexa-coordinate complex $[UO_2(OOCCH_3)(H_2O)_4]^+$ is stabilized more than the monodentate complex $[UO_2(OOCCH_3)(H_2O)_5]^+$. This result can be rationalized by steric considerations. The angle of carboxylic oxygen with uranium and each of the two adjacent aqua ligands, O_c-U-O_w, are wider, on an average 72°, in the monodentate penta-coordinate complex than the O_c-U-O_c angle in the bidentate complex, 54°. Thus, in the bidentate complex there is more space for an additional aqua ligand.

At the level of free energies ΔG (when entropy effects are included), the exothermicity is significantly reduced in the gas phase ~60 kJ mol^{-1} (Table 4.8). The reaction becomes even endothermic in solution: ΔG = 18 kJ mol^{-1} for bidentate and 32 kJ mol^{-1} for monodentate coordination. Also Gibbs free energies suggest, that the higher coordination of N = 6 is somewhat more probable for complexes with bidentate carboxylate coordination. Based on these reaction free energies and taking into account

the accuracy of the present theoretical approach (about 10–20 kJ mol^{-1}), one would expect that hexagonal coordination is possible for the carboxylate complexes studied. However, applying a Boltzmann weighting to the calculated Gibbs free energies, only a relative population of about 10^{-4} results for the hexa- coordination. The calculated results are inline with the experimental determination of N= 5.0–5.4.[133,137,158]

Another comparison of five- and six-coordinate complexes relies on a five-coordinate species with an additional water molecule in the second coordination sphere (Fig. 4.8 c, d). It is not easy to include a complete second shell in the models, because of the high computational cost as well as optimization complications due to a large number of soft degrees of freedom. Therefore, models with a single water molecule in the second solvation sphere were studied. This additional water molecule was placed next to an aqua ligand in *anti* position to the carboxylate ligand (Fig. 4.8). In this model, the impact of the additional water molecule will be overestimated because of the localized character and the neglect of bond competition with further water molecules in the second shell. Effects on all characteristic distances are small, less than 1 pm, both for bidentate and monodentate complexes (Table 4.7). The axial uranyl distances are slightly affected by this addition of an aqua ligand in the second shell; they elongate by 0.4 pm for bidentate and by 0.2 pm for monodentate (Table 4.7). Concomitantly, the uranyl stretching frequencies are slightly lowered. U-O_c bond gets minimally elongated (1 pm) both for bidentate and monodentate complexes. Also, the U-O_{eq} distance is hardly affected. As expected, the U-O_w bond of the aqua ligand, which is coordinated by the second shell water, is noticeably shortened, by about 7 pm, compared to the penta- and hexa-coordinate models, while the adjacent U-O_w bonds are elongated by up to 2 pm. This shortening is attributed to a charge accumulation on the oxygen center of the aqua ligand, which forms a hydrogen bond with the second-shell water molecule. This hydrogen bond to the first coordination sphere is characterized by an O···H distance of about 139 pm and an O···H-O_w angle of about 177º (Fig. 4.8). A comparison with characteristic parameters of hydrogen bonds indicates a rather strong bond (typically 120–150 pm, 175–180º).[249] Effects of an additional aqua ligand in the second hydration shell are smaller than the effects of adding an aqua ligand in the first hydration shell. However, one expects that inclusion of a complete second shell in the model will lead to more pronounced effects on the local environment of uranyl.[247,250]

Due to the small structural changes in the complex $[UO_2(OOCR)(H_2O)_n]^+ \bullet H_2O$ compared to $[UO_2(OOCR)(H_2O)_n]^+$, the main deviations to the experimental data discussed above remain. The corresponding energy change ΔE according to the (formal) reaction

$$[UO_2(OOCR)(H_2O)_n]^+ + \ H_2O \ \rightarrow \ [UO_2(OOCR)(H_2O)_n]^+ \bullet H_2O \qquad (4.4)$$

amounts to -38 kJ mol^{-1} for the bidentate and -34 kJ mol^{-1} for the monodentate complex (Table 4.8). However, the corresponding free energies ΔG are slightly endothermic, 12 kJ mol^{-1} for the bidentate and 16 kJ mol^{-1} for the monodentate complex. When standard state corrections are applied, the change in the free energy is reduced by 18 kJ mol^{-1}, resulting in an essentially negligible binding of the second shell aqua ligand (Table 4.8).

To examine the relative stability of five- and six-coordinate complexes, yet another model reaction Eq. (4.5) can be used, where an aqua ligand from the second shell moves to the first coordination shell.

$$[UO_2(OOCR)(H_2O)_n]^+ \bullet H_2O \ \rightarrow \ [UO_2(OOCR)(H_2O)_{n+1}]^+ \qquad (4.5)$$

The corresponding energies and free energies are also shown in Table 4.8. Both electronic and free energies show that the hexa-coordinate species are slightly less stable than the penta-coordinate. This leads to instability of the additional water, in the first coordination shell than in the second shell. Bringing water from infinity to the second shell is an exothermic process (Eq. 4.4); on the other hand, it is rather energy consuming to introduce another water molecule into the first coordination shell, owing to the steric hindrance therein. Here, as observed before,[62] the trend that in bidentate coordination, the hexa-coordinate species is slightly more stable than in monodentate is noticed.

From the above discussion of different model approaches to inspect the stability of penta- and hexa-coordinated uranyl monocarboxylate species, further evidence is provided that five-coordination of uranyl monoacetate is more stable than six-coordination.

4.2.2 Complexes of aromatic carboxylic acids

Aromatic carboxylic acids are investigated as models of corresponding functional groups in humic acids. This study complements an earlier one on small aliphatic carboxylic acids.[62] The combined results of both studies give an overview over the variability of carboxylic groups in humic substances and as models of complexating sites of humic acids and will also be useful when one construct empirical complexation models of natural organic compounds.[251]

The focus of this section is on uranyl monocarboxylate complexes $[UO_2(OOCR)]^+$ with an aromatic residue R; such complexes are suggested at low pH (see Section 2.2.2). The structure and energies of monocarboxylate model complexes of uranyl for the ligands benzoate $C_6H_5COO^-$, p- and o-methyl benzoate $C_6H_4(CH_3)COO^-$, o-dimethyl benzoate

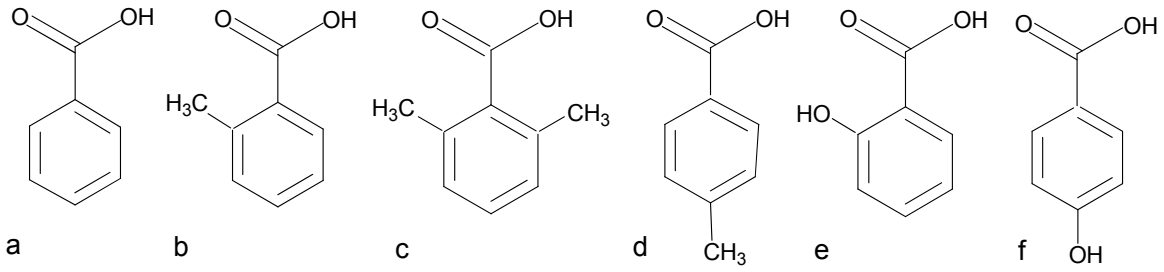

Figure 4.9. Schematic structures of various aromatic carboxylic acids studied: (a) benzoic acid, (b) o-methyl benzoic acid, (c) o-dimethyl benzoic acid, (d) p-methyl benzoic acid, (e) o-hydroxy benzoic (salicylic) acid, and (f) p-hydroxy benzoic acid.

$C_6H_3(CH_3)_2COO^-$, and p- and o-hydroxy benzoate $C_6H_4(OH)COO^-$ in solution are explored (Fig. 4.09). While all the ligands studied may act as mono- or bidentate ligands, o-hydroxy benzoic acid (salicylic acid) offers in addition the possibility of chelate coordination. Compared to acetic acid with a pK_a of 4.8 and the simple model of benzoic acid with a pK_a of 4.2, derivatives of benzoic acid exhibit pK_a values from 3.0 (o-hydroxy benzoic acid) to 4.6 (p-hydroxy benzoic acid).[128] In addition to the electronic substitutional effect, also steric effects may arise for substituents in ortho position. To examine that possibility, o-dimethyl benzoic acid was included in the models.

4.2.2.1 Acidity of aromatic carboxylic acids

Before going into the details of uranyl carboxylate complexes, the acidity of aromatic acids themselves is explored and compared with corresponding experimental results. This investigation is performed as accuracy check of the computational approach used and to support the interpretation of corresponding effects in uranyl monocarboxylate complexes. According to the Brønsted-Lowry definition, both UO_2^{2+} carboxylate complexes and carboxylic acids are compounds of acid type. In the carboxylate complex, the UO_2^{2+} ion acts as acceptor of the anion, while a proton accepts the anion in the formation of carboxylic acid. However, there is a considerable difference between the formation or dissociation of carboxylic acid and of the UO_2^{2+} complexes with the corresponding carboxylate anion, because in the latter case water molecules of the primary hydration shell of the UO_2^{2+} ion are displaced and substituted.

Substitution effects were examined for methyl, hydroxyl, and fluoro benzoic acid in ortho, meta, and para positions. The choice of this test set can be regarded as representative and was guided by the availability of experimental results. Only the low

energy conformers of each acid were considered.[252] Experimental ΔG values of deprotonation in solution were calculated from the pK_a values.[128] The isodesmic reaction

$$X\text{-}C_6H_4COOH + C_6H_5COO^- \Leftrightarrow X\text{-}C_6H_4COO^- + C_6H_5COOH \qquad (4.6)$$

was chosen to describe the differences of acidity of substituted acids X-C_6H_4COOH, X = CH_3, OH, F, with benzoic acid as a reference. Results are presented in Table 4.9.

In the gas phase, fluoro benzoic acids show a little stronger acidity compared to benzoic acid owing to the electron withdrawing nature of the F substituent. The rather high acidity of o-hydroxy benzoic acid is caused by a strong intermolecular hydrogen bond between hydroxyl and carboxyl groups in the anion. Meta and para isomers lack this effect, but an increased acidity of p-hydroxy benzoic acid occurs due to resonance stabilization of the corresponding anion.[253,254] For p-hydroxy benzoate, carboxylate and phenolate anions coexist in about equal amounts.[255] Correspondingly, when one calculates the average ΔG value of deprotonated carboxyl and hydroxyl groups, one obtains reasonable agreement with experiment. For o-hydroxy benzoate the situation is more complicated due to the existence of an internal hydrogen bond. Nevertheless, similar results were found for phenolate and carboxylate anions, with a slight preference of 0.2 kJ mol^{-1} for the phenolate isomer, which also was determined in another

Table 4.9. Gibbs free energies of the proton exchange reaction between substituted benzoic acids X-C_6H_4COOH and the benzoate anion, (Eq. 4.6), in kJ mol^{-1}. Results are given for the reaction in the gas phase (GP) and in aqueous solution (PCM). Energetics are based on the LDA/BP approach. The pK_a of benzoic acid is 4.18. Δ indicates differences of calculated and experimental free energy values.

	GP			PCM			
X	Exp.[a]	ΔG_{calc}	Diff	pK_a[b]	ΔG_{exp}[c]	ΔG_{calc}	Δ
o-F	-10	-7	3	3.27	-5	-3	2
m-F	-16	-18	2	3.87	-2	-8	-6
p-F	-12	-13	-1	4.14	0	-3	-3
o-OH	-56	-68[d]	-	2.98	-7	-35[d]	-
m-OH	-6	-7	-1	4.08	-1	-2	-2
p-OH	-17	-18[e]	-1	4.58	2	6	3
o-CH_3	-3	-3	0	3.91	-2	2	4
m-CH_3	3	-2	5	4.24	0	-4	-4
p-CH_3	5	1	4	4.34	1	-1	-2

[a] Ref. 257 [b] Ref. 128. [c] Calculated from pK_a. [d] Calculated value provided for the most stable isomer (phenolate). [e] Averaged over most stable isomers of carboxylate and phenolate anions, in line with experimental finding; Ref. 255.

computational study.[256] Since the distribution of isomers for o-hydroxy benzoate is not clear in experiment,[257] this species is excluded from the comparison in the following. The differences of experimental acidity values in the gas phase[257] among the various derivatives of benzoic acids are well reproduced in the calculations with an average deviation of 2 kJ mol^{-1} in the proton exchange Gibbs free energy (Table 4.9). In addition, the trends between different substituents are qualitatively recovered.

In solution, the variation of proton exchange energies between different substituted benzoic acids compared to benzoic acids is considerably smaller than in the gas phase (Table 4.9). For p-hydroxy benzoate deprotonation of the carboxyl group is favored.[255] For the o-hydroxyl substituent, a strong deviation from experiment is obtained, which may be due to the coexistence of several isomers. A similar difference has also been obtained by other computational methods.[258,259] Although the average absolute deviation of 4 kJ mol^{-1} between calculated and experimental data in solution is still acceptable, trends between different isomers are no more reproduced. As an example meta-fluoro and meta-methyl isomers can be mentioned, which are calculated to be slightly more acidic than their ortho and para congeners, at variance with the experimental trend. Similar deviations in relative acidities have been obtained before for chloro substituted benzoic acids[260] and most probable can be traced back to the application of a PCM model. In summary, one is lead to conclude that small differences in acidity of substituted benzoic acids are not well reproduced by a standard density functional approach including a PCM treatment of solvation effects. Thus, small differences below about 5 kJ mol^{-1} in complexation energies of uranyl with these ligands should be interpreted with due care.

4.2.2.2 C_s models

Model aspects

As a preparatory step, all uranyl monocarboxylate complexes are pre-optimized with C_s symmetry constraints, where the equatorial plane of uranyl was chosen as reflection plane. This procedure reduces the computational effort of the complete optimization (without symmetry) and allows a direct comparison to earlier calculations on aliphatic carboxylates.[62,219] Symmetric model complexes will also be helpful in some cases for reaching a deeper understanding of structure and relative stability of these complexes optimized without symmetry constraints. Before discussing the results of fully optimized uranyl monocarboxylates with various aromatic ligands in the next section, some basic structural aspects of the energetically more stable conformers will be considered here. Solvation effects of uranyl monobenzoate will also be characterized for the present

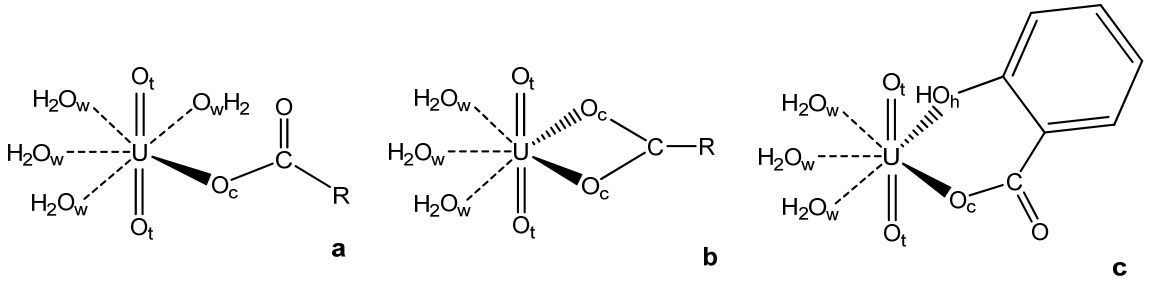

Figure 4.10. Possible coordination modes of carboxylate groups at uranyl: (a) monodentate (b) bidentate and (c) chelate coordination.

symmetric models.

For uranyl monocarboxylate, mono, bi- and chelate coordination (Fig. 4.10) of the carboxylic ligand are considered. In the monodentate and chelate systems, the equatorial uranyl plane, spanned by O centers of the carboxylate ligand (O_c) and the aqua ligands (O_w), was chosen as symmetry plane (Fig. 4.10 a, c). For the bidentate uranyl benzoate complex (Fig. 4.10 b), the equatorial plane as well as a plane perpendicular to it, which includes the uranyl moiety, were considered. In general, differences between the two bidentate models are small, i.e. distances differ at most by 2 pm, angles at most by 2°, and total energies at most by 10 kJ mol^{-1}. In the following, only results for the energetically more stable conformers, namely those with an equatorial mirror plane, will be discussed. Short-range solvent effects were accounted for by adding explicit aqua ligands (*n*) in the first hydration sphere, three for bidentate and chelate and four for monodentate

Table 4.10. Calculated structural parameters (LDA, distances in pm), symmetric uranyl stretching frequency ν_{sym} (in cm^{-1}) and ligand substitution energy (E_{sub} in kJ mol^{-1}), corresponding to Eq. (4.7) of bidentate (bi) and monodentate (mono) uranyl monobenzoate complexes (C_s models). Results from calculations on complexes in the gas phase (GP) and in solution (PCM) calculations as well as calculated solvation effects (ΔPCM = PCM-GP). For atom designations, see Fig 4.10.

Complex		$U=O_t$	$U-O_c$	U-C	$U-O_w$	$U-O_{eq}$	ν_{sym}	ΔE_{sub}
bi	GP	177.9	232	273	243	238	876	-835
	PCM	178.5	237	277	236	237	854	-83
	ΔPCM	0.6	4.5	3.7	-7	-1		
mono	GP	178.4	217	338	245	239	866	-849
	PCM	178.9	221	341	241	237	849	-81
	ΔPCM	0.5	4.3	3.4	-4	-2		

coordination (Fig. 4.10). In this way, the typical pentagonal coordination of uranyl moiety was achieved.

For bidentate coordination, complexes in C_s symmetry in the gas phase and in solution are examined, where the benzene ring was oriented parallel and perpendicular to the plane of the carboxylate group COO^- (Fig. 4.11), which in turn coincides with the equatorial plane of uranyl. Of the two orientations, the complex with the benzene ring in the equatorial plane is 35 kJ mol^{-1} more stable in the gas phase and 28 kJ mol^{-1} in aqueous solution, due to resonance stabilization of the benzoate moiety in the coplanar configuration. The structural differences between both orientations are rather small; distances differ by about 2 pm and angles up to 2º. Thus, for all species examined, parallel orientation of the benzene ring is chosen as starting structures for the optimizations.

Uranyl benzoate

Table 4.10 summarizes results for mono- and bidentate uranyl benzoate model complexes $[UO_2(OOCC_6H_5)(H_2O)_n]^+$, with n = 3 (bidentate) or 4 (monodentate), optimized in C_s symmetry in the gas phase and in solution. Geometric parameters indicate a stronger uranyl-carboxylate bond in the case of monodentate coordination. The bonds U-O_c between uranium and the oxygen center of the carboxylate are 16 pm shorter than in the bidentate complex. In the gas phase as well as in solution the uranyl bond U=O_t is slightly

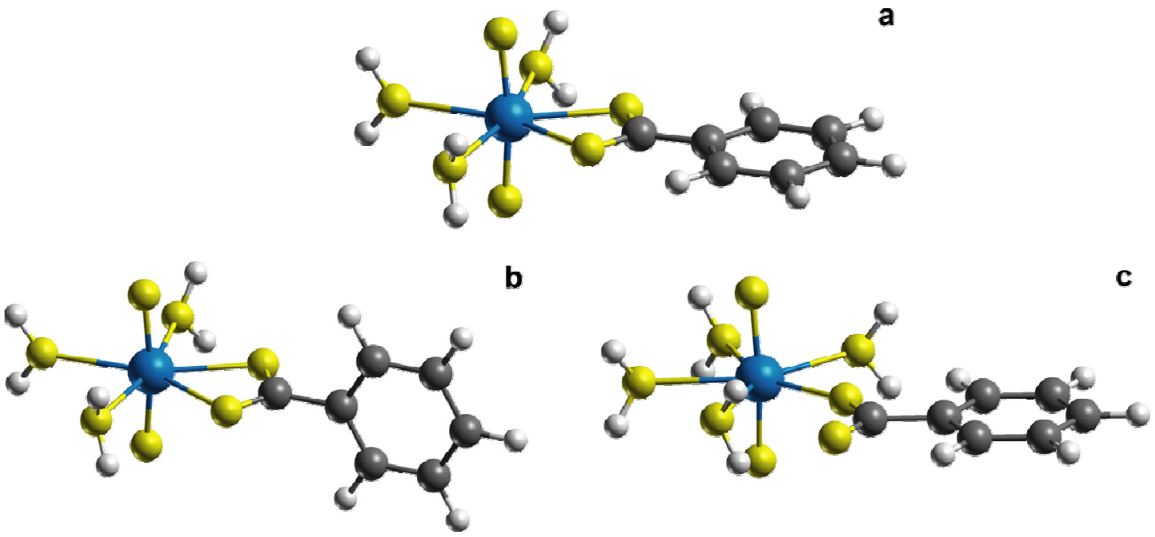

Figure 4.11. Optimized structures of uranyl monobenzoate complexes (C_s models) $[UO_2(OOCC_6H_5)(H_2O)_n]^+$. The carboxylate ligands are coordinated in bidentate and monodentate fashion to the uranyl ion: bidentate coordination (n=3) with parallel (a) and perpendicular (b) aromatic ring orientation and monodentate coordination (n=4) (c).

activated for monodentate coordination, i.e. it is by 0.5 pm longer; also, the vibrational frequencies ν_{sym} are marginally lower, by 10 cm^{-1} in the gas phase and 5 cm^{-1} in solution.

Long-range solvent effects slightly activate the uranyl and uranyl-carboxylate bonds; for both coordination modes, the distance $U{=}O_t$ increases by ~0.5 pm and the bond $U\text{-}O_c$ by 5 pm. This can be rationalized as screening of polar bonds due to the polarizable solvent environment.[219,261] The slight weakening of the uranyl bond is also reflected in a reduction of the symmetric uranyl stretching frequency, by 22 cm^{-1} in the bidentate and by 17 cm^{-1} in the monodentate complex (Table 4.10). In contrast to the other U-O bonds, uranium-water distances decrease significantly, by about 5 pm, due to the PCM treatment. The solvation induced changes in bond lengths result in an overall decrease of the average U-O bond length of uranyl to its ligands, $U\text{-}O_{eq}$, by 1–2 pm. Comparable effects of solvation for uranyl complexes were obtained also in other computational studies using a molecular shaped cavity.[220] With the approximation of a spherical shaped cavity, the trend of the metal-water distance in the first coordination shell goes in the opposite direction; however, the results with a molecular shaped cavity are in better agreement with discrete solvation models. [262]

To examine the competition between aqua and carboxylate ligands one invokes the formal substitution of aqua ligands of the solvated uranyl ion $[UO_2(H_2O)_5]^{2+}$ by a carboxylate ligand:

$$[UO_2(H_2O)_5]^{2+} + [RCOO]^- \rightarrow [UO_2(OOCR)(H_2O)_n]^+ + (5-n)\ H_2O \qquad (4.7)$$

The corresponding reaction energies ΔE_{sub} are also listed in Table 4.11. In the gas phase, the ligand substitution reaction, Eq. (4.7), slightly favors the monodentate complex (by 14

Table 4.11. Models with C_s symmetry of $[UO_2(OOCR)(H_2O)_n]^+$ (R = H, CH_3, and C_6H_5) for bidentate (bi, n = 3) and monodentate (mono, n = 4) coordination of carboxylate, calculated in solution (LDA): comparison of structural parameters (in pm), symmetric uranyl stretching frequency ν_{sym} (in cm^{-1}), and ligand substitution energy, Eq. (4.7) (LDA/BP, in kJ mol^{-1}).

Complex	R	$U{=}O_t$	$U\text{-}O_c$	U-C	$U\text{-}O_w$	$U\text{-}O_{eq}$	ν_{sym}	ΔE_{sub}
bi	H	178.3	239	277	236	237	860	-75
	CH_3	178.7	237	277	236	236	858	-97
	C_6H_5	178.5	237	277	236	237	854	-83
mono	H	178.8	222	340	242	238	850	-82
	CH_3	179.0	220	340	242	238	846	-96
	C_6H_5	178.9	221	341	241	237	849	-81

kJ mol^{-1}), but the complexes with mono- and bidentate coordination are essentially isoenergetic in solution. Thus, for symmetric models in solution both structures can be considered to be in equilibrium.

Comparison to aliphatic carboxylic acids

C_s symmetric models in solution had also been invoked in an earlier study of uranyl monocarboxylate complexes with formate, acetate, and propionate.[62,219] As acetate and propionate complexes are very similar,[62] the uranyl monobenzoate is compared to acetate and formate. In line with the pK_a values (formic acid 3.8, benzoic acid 4.2, acetic acid 4.8)[128] and the weaker inductive effect of the benzene ring in comparison to a methyl substituent, results for the benzoate complex tend to fall between those of acetate and formate complexes.

All characteristic bond lengths of uranyl-benzoate were calculated very similar to those of aliphatic species (Table 4.11). This similarity extends to substitution energies, which tend to be lowest for formate, higher for benzoate, and highest for acetate complexes (Table 4.11). Also the typical differences between mono- and bidentate complexes are the same as for acetate.[62,219] For benzoate coordinated in monodentate (~340 pm) the distance U-O_c is ~20 pm shorter than in bidentate fashion (~280 pm) and the distance U-C to the carbon center of the carboxylate group is considerably longer. As for aliphatic monocarboxylates, the average U-O_{eq} turned out to be essentially insensitive to the coordination mode.

Substituted benzoate: geometry

Next, the results of C_s symmetric models of various methyl and hydroxyl substituted benzoate ligands and the effect on benzoate complexation to uranyl will be discussed.

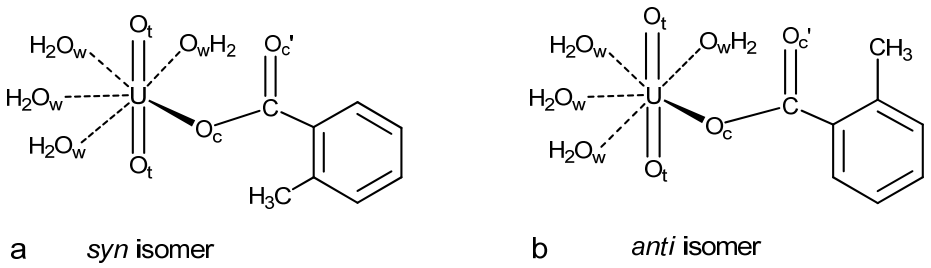

Figure 4.12. Schematic structure of uranyl methyl benzoate complexes $[UO_2(OOCC_6H_4CH_3)(H_2O)_4]^+$. For monodentate coordination mode both (a) *syn* and (b) *anti* conformers are shown.

Table 4.12. Calculated structural parameters (in pm) and symmetric uranyl stretching frequency ν_{sym} (in cm^{-1}) of $[UO_2(OOCR)(H_2O)_n]^+$ for R = C_6H_4X with X = H, CH_3, and OH or R= C_6H_3X with X= $(CH_3)_2$. Models with C_s symmetry exhibiting monodentate (mono, n = 4), bidentate (bi, n = 3) and chelate (chelate, n=3) carboxylate coordination in comparison with uranyl-benzoate. For the designations of the atoms, see Fig. 4.10.

Complex	RX	U=O_t[a]	U-O_c	U-C	U-O_w[a]	U-O_{eq}	ν_{sym}
mono	C_6H_5	178.9	221	341	241	237	849
syn	C_6H_4(o-CH_3)	178.9	222	340	242	238	851
anti	C_6H_4(o-CH_3)	179.0	219	342	242	237	843
	C_6H_4(o-$(CH_3)_2$)	179.0	223	341	241	237	850
	C_6H_4(p-CH_3)	179.0	221	341	241	237	847
syn	C_6H_4(o-OH)	178.5	227	345	240	237	855
anti	C_6H_4(o-OH)	178.6	224	341	241	237	856
	C_6H_4(p-OH)	179.0	220	340	242	237	851
bi	C_6H_5	178.5	237	277	236	237	854
	C_6H_4(o-CH_3)	178.6	237	277	237	237	853
	C_6H_4(o-$(CH_3)_2$)	178.7	236	278	237	237	852
	C_6H_4(p-CH_3)	178.5	236	276	236	236	867
	C_6H_4(o-OH)	178.3	239	279	236	237	874
	C_6H_4(p-OH)	178.6	236	276	237	237	846
chelate	C_6H_4(o-OH)	178.9	218, 246[b]	341	239	237	858

[a] average [b] U-O_H bond to hydroxyl group

Inspection of Table 4.12 shows that the geometries of uranyl monocarboxylate complexes with aromatic ligands are mainly determined by the complexation mode. The structure variations due to substitution are notably smaller. As for benzoate, complexes are optimized with mono- and bidentate coordination of the carboxylate ligand; for o-hydroxy benzoate, due to the OH group neighboring the carboxylate group, also chelate complexation is possible. For bidentate complexes, the uranyl bond U=O_t was calculated ~0.35 pm shorter than for the monodentate complexes, indicative of a slightly stronger ligand interaction in the latter complexes. The uranyl-ligand bond U-O_c exhibits a clear trend: in monodentate complexes, it is shorter (219–227 pm) than in bidentate complexes (236–239 pm) while it is shortest, 218 pm, in the chelate complex of salicylate. The latter complex also features a weak second bond to the β-OH group, 246 pm. In turn, in the chelate complex of salicylate, a relatively long U=O_t bond, 178.9 pm is calculated. This is taken as indication of a strong ligand bond, comparable to monodentate complexes.

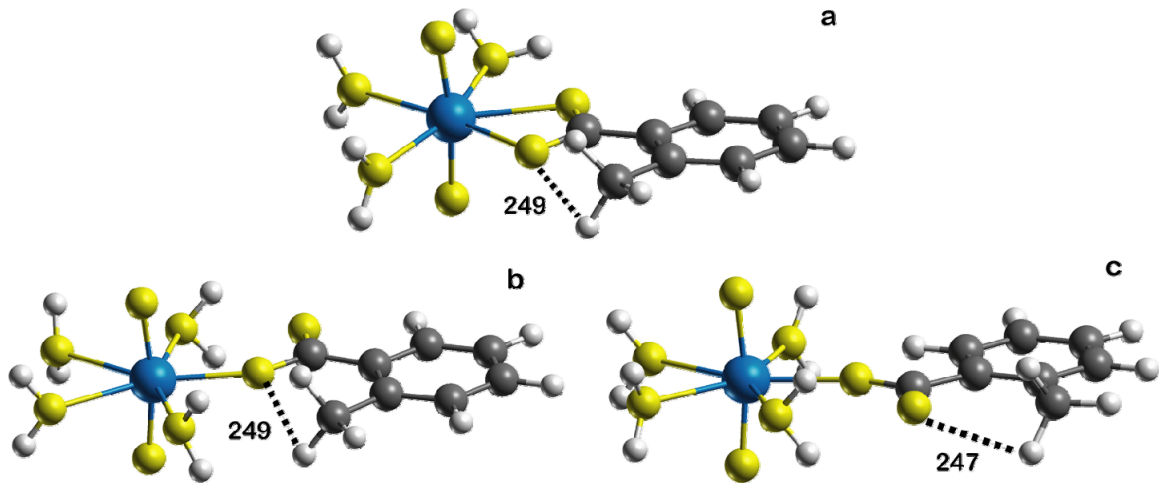

Figure 4.13. Optimized structures of monomethylated uranyl-benzoate $[UO_2(OOC C_6H_4CH_3)]^+$ in mono and bidentate coordination modes: (a) bidentate (b) *syn* and (c) *anti* isomers of monodentate complex. Also shown are calculated O···H distances (in pm) of hydrogen bonds that are formed within the ligand sphere.

Geometry of monodentate complexes

The substitution effects are examined for methyl groups in ortho and para positions of benzoate ligand. For the monodentate complex of ortho methyl and hydroxyl substituted benzoate, two possible substitution sites, the *syn* position with the methyl/hydroxyl group adjacent to the carboxylic oxygen bound to the uranyl moiety and the *anti* position with methyl/hydroxyl close to the unbound oxygen atom of the carboxylic group are examined (Fig. 4.12). Table 4.12 summarizes computational results on uranyl-methyl and hydroxyl benzoate complexes in different coordination modes. All measured geometry parameters remain almost unaltered (< 1 pm) with substitution except the U-O_c bond, which shows a variation up to ±3 pm for methyl and up to 7 pm for hydroxyl substituted complexes. The substitution effect is slightly larger in ortho than in para positions. The effect is more significant in hydroxyl than in methyl-substituted complexes due to the presence of internal hydrogen bonding in the salicylate ligand. The *anti* isomer of ortho-methyl benzoate shows a shorter U-O_c bond by 2 pm owing to the inductive effect of the methyl group. Alternatively, in the *syn* isomer steric effects between methyl and carboxyl groups weaken the bonding of the carboxyl moiety to the uranium center (Fig. 4.13). This counteracts the inductive effect and leads to a longer U-O_c bond (by 1 pm) than in the benzoate congener. Introduction of two methyl groups results in a longer U-O_c distance (by 2 pm) than in the complex with unsubstituted benzoate due to an enhanced crowding of the complexation site (Fig. 4.14).

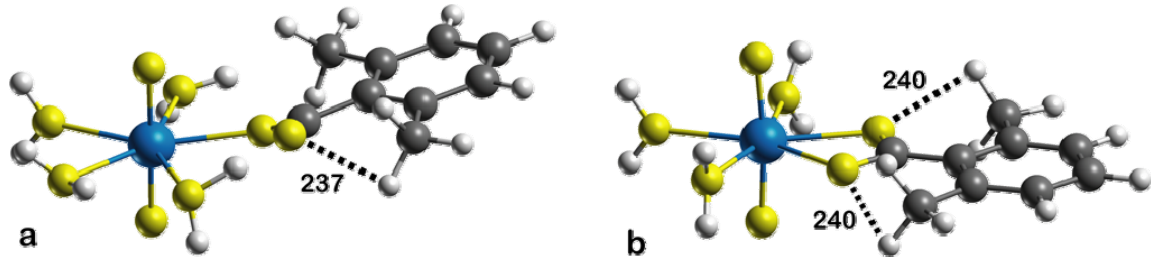

Figure 4.14. Optimized structures of dimethylated (a) mono- and (b) bidentate benzoate complexes $[UO_2(OOCC_6H_3(CH_3)_2)]^+$ with additional four and three aqua ligands, respectively, to reach penta-coordination. Also shown are O···H distances (in pm) of hydrogen bonds that are formed within the ligand sphere.

Two different orientations of methyl hydrogens with respect to carboxylic oxygen were examined for methyl-substituted complexes (Fig. 4.15). There is gain of 3 kJ mol^{-1} in substitution energies for complexes with two methyl hydrogens oriented towards O_c. In the complex with an o-hydroxy benzoate ligand, an internal hydrogen bond of length (O···H = 162 pm, Fig. 4.16) between the carboxylic oxygen O_c and the hydroxyl group leads to an elongated U-O_c bond for the *syn* isomer (by 6 pm). In the *anti* isomer, the hydrogen bond is shorter (O···H = 148 pm) and its effect on U-O_c is smaller (+3 pm), as there is no direct bond competition. Para isomers of methyl and hydroxyl substituted monodentate complexes display characteristics very similar to unsubstituted benzoate complexes.

Geometry of bidentate complexes

For bidentate benzoate complexes, no major changes are noticed in the measurable structural parameters with the exception of the salicylate ligand (Table 4.12). At variance with monodentate complexes, U-C and U-O_c vary only marginally (~1 pm). For the o-hydroxy benzoate ligand, the hydrogen bond between O_c and the hydroxyl group of 161

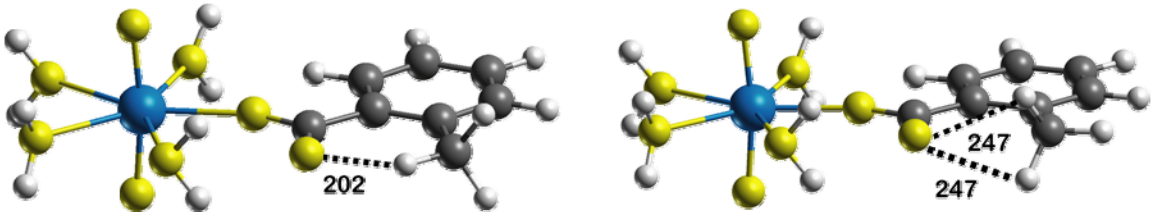

Figure 4.15. Optimized structures of *anti* isomer of monodentate uranyl methyl benzoate complexes $[UO_2(OOCC_6H_3(CH_3)_2)]^+$ with 1 hydrogen and 2 hydrogen atoms of methyl group oriented towards carboxyl group.

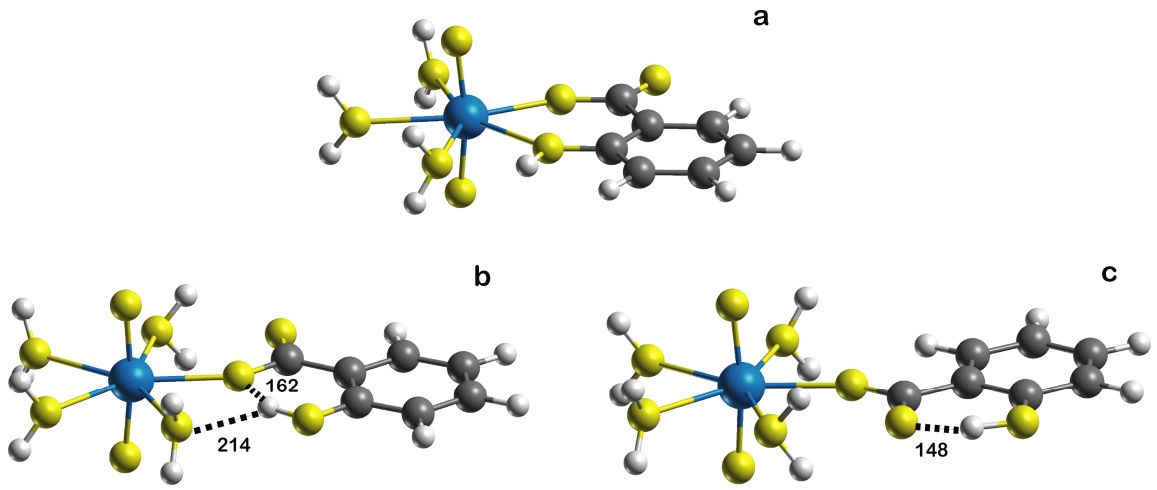

Figure 4.16. Optimized structures from PCM calculations of $[UO_2(OOCC_6H_4OH)]^+$ with different coordination modes of the salicylate ligand: (a) chelate complex (b) *syn* isomer and (c) *anti* isomer of monodentate complexes. Also shown are calculated O···H distances in pm of hydrogen bonds that are formed within the ligand sphere.

pm leads to an elongation of U-O_c by 2 pm, which in turn slightly tightens the terminal uranyl bond (0.3 pm). Terminal uranyl bonds are almost unchanged by substitution, in line with virtually constant symmetric stretching frequencies ν_{sym}. The only exception was the p-methyl benzoate complex, where a difference of 13 cm^{-1} in ν_{sym} compared to the unsubstituted benzoate complex is determined (Table 4.12), although terminal uranyl bonds U=O_t are the same in both complexes. Such a small difference is at the border of the estimated uncertainty of the normal mode calculations. The average uranyl-equatorial oxygen distance U-O_{eq} of about 237 pm is found to be indifferent to substitution effects and even to the coordination mode, as observed earlier for aliphatic uranyl monocarboxylates.[62]

Geometry of chelate complex

In addition to monodentate and bidentate coordination, also chelate coordination is considered for o-hydroxy benzoate ligand (Fig. 4.10 c). Deprotonation of the OH group will not be studied for the monocarboxylate complexes that are expected to be present at low pH; however, it might be relevant in chelate complexes at higher pH values.

In the chelate complex of o-hydroxy benzoate, the uranyl bond to the hydroxyl group U-O_h is much longer (246 pm) than other uranium-oxygen bonds in the first coordination shell. Concomitantly the carboxylic oxygen is shortened, to only 218 pm (Fig. 4.16), even shorter than the bonds U-O_c of the monodentate complexes (Table 4.12).

As a result, the average uranium-water distance elongates by 3 pm, with the equatorial uranium-oxygen distance U-O_{eq} invariant.

Substituted benzoate: energetic

The structural discussion will be completed with energetic aspects of uranyl monocarboxylate species. To examine the stability of the various complexes, first the fragmentation energy ΔE_{frag} of the complexes into uranyl, carboxylate, and aqua ligands is examined according to the equation:

$$[UO_2(OOCR)(H_2O)_n]^+ \rightarrow [UO_2]^{2+} + [RCOO]^- + n\,H_2O \qquad (4.8)$$

Trivially, all complexes are stable with respect to fragmentation both in the gas phase and in aqueous solution. Fragmentation energies in the gas phase are very large: ~1940–1960 kJ mol^{-1} for bidentate complexes and ~1945–1970 kJ mol^{-1} (Table 4.13) for

Table 4.13. Fragmentation energies ΔE_{frag} (Eq. 4.8) and ligand substitution energies ΔE_{sub} (Eq. 4.9) for C_s models (in kJ mol^{-1}) of complexes $[UO_2(OOCRX)(H_2O)_n]^+$ with R = C_6H_4 and C_6H_3 for X = H, CH_3, OH and $(CH_3)_2$ for bidentate (bi, n = 3), monodentate (mono, n = 4), and chelate coordination (chelate, n = 3). Results are given for systems in the gas phase (GP) and in solution (PCM), applying an LDA/BP approach.

		ΔE_{frag}		ΔE_{sub}	
Complex	RX	GP	PCM	GP	PCM
mono	C_6H_5	1954	602	-849	-81
syn	C_6H_4(o-CH_3)	1949	594	-844	-74
anti	C_6H_4(o-CH_3)	1962	604	-857	-84
	C_6H_4(o-$(CH_3)_2$)	1944	598	-839	-77
	C_6H_4(p-CH_3)	1962	603	-857	-84
syn	C_6H_4(o-OH)	1871	565	-766	-44
anti	C_6H_4(o-OH)	1888	576	-782	-56
	C_6H_4(p-OH)	1969	606	-864	-85
bi	C_6H_5	1941	603	-835	-83
	C_6H_4(o-CH_3)	1948	609	-843	-88
	C_6H_4(o-$(CH_3)_2$)	1945	615	-839	-96
	C_6H_4(p-CH_3)	1952	607	-846	-87
	C_6H_4(o-OH)	1862	568	-756	-48
	C_6H_4(p-OH)	1957	611	-852	-91
chelate	C_6H_4(o-OH)	1799	534	-692	-14
	CH_2OH	1869	585	-764	-64

the monodentate complexes owing to the unfavorable charge separation, (Eq. 4.8). An exception is the salicylate complex in all coordination modes: ΔE_{frag} is lower by about 70 kJ mol^{-1} for mono- and 50 kJ mol^{-1} for bidentate, compared to other complexes in the corresponding series. This energy is particularly low, only 1799 kJ mol^{-1}, for the chelate complex of salicylate. The internal hydrogen bonding in the salicylate anion stabilizes the ligand; thus, salicylate complexes feature the lowest ligand abstraction energies among the complexes studied.

In solution, the fragmentation energies drop to about one third of the GP values: ~570–615 kJ mol^{-1} for bi- and ~565–610 kJ mol^{-1} for monodentate complexes. This reduction can be rationalized by the large solvation energy of the small, charged uranyl moiety (-1245 kJ mol^{-1}) which stabilizes the fragmentation products. Solvation of the carboxylate ion (~-240 kJ mol^{-1}) contributes to a smaller extent. The rather weak preference of bidentate coordination obtained in the gas phase vanishes for the aromatic complexes if solvation is taken into account. The mono- and bidentate coordination modes of salicylate exhibit also similar fragmentation energies that differ only by ~5 kJ mol^{-1} (Table 4.13). Again, salicylate chelate coordination is found to be the least stable complex with a fragmentation energy of 534 kJ mol^{-1}.

The competition between aqua and carboxylate ligands is examined via the formal substitution of aqua ligands of the solvated uranyl ion $[UO_2(H_2O)_5]^{2+}$ by a carboxylate ligand:

$$[UO_2(H_2O)_5]^{2+} + [RCOO]^- \rightarrow [UO_2(OOCR)(H_2O)_n]^+ + (5-n)\ H_2O \qquad (4.9)$$

The corresponding reaction energies ΔE_{sub} are listed in Table 4.13. In the gas phase, substitution energies ΔE_{sub} are large (by absolute value), about -850 kJ mol^{-1} for monodentate complexes and about -840 kJ mol^{-1} for bidentate complexes. The salicylate complexes again yield somewhat reduced substitution energies, by ~80 kJ mol^{-1} for mono- and bidentate and 150 kJ mol^{-1} for the chelate coordination mode. Substitution is strongly exothermic because oppositely charged moieties are combined. In aqueous solution, the reactants are strongly stabilized. Hence, the reaction energies are significantly smaller, 74–94 kJ mol^{-1} for most mono- and bidentate benzoate complexes and about 50 kJ mol^{-1} for salicylate. This latter lower value is rationalized by a stabilizing hydrogen bond between carboxyl and hydrogen in the anion. Once again, the slight preference for monodentate coordination, calculated for the gas phase, vanishes in solution. Only a weak preference is calculated for bidentate complexes, less than 10 kJ mol^{-1}. The ligand substitution energy of the chelate complex of salicylate is significantly smaller, -12 kJ mol^{-1}, owing to the thermodynamic instability of the six-membered

chelate ring. This ring via a β-hydroxyl group yields a much weaker complex than the five-membered chelate ring of glycolate (Table 4.13, ΔE_{sub} = -64 kJ mol^{-1}). Recent studies on the complexation of dicarboxylic acids with lanthanide(III) ions also show six-rings to be less favorable than five-rings.[263]

The effects of substitution on ΔE_{sub} will now be discussed for the data in solution. Considering the monomethylated monodentate complexes, the substitution effect is noticeable in ortho position for the *syn* isomer (+7 kJ mol^{-1}, ΔE_{sub}); but the *anti* isomer shows a smaller variation (-3 kJ mol^{-1}). In line with these energies, in the *anti* isomer, the bond to the ligand is shorter by 3 pm (Table 4.12) than in the *syn* isomer. Also, the para isomer shows a slight increase of the substitution energy by 3 kJ mol^{-1} compared to the unsubstituted complex. The *anti* ortho and para isomers experience no steric hindrance; their slight increase in substitution energy is rationalized by the weak donating effect of the methyl group. This trend agrees with the assumed steric repulsion in the *syn* ortho isomer, as suggested already based on geometry results (see above).

The dimethylated complexes show different trends in substitution energy for mono and bidentate coordination. A decrease in ΔE_{sub} for monodentate (3 kJ mol^{-1}) and an increase for bidentate coordination by -11 kJ mol^{-1} compared to the unsubstituted uranyl-benzoate complexes are calculated. This trend is rationalized by the electron donating effect of two methyl groups in the bidentate complex, which is counteracted by the steric effects in the monodentate complex. This is in line with slightly larger distance, 240 pm, between methyl hydrogen and carboxyl oxygen in the bidentate complex compared to 237 pm in the monodentate complex. Para and ortho isomers of bidentate coordination as well as para and *anti* ortho monodentate complexes feature comparable substitution effects.

In comparison to methyl substituents, the hydroxyl group in ortho position to the carboxyl group displays a strong intermolecular hydrogen bond. As discussed earlier, this interaction significantly affects the complexation process. Thus, a large drop in substitution and fragmentation energy (~40 kJ mol^{-1}) is noticed for both mono- and bidentate salicylate complexes, which is in line with the elongated U-O_c bond (Table 4.12).

Overall, rather similar substitution energies were calculated for complexes with different carboxylate coordination modes (Table 4.13). Although the energy variation due to substitution effects are small compared to the estimated computational accuracy (see Section 4.2.2.1), they allow a consistent interpretation and thus can be regarded as qualitatively correct. This assumption will be further corroborated in Section 4.2.2.3 by results obtained without symmetry constraints. With the exception of salicylate, a very

weak preference for bidentate coordination was noticed for C_s symmetric models, which reflects the pure ligand binding without additional stabilization effects. Therefore, in aqueous solution, there is no clear energetic preference for any of the two coordination modes when solvation effects are taken into account. One should keep in mind that this conclusion was obtained by assuming pentagonal coordination of uranyl in all cases.

This analysis will be refined in the following chapter on the basis of structures that were obtained from unconstrained optimization. These latter approach allows a more flexible orientation of the ligand to form interligand contacts or to avoid steric strain.

4.2.2.3 C_1 models

Geometry

After discussing the basic properties of uranyl monobenzoate as well as the corresponding solvation and substitution effect on the complexation within the framework of simplified models, now various substituted benzoate ligands are examined on the basis of fully optimized five-coordinated uranyl monocarboxylate model complexes. Table 4.14 collects the corresponding results for geometry parameters and compares them to available experimental data for carboxylate and humate complexes of uranyl. The most important approximation of pre-optimized C_s models was the symmetry restriction which prevented the free orientation of ligands in the first coordination shell. Essential relaxation effects due to release of the C_s symmetry constraints are similar for all ligands

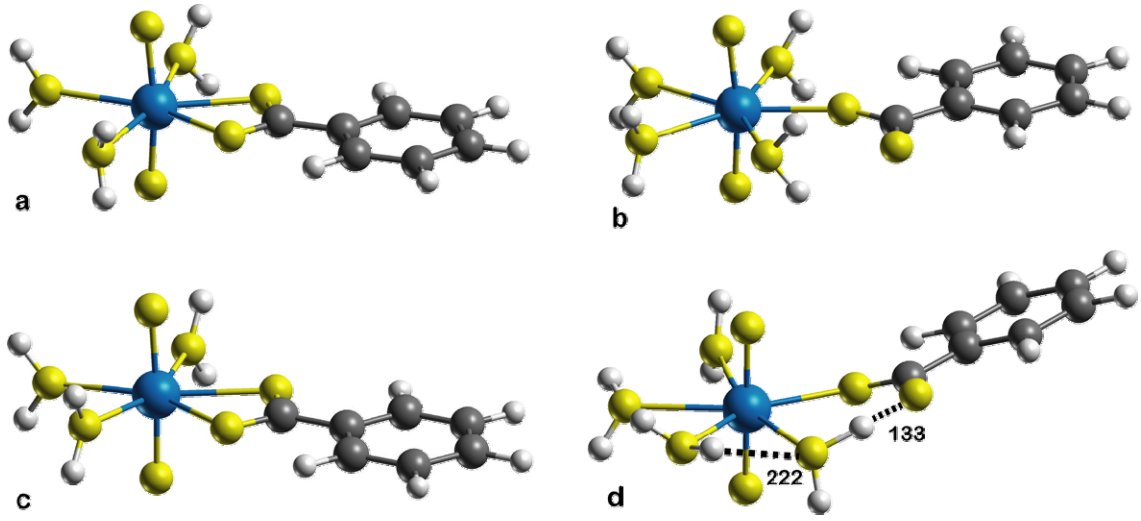

Figure 4.17. Optimized structure of uranyl monobenzoate complexes $[UO_2(OOCC_6H_5)(H_2O)_n]^+$ in solution: (a) bidentate and (b) monodentate modes in C_s symmetry as well as (c) bidentate and (d) pseudo-bridging modes without symmetry constraints (C_1).

examined and will be discussed for the example of benzoate (Tables 4.12 and 4.14). Notable changes were calculated for the uranyl complex with benzoate coordinated in monodentate fashion (Fig 4.17). The aqua ligand close to the non-coordinated carboxyl oxygen center turns to form a hydrogen bond with that oxygen center (O···H = 133 pm) and with an O_w-H-O_c angle of ~170°. Concomitantly the U-O_c bond is weakened as it elongates from 221 pm to 227 pm. Nevertheless, the distance U-C decreases from 341 to 331 pm because of the newly formed intermolecular hydrogen bond with the aqua ligand. Despite this strong rearrangement of the first ligand shell, also for the monodentate

Table 4.14. Calculated structural parameters (in pm, LDA, C_1 symmetry) of $[UO_2(OOCRX)(H_2O)_n]^+$ (R = C_6H_4 for X = H, CH_3, and OH; R= C_6H_3 for X= $(CH_3)_2$) exhibiting bidentate (bi, n = 3), monodentate (mono, n = 4), and chelate (chelate, n = 3) coordination of the carboxylate. Results for monodentate and bidentate acetate complexes (RX = CH_3) are given for comparison.

	RX	U=O_t	U-O_c	U-C	U-O_w	U-O_{eq}
mono	CH_3	178.9	228	333	238	236
	C_6H_5	178.8	227	331	239	237
syn	C_6H_4(o-CH_3)	178.9	230	334	238	236
anti	C_6H_4(o-CH_3)	179.0	226	335	239	237
	C_6H_3(o-$(CH_3)_2$)	178.9	229	334	238	237
	C_6H_4(p-CH_3)	178.8	229	329	239	237
syn	C_6H_4(o-OH)	178.6	232	338	238	237
anti	C_6H_4(o-OH)	178.8	227	338	239	236
	C_6H_4(p-OH)	178.9	227	334	239	237
bi	CH_3	178.6	237	277	237	237
	C_6H_5	178.5	237	277	236	237
	C_6H_4(o-CH_3)	178.7	236	277	237	237
	C_6H_3(o-$(CH_3)_2$)	178.8	236	277	237	237
	C_6H_4(p-CH_3)	178.6	237	276	237	237
	C_6H_4(o-OH)	178.3	237	277	237	237
	C_6H_4(p-OH)	178.7	237	277	237	237
chelate	C_6H_4(o-OH)	179.0	218, 246	341	240	237
Exp.[a]	C_6H_5[b]	177				242
	C_6H_5[c]	178		291		241
	C_6H_4(p-OH)[c]	177		288		243
	HA[d]	177-178(2)				238-240(2)

[a] EXAFS results of uranyl benzoate, p-hydroxy benzoate, humate (HA) in solution are provided for comparison. [b] Ref. 267 [c] Ref. 266 [d] Refs. 61,121,131

complex, the average U-O_{eq} remains unchanged at 237 pm, as in the bidentate complex. Also U=O_t is unaffected (changed by 0.1 pm). Analogous rearrangements as described above have previously been observed for uranyl monoacetate upon release of symmetry constraints.[62,219]

For monodentate complexes, the uranyl bond U=O_t was calculated ~0.25 pm longer than for bidentate complexes, indicating a slightly weaker ligand interaction in the latter complexes. The uranyl-ligand bond U-O_c exhibits again a clear trend: in monodentate complexes, it is shorter (226–232 pm) than in bidentate complexes (236–237 pm) while it is shortest, 218 pm, in the chelate complex of salicylate. U-C distances, which commonly are used in experiment to identify the complexation mode,[133,134] are calculated at ~340 pm in the chelate complex, 330–340 pm in monodentate complexes, and 277 pm in the bidentate complexes. Thus, as illustrated by the o-hydroxy benzoate complexes (Table 4.14), monodentate and chelate coordination may not always be distinguishable by means of U-C distances. Average bond lengths U-O_w to aqua ligands increase slightly when the interaction of uranyl with the carboxylate strengthens, as inferred from the discussion above. Distances, U-O_w were calculated more similar than in the C_s models, at 237 pm for bidentate and 238–239 pm for monodentate complexation as well as 240 pm for the chelate structure. Nevertheless, bonding competition ensures that the average bond distance U-O_{eq} to equatorial ligands remains at 237 pm, independent of the coordination mode (Table 4.14). All these findings strongly parallel the results of an earlier study on

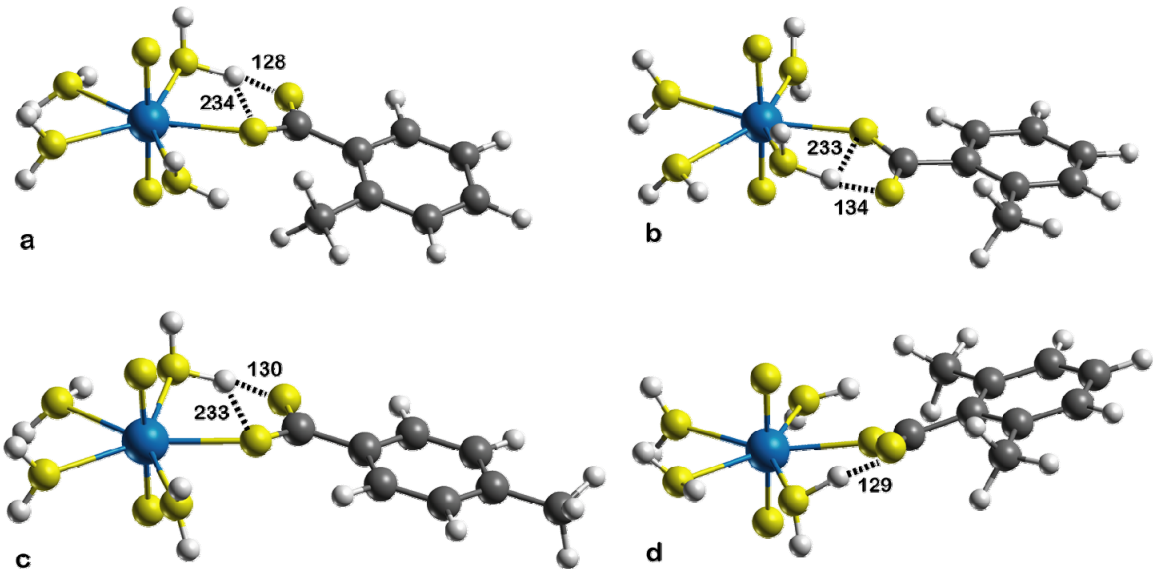

Figure 4.18. Optimized structures of monodentate complexes of uranyl monomethyl benzoate $[UO_2(OOCC_6H_4CH_3)]^+$ in solution – (a) *syn* and (b) *anti* isomers of the o-methyl complex, (c) the p-methyl complex – as well as (d) the o-dimethyl uranyl-benzoate complex $[UO_2(OOC_6H_3(CH_3)_2)]^+$.

monocarboxylate complexes with aliphatic ligands.[62,219] Note in particular that the insensitivity of U-O_{eq} to the coordination mode of the ligands, noted earlier,[62,219] is nicely corroborated by the present results.

For the different monodentate complexes, slight variations of the uranyl-carboxylate distances were calculated (Table 4.14). For para substituted aromatic acids, these are small, up to 2 pm for U-O_c and 3 pm for U-C. Somewhat larger effects were obtained for ortho substituted species. While U-O_c varies by up to 5 pm around the value of 227 pm for benzoate, the U-C distance is always longer for ortho substituted species. It amounts to 331 pm for benzoate and is largest for o-hydroxy benzoate, 338 pm. In the case of methyl substituents, this effect was already rationalized by a slight steric repulsion (Fig. 4.18). In the complex with salicylate, the uranyl-carboxyl bond is 5 pm longer in the *syn* isomer because of the hydrogen bond formed between the hydroxyl and the carboxyl groups (Fig. 4.19).

The structures of the two isomers of singly ortho substituted aromatic carboxylate complexes still feature notably differences. For methyl substituents in ortho position, the *syn* isomer shows a longer U-O_c bond (230 pm) due to steric repulsion between the methyl and the carboxyl groups. Also, the long bond of 232 pm calculated for the o-OH substituent with *syn* orientation due to the strong intermolecular hydrogen bond between the carboxyl oxygen center and the β-hydroxyl group remains (Fig. 4.19). The corresponding *anti* isomers yield relatively short U-O_c bonds, 226 pm for the o-CH_3 and 227 pm for the o-OH substituents. In the *anti* isomer with the o-OH substituent, the distance U-O_c is hardly elongated when the symmetry is relaxed (3 pm) as measured by

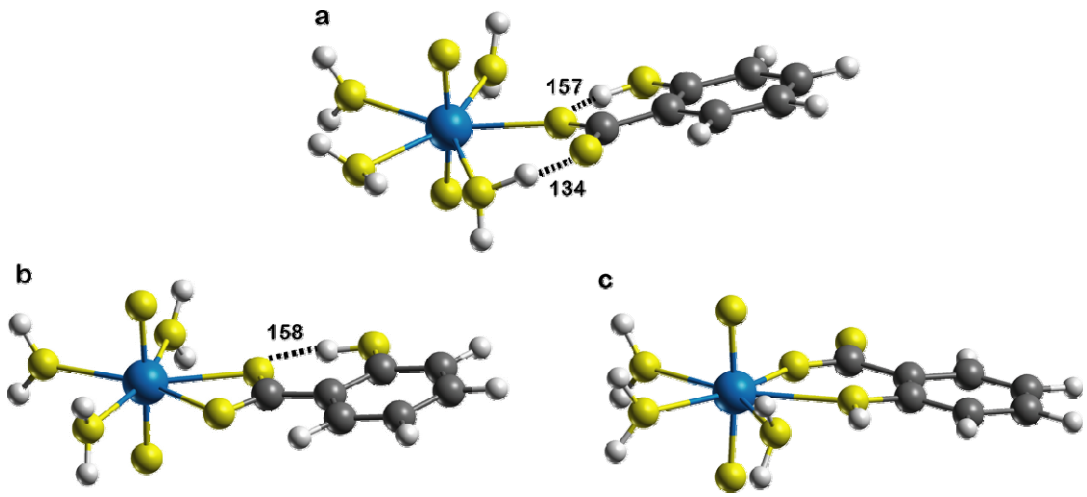

Figure 4.19. Optimized structures of uranyl-salicylate complexes in solution for various coordination modes: (a) *anti* monodentate isomer, (b) bidentate complex, and (c) chelate complex.

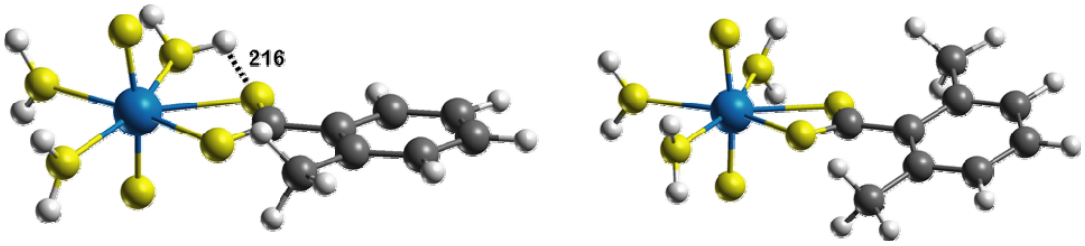

Figure 4.20. Optimized structures of bidentate uranyl mono- and dimethyl benzoate complexes in solution $[UO_2(OOCR)(H_2O)_3]^+$ (R = $C_6H_4CH_3$ and $C_6H_3(CH_3)_2$).

the relaxation of the other complexes studied (7 pm). This may be related to the longer, hence weaker hydrogen bond with the adjacent aqua ligand (237 pm), whereas this bond is somewhat shorter (233 pm) in other monodentate complexes.

The o-dimethyl substituted benzoate yields a monodentate uranyl complex with key structural parameters rather similar to those of the *syn* ortho methyl species. The distance U-O_c is 1 pm shorter, 229 pm, than in its monosubstituted congener while the U-C distances are equal, 334 pm. The angle between the carboxyl group and the benzene ring also reflects the fact that the small geometry variations calculated for ligands with ortho substituted OH and CH_3 group have different origin. In most complexes these two groups are essentially coplanar (the corresponding dihedral angles are less than 5°), but the steric repulsion mentioned earlier for C_s models, induces orientations of the benzene ring relative to the carboxyl group characterized with larger dihedral angles: 7° for the CH_3 substituted *anti* structure, 13° for its *syn* congener, and even 19° for the o-dimethyl substituted complex (Fig. 4.18). Yet, substituent effects on the geometry of monodentate complexes are rather small, beyond these hints for weaker uranyl-carboxylate bonds in complexes with *syn* substituted benzoates and o-dimethyl substituted ligands. The small elongation in U-O_c for the para methyl isomer is due to the internal hydrogen bond from an adjacent aqua ligand at (O···H = 233 pm) (Fig. 4.20). In these complexes, the distance U-C also changes accordingly, even though U-O_{eq} and U-O_w remain almost unaltered.

In the uranyl-benzoate with bidentate coordination, symmetry reduction has essentially no effect: characteristic structure parameters remain unaltered. The average changes of bond lengths for all complexes are ~1 pm. Unlike monodentate complexes, the orientation of ligands is almost unaltered upon symmetry relaxation, except in the ortho methyl complex (Fig. 4.18). In that case, the distance U-O_w is slightly shorter (~2 pm) than in the monodentate complexes, but the uranyl-carboxyl distance is longer by about 10 pm. These results are in line with those obtained for the uranyl-acetate (Table 4.14) complexes. Thus, the use of C_s models is well justified for bidentate coordination.

For bidentate coordinated complexes, substituent effects on geometry parameters are negligible for all species investigated and amount to changes of pertinent distances by at most 1 pm (Table 4.14). This may be interpreted as result of a compensation of effects where a stronger interaction due to the electron donating effect of methyl groups is counteracted by steric repulsion. This conclusion is again corroborated by variations of the dihedral angle between the carboxyl group and the benzene ring. That angle is zero for benzoate and increases with increasing ortho methylation. As a reaction to steric repulsion of the methyl groups with the carboxyl group, the benzene ring rotates relative to the carboxyl group, by 5° when the ligand is substituted by a methyl group in ortho position and by 19° in the case of two methyl substituents in ortho positions (Fig. 4.20). This feature also occurs in the dimethyl benzoate ligand where the carboxyl group is flipped by 60° from the planar structure. This structure motif has previously been discussed.[264,265] It leads to an increased acidity of dimethyl benzoic acid, pK_a = 3.21, compared to that of benzoic acid, pK_a = 4.18.[128]

Comparison to experiment

In Table 4.14 the results for complexes of uranyl with aromatic carboxylic acids are also compared to available structural data as determined by means of EXAFS.[266,267] In these experimental studies, the existence of monocarboxylate complexes of uranyl, as examined in this study is claimed. Nevertheless, the experimental results should be interpreted with due caution, as the measurements were carried out on probes where the complexes are in equilibrium with solvated uranyl and its hydrolysis products.[266,267] Also complexes with more than one carboxylate ligand may have been present in the samples, as indicated by the U-C coordination numbers of 2.2 ± 0.4 for benzoate and 3.0 ± 0.4 for p-hydroxy benzoate.[266] Based on U-C distances of about 290 pm, resolved for benzoate and p-hydroxy benzoate, a bidentate carboxylate coordination was assigned.[266] Also, based on crystal data as reference, the $U\text{-}O_{eq}$ value of ~242 pm for both monocarboxylate complexes was interpreted to indicate bidentate coordination.[266,267] For monodentate coordination, average equatorial ligand bonds $U\text{-}O_{eq}$ are expected to be ~5 pm shorter than for bidentate coordination.[131]

The present results for uranyl bonds $U{=}O_t$, 179 pm on average, of all aromatic carboxylates and coordination modes studied, agree well with measured results, 177–178 pm.[266,267] From this overestimation of the terminal uranyl bond, one expects an underestimation of the average distance, $U\text{-}O_{eq}$ of U-O bonds to equatorial ligands. Indeed, the EXAFS derived value, ~242 pm,[266,267] is ~5 pm longer than present

computational results (Table 4.14). Recall a similar discrepancy between calculated and EXAFS values in an earlier study of aliphatic monocarboxylates.[62,219] Just as in that preceding work where essentially the same computational strategy had been used, this study fails to obtain any difference between U-O_{eq} values of mono- and bidentate coordinated carboxylate ligands (Table 4.14). The discrepancy between measured and calculated U-O_{eq} values can be rationalized as a consequence of a change of coordination number of uranyl,[62,219]a trend that was also apparent in pertinent crystal structures.[140] The present results corroborate the earlier interpretation: U-O_{eq} values of ~237 pm is assigned as typical for five-fold coordination of uranyl and larger values of ~242 pm for six-coordinated uranyl. In consequence, the most commonly determined structure parameters of uranyl complexes, U=O_t and U-O_{eq}, are not sensitive to the coordination mode of the carboxylate ligand.

Rather, a determination of the coordination mode has to resort to U-C distances. The experimentally determined U-C distances of 291 pm for benzoate and 288 pm for p-hydroxy benzoate[266] are closer to the calculated value, 277 pm, calculated for bidentate complexes than to the values of 330–340 pm, calculated for monodentate ligand coordination. This qualitative agreement corroborates the assignment of aromatic monocarboxylate complexes as bidentate coordinated.[266]

Other experimental crystal data are available on oxonium tris(2-hydroxo benzoato)dioxouranate(VI) pentahydrate $[H_3O][UO_2(C_6H_4OHCOO)_3]\cdot 5H_2O$[268] where uranyl is six-fold coordinated. To ensure better comparison, hexa-coordinated UO_2^{2+} with three equatorial salicylate ligands was modeled in the gas phase. With this model, U-O_c and C-O_c bonds are slightly underestimated by 2 pm, and the terminal uranyl bond of 178.2 pm is in good agreement with experiment (177±16 pm). These small geometrical differences from experiment may well be interpreted as an effect of the crystal environment, where six water molecules per unit cell connect adjacent uranyl salicylate complexes.

Energetic

In order to predict the relative stability of monodentate and bidentate complexes, the substitution reaction was taken into account, where one or two water molecules of $[UO_2(H_2O)_5]^{2+}$ are replaced by a carboxyl ligand to form the complex $[UO_2(OOCR)(H_2O)_n]^{+}$. The competition between aqua and carboxyl ligands is quantified again via a formal substitution energy calculated according to Eq. 4.9 (Section 4.2.1). Substitution energies (in solution) corresponding to Eq. 4.9 for C_s and C_1 models are

compared in Table 4.15. All complexes are stable with respect to the formation of bi- and monodentate species by substituting aqua by carboxylate ligands, both in the gas phase and in aqueous solution.

While structural parameters of the complexes examined are rather uniform (Table 4.14), these energetic parameters exhibit notable variations. As noted earlier (Section 4.2.2.2), substitution energies $\Delta E_{sub}(C_s)$ of mono- and bidentate coordinated uranyl monocarboxylate complexes reveal both coordination modes to similarly stabile, with an average absolute difference of 6 kJ mol^{-1}. Without symmetry constraints, formation of monodentate complexes is favored on average by 27 kJ mol^{-1}; see the $\Delta E_{sub}(C_1)$ values in Table 4.15. This trend can be rationalized by strong internal H-bonding in monodentate complexes, which stabilizes the complex by ~40 kJ mol^{-1} in the gas phase and ~30 kJ mol^{-1} in solution. This "pseudo-bridging" conformation enhances ΔE_{sub} for all monodentate systems, irrespective of the position of the substituents. For bidentate complexes, the substitution energy is almost indifferent to a reduction of symmetry. The only exception is the complex with the o-dimethyl substituted benzoate ligand, where 19 kJ mol^{-1} are gained due to a rotation of the benzene ring with respect to the plane of the carboxyl group to avoid steric strain. A significant stabilization in ligand energy decrease ΔE_{sub} (by ~12 kJ mol^{-1}) for the monodentate complex compared to the relaxation energy ($C_s \rightarrow C_1$) calculated for other monodentate systems. In total, species with monodentate coordination species are clearly preferred in energy when optimized without symmetry constraints. The following discussion focuses on these latter structures.

The propensities for substitution of all aromatic carboxylates studied here are lower (substitution energies are less exothermic) than for the corresponding monoacetate complex: by more than 10 kJ mol^{-1} for monodentate and more than 5 kJ mol^{-1} for bidentate coordinated species (Table 4.15).

For most complexes, ligand substitution energies determined are close to the values of uranyl monobenzoate: -111 kJ mol^{-1} for monodentate and -83 kJ mol^{-1} for bidentate coordination. Slightly larger values are calculated (in absolute terms, up to 7 kJ mol^{-1}) for complexes with para substituted benzoate ligands, both for methyl and hydroxyl substitution, as well as with ortho methyl substituted ligands. In line with minor steric repulsion, less exothermic substitution energies were obtained for the o-dimethyl benzoate ligand: 95 kJ mol^{-1} for monodentate and 75 kJ mol^{-1} for bidentate coordination. Even lower ligand substitution energies resulted for the complex with the o-hydroxy benzoate ligand, ~80 kJ mol^{-1} for the monodentate isomers and 47 kJ mol^{-1} for the bidentate species. These complexation propensities are notably lower for two reasons.

The bonding competition with the uranyl carboxyl bond weakens the hydrogen bond between the OH substituent and the carboxyl group; also, the reference salicylate anion is particularly stabilized by the internal hydrogen bond. The structural variations calculated for *syn* and *anti* isomers of monodentate ortho substituted complexes go along with rather moderate variations in energy. In line with structural trends (see above), complexes with ligands in *anti* configuration yielded slightly higher (in absolute terms) substitution energies than *syn* isomers, by only 3 kJ mol^{-1} for methyl and 7 kJ mol^{-1} for hydroxyl substituents (Table 4.15). Surprisingly, a rather small energetic propensity for ligand substitution, only -12 kJ mol^{-1}, was calculated for the complex with salicylate in chelate

Table 4.15. Ligand substitution energies ΔE_{sub}, enthalpies $\Delta H_{sub}(C_1)$, and Gibbs free energies $\Delta G_{sub}(C_1)$ (Eq. 4.9) from models with C_s and C_1 symmetry (in kJ mol^{-1}) of uranyl monocarboxylate complexes $[UO_2(OOCRX)(H_2O)_n]^+$ (R = C_6H_4 for X = H, CH_3, and OH for bidentate (bi, n = 3) and chelate (chelate, n = 3) and R= C_6H_3 for X = $(CH_3)_2$) for monodentate (mono, n = 4)) coordination. Results for monodentate and bidentate acetate complexes (RX = CH_3) are given for comparison. The values $\Delta G_{sub}{}^{corr}$ refer to the standard state.

		E_{sub}				
	RX	$\Delta E_{sub}(C_s)$	$\Delta E_{sub}(C_1)$	$\Delta H_{sub}(C_1)$	$\Delta G_{sub}(C_1)$	$\Delta G_{sub}{}^{corr}$
mono	CH_3	-96	-127	-130	-117	-107
	C_6H_5	-81	-111	-114	-99	-89
syn	C_6H_4(o-CH_3)	-74	-112	-114	-96	-86
anti	C_6H_4(o-CH_3)	-84	-115	-120	-103	-93
	C_6H_4(o-$(CH_3)_2$)	-77	-95	-96	-77	-67
	C_6H_4(p-CH_3)	-84	-115	-118	-105	-95
syn	C_6H_4(o-OH)	-44	-74	-68	-52	-42
anti	C_6H_4(o-OH)	-56	-81	-80	-66	-56
	C_6H_4(p-OH)	-85	-118	-120	-103	-93
bi	CH_3	-97	-96	-102	-137	-109
	C_6H_5	-83	-83	-88	-125	-98
	C_6H_4(o-CH_3)	-88	-88	-93	-125	-98
	C_6H_4(o-$(CH_3)_2$)	-96	-75	-81	-116	-88
	C_6H_4(p-CH_3)	-87	-86	-91	-128	-100
	C_6H_4(o-OH)	-48	-47	-48	-89	-61
	C_6H_4(p-OH)	-91	-90	-98	-133	-105
chelate	C_6H_4(o-OH)	-14	-12	-12	-77	-49
	CH_2OH	-64	-64	-71	-110	-82

coordination. Thus, the corresponding six-ring structure of the salicylate ligand (Fig. 4.19) is energetically less favorable than mono- or bidentate coordination. The especially low value of ΔE_{sub} is rationalized by the loss of the hydrogen bond between the hydroxyl and the carboxyl group in the salicylate anion.

Unlike the methyl-substituted complexes, the bidentate complex of ortho hydroxy-benzoate (Fig 4.19 b) shows a strong electrostatic effect and the substitution energy is significantly reduced, by about ~40 kJ mol^{-1} (Table 4.15), compared to the unsubstituted benzoate complex. To understand the result more clearly, the salicylate ligand was modeled with one additional water molecule (Fig. 4.21), to examine the effect of an internal hydrogen bond of the salicylate ligand on complexation. This external water molecule is hydrogen bonded to the hydroxyl group at a distance of 149 pm, and oriented away from the complexation site. Its effect is quite prominent: the substitution energy increases by 53 kJ mol^{-1}. This confirms the concept of internal hydrogen bonding reducing the propensity for complexation.

Finally, the Gibbs free energies calculated for species in solution will be discussed. The complexation propensities, as described above changed when thermodynamic corrections are applied, which are 15 kJ mol^{-1} on average for monodentate complexes and -41 kJ mol^{-1} for bidentate complexes, thus clearly favoring bidentate coordination. In fact, bidentate coordination becomes preferred at the level of Gibbs free energies, by ~30 kJ mol^{-1} on average for all ligands inspected, largely due to entropy effects; this can be seen by comparing values of $\Delta G_{sub}(C_1)$ and $\Delta H_{sub}(C_1)$ in Table 4.15. In contrast, all monodentate complexes are slightly destabilized. These different effects can be rationalized by considering Eq. 4.9. The carboxylate ligand occupies two equatorial coordination sites of the uranyl ion in the case of bidentate coordination (n = 3); therefore, two aqua ligands are released in the substitution reaction. However, in monodentate complexes (n = 4) only one aqua ligand is split off. Thus, the number of reactants remains unchanged in the monodentate case, whereas the second aqua ligand, released in the bidentate case, leads to a favorable entropy contribution due to an increased disorder.

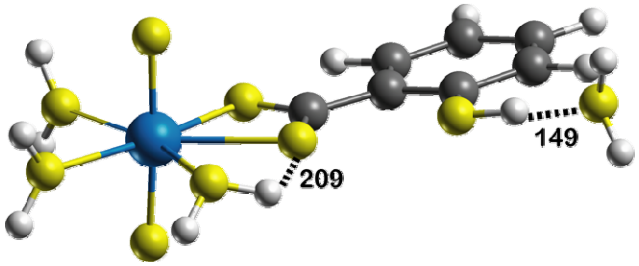

Figure 4.21. Optimized structures of bidentate uranyl-salicylate complex $[UO_2(OOCC_6H_4OH)(H_2O)_3.H_2O]^+$ with one additional water in the second shell.

Concomitantly, the preference for monodentate coordination is reduced. Additionally the correction terms corresponding to the conversion of standard states are considered for substitution energy. The trend of bidentate complexes being more stable than monodentate ones is partially cancelled after standard state corrections have been taken into account.

The thermodynamic corrections, which convert reaction energies into Gibbs free energies, are uniform. Therefore free energies $\Delta G_{sub}(C_1)$ of the ligand substitution reaction, Eq. 4.9, follow closely the trends of the $\Delta E_{sub}(C_1)$ values of various benzoate derivatives just discussed. As single exception, a rather strong entropy correction, -65 kJ mol^{-1}, for the salicylate chelate complex shall be mentioned; this complex is energetically least favorable among the species studied (Table 4.15). This rather strong, favorable entropy effect renders the free energy of ligand substitution to the chelate complex slightly more negative, up to -77 kJ mol^{-1}, than the reaction free energy to the isomers with a monodentate salicylate ligand, -52 and -66 kJ mol^{-1}.

Finally, a cautionary remark. The complexes under scrutiny and also the reference aqua complex exhibit relatively flexible structures due to the complex nature of the ligand sphere. They may have also energetically close lying isomers. Therefore, one has to consider the presented free energies of the ligand substitution as estimates. Potentially more accurate free energies from *ab initio* molecular dynamics, especially including more explicit solvent molecules, would not only be rather costly, but also not trivial to obtain under the circumstances.

4.2.2.4 Stability constants

A stability constant is an equilibrium constant that measures the stability of a complex with respect to its decomposition. It is directly related to the ΔG value of the corresponding complexation reaction (Eq. 2.3, Section 2.1.2). In recent years, this information on the interaction of uranium(VI) with carboxylate ligands has become available from experimental investigations.[65,83] In the following, stability constants of uranyl-carboxylate complexation in solution from computed ΔG values will be discussed, using the same two sets of reactions as already introduced (Section 2.1.2):

$$UO_2^{2+} + RCOO^- \rightarrow [UO_2OOCR]^+ \quad (4.10)$$

$$UO_2^{2+} + RCOOH \rightarrow [UO_2OOCR]^+ + H^+ \quad (4.11)$$

Eq. 4.10 describes the complexation of a carboxylate anion with uranyl, the corresponding complexation constant is β. Complexation constant β^* of Eq. 4.11 includes

the dissociation of carboxylic acid in the complexation process. Both types of constants, β and β*, are related by the dissociation constant (pK_a) of the corresponding carboxylic acid. In the literature exists some uncertainty regarding the use of β and β*. Several studies[269–271] describe the complexation process by Eq. 4.11, but use the notation β. Alternatively many experimental studies[133,248,272] describe the complexation process via Eq. 4.10; they arrive at quite similar values.

Several uncertainties exist when stability constants are determined experimentally. Stability constants are known to vary with the ionic strength.[269] Additionally the aqueous chemistry of UO_2^{2+} complexes is complicated; many side reactions such as hydrolysis affect the complexation already at low pH and lead to complicated equilibria. Stability constants are usually determined in a semi-empirical fashion, where one assumes a set of model reactions to be in equilibrium and extrapolates log β at infinite dilution.[269] As the complexation modes of the species normally are not known, comparison to calculated data for species with definite structure is not easy.

Stability constants are rather difficult to determine computationally in an accurate fashion. One unit in log β or log β* corresponds to only 5 kJ mol^{-1} in ΔG (Eq. 4.10, 4.11). Thus, the calculated stability constants may show a large error bar of 1 to 2 logarithmic units. In the present work, stability constants for uranyl-carboxylate complexation were determined by considering the penta-coordinated uranyl-aqua complex $[UO_2(H_2O)_5]^{2+}$ and resorting to model reactions Eq. 4.12 and 4.13.

$$[UO_2(H_2O)_5]^{2+} + RCOO^- \rightarrow [UO_2(OOCR)(H_2O)_n]^+ + (5–n)\ H_2O \quad (4.12)$$

$$[UO_2(H_2O)_5]^{2+} + RCOOH \rightarrow [UO_2(OOCR)(H_2O)_n]^+ + (3\text{-}n)\ H_2O + H_5O_2^+ \quad (4.13)$$

In Eq. 4.13, the solvated proton is described as the "Zundel ion" $H_5O_2^+$ which is one of the major structures of a hydrated proton along with the "Eigen ion" $H_9O_4^+$.[273,274] $H_5O_2^+$ is chosen as model to describe solvated proton, as discussed in previous Section 4.1.4, solvation energies of proton can be better described by $H_5O_2^+$ than H_3O^+. Since the solvation energy of anions is not easily determined accurately by means of PCM models,[221,223] it is expected that calculated values of β* are more reliable than results for β, because the reaction equation underlying the definition of β* does not contain an anion.

The stability constant of the uranyl-monoacetate complex will be discussed as reference with respect to the free energy values corresponding to Eqs. 4.12 and 4.13. log β* was calculated as 2.5 for bidentate and 2.6 for monodentate uranyl monoacetate. These values agree very well with the experimental result 2.86 at infinite dilution.[155] At different ionic strengths, log β* was determined to vary from 2.32 to 2.86 by potentiometry titration.[155] Comparison to bidentate coordination of uranyl monoacetate complex seems appropriate, as many studies show this coordination mode to be preferred.[133,136,215,275] This very good agreement of calculated and experimental stability constants has to be regarded as somewhat fortuitous.

Table 4.16. Reaction Gibbs free energies ΔG (Eq. 4.12) and ΔG* (Eq. 4.13) (including standard state corrections, in kJ mol^{-1}) for a series of monodentate (mono) and bidentate (bi) uranyl-carboxylate complexes $[UO_2(OOCRX)(H_2O)_n]^+$ ((RX = H and CH_3; R = C_6H_4 for X = H, CH_3, and OH; R= C_6H_3 for X= $(CH_3)_2$) and the corresponding stability constants log β and log β*, respectively. Experimental values for uranyl complexes with acetate, benzoate and humate are also provided.

Complex	R	ΔG	log β	ΔG^*	log β^*
mono	H	-101	17	-20	3.54
	CH_3	-110	19	-15	2.63
	C_6H_5	-98	17	-10	1.81
	C_6H_4(o-CH_3)	-93	16	-11	1.90
	C_6H_4(p-CH_3)	-96	17	-16	2.88
	C_6H_4(o-OH)	-56	10	-11	1.94
	C_6H_4(p-OH)	-93	16	-10	1.77
bi	H	-79	14	1.5	-0.26
	CH_3	-109	19	-15	2.54
	C_6H_5	-98	17	-19	3.37
	C_6H_4(o-CH_3)	-98	17	-15	2.70
	C_6H_4(p-CH_3)	-100	17	-21	3.69
	C_6H_4(o-OH)	-61	11	-27	4.64
	C_6H_4(p-OH)	-105	18	-19	3.41
Exp.	CH_3			-16	2.9[a]
	C_6H_5			-17, -14	2.9[b], 2.4[c]
	Humic acid				2.5–4.0,[d]
					5.5–7.8,[e]
					6.08±0.21,[f]
					6.41±0.70[g]

[a] Ref. 155 [b] Ref. 277 and [c] Ref. 278 (at infinite dilution)
[d] Refs. 278, 279, 280, 281 for 1:1 stoichiometry of uranyl-humate [e] Refs. 277, 278, 279, 280, 283 for1:2 stoichiometry of uranyl-humate
[f] Ref. 145, 284; charge neutralization model

According to Eq. 4.12, the corresponding values of log β are determined at 24 for the bidentate complex and at 21 for the monodentate complex. With standard state corrections taken into account for Eq. 4.12, log β decreases to 19 for both mono- and bidentate complexes (Table 4.16). The correction term is larger for the bidentate complex, due to the removal of one extra water ligand. The difference between log β and log β* should to be the pK_a of acetic acid, *i.e* 4.76.[128] However, a large difference of 16 units was obtained. This large difference mainly is caused by an inaccurate value of the solvation energy of the acetate anion, Eq. 4.12. Compared to the experimental solvation energy of the acetate anion, -323 kJ mol^{-1},[276] the present calculation using van der Waals radii underestimates that energy considerably, -273 kJ mol^{-1}. With a solute cavity constructed on the basis of van der Waals radii, a polarizable continuum model tends to provide rather inaccurate solvation energies for anions.[221,223] Empirical radii according to the UA0 scheme[215] for acetate yielded improved results:[215] the difference between log β and log β* decreased by 5 units and log β was calculated at 14 for both bi- and monodentate complexes. If one invokes the experimental solvation energy of acetate, one reaches even better agreement; log β is reduced to 10 and the difference between log β and log β* decreases to 7. The latter value agrees with the pK_a of acetic acid, 4.8, within the computational uncertainties. This discussion shows that most of the deviations of log β from experiment is related to improper modeling of the anion in Eq. 4.12.

The stability constants log β* of uranyl monobenzoate were calculated at 3.4 for the bidentate and at 1.8 for the monodentate complexes. These values agree fairly with the experimental results of 2.92±0.14[277] and 2.37±0.08.[278] The calculated values of log β* for uranyl formate are 3.54 for the mono- and -0.26 for the bidentate complex (Table 4.16). The experimental value log β* = 1.8 (not at infinite dilution)[65] corresponds to the formation of uranyl-diformate. Hence, the difference of 2.1 logarithmic units from experiment in part reflects the different stoichiometry of complexation. For the uranyl-monosalicylate complex log β* = 1.43 has been measured[262] for a ligand with a protonated hydroxyl group whereas the calculations yielded 1.94 and 4.64 for mono- and bidentate complexes, respectively. For p-methyl benzoate, the value log β* = 3.7 calculated for the bidentate complex agrees rather well with the experiment[278] which gave log β* = 2.71±0.04 at 0.1m/L for p-methyl benzoate ligand. As quoted above for acetate, the change in log β* is small when extrapolated to zero ionic strength.[155] This is in perfect agreement with the calculated value log β* = 2.9 for the monodentate p-methyl species. Nevertheless, differences between mono- and bidentate complexes are in the range of typical deviations from experiment. Thus, a decision on the complexation mode by means of complexation constants would demand calculations on more accurate solvation models.

Comparison of all species calculated reveals that differences from experiment are in the range of computational uncertainty, but trends among various species are reasonably well reproduced. Therefore, computational results even at the level given here provide a valuable guideline.

4.2.2.5 Implications for uranyl complexation by humic acids

Finally, the model results discussed thus far are to be compared to experimental findings on the interaction of the uranyl dication with humic substances. Such complexes with humic acids are commonly interpreted as a result of coordinated carboxylate groups.[3,2,11,12] EXAFS investigations of uranyl humate complexes determined U=O_t bond lengths at 177–178 pm and U-O_{eq} values at 237–240 pm (Table 4.14).[121,131,132] Just as in the case of uranyl carboxylate complexes (see above)[62] the short U-O_{eq} values were interpreted to indicate monodentate complexation of uranyl by a carboxylate[270] in contrast to the common preference of carboxylate complexes to bidentate coordination. The present results for aromatic carboxylates corroborate the earlier suggestion, based on calculated results for aliphatic carboxylates that average U-O_{eq} distances do not depend on the coordination mode (see Section 4.2.1). Accordingly, U-O_{eq} values of 237–240 pm, as determined for uranyl humate complexes[121,131,132] can also be assigned to bidentate uranyl carboxylate complexes with preferential five-fold coordination.[62,219]

On the other hand, bidentate complexation should go along with relatively short U-C distances of ~290 pm;[131] yet, such distances are missing in EXAFS studies of uranyl humate.[61] Unequivocal experimental determination of U-C distances may be hampered because (*i*) other functional groups of humic substances may contribute to uranyl complexation[59,121] and (*ii*) chelate structures of carboxyl groups cannot be excluded. Thus, the contribution of bidentate carboxylate complexes to the overall uranyl complexation by humic acids may be not prevailing enough to yield an unequivocal signal in EXAFS. Still, this study shows that carboxylates, attached in various ways to the organic skeleton of humic substances, should lead to rather similar geometric characteristics U=O_t and U-O_{eq} of uranyl complexes, irrespective of the coordination *type*, as long as the coordination *number* remains unchanged.

Any empirical modeling of actinide complexation by humic substances should take into account that the complexation strength of carboxylic sites may vary more strongly even though pertinent structural features can be rather similar. For the aromatic carboxylates treated here and their aliphatic congeners[62,219] ligand substitution Gibbs free

energies ranging from 70 to 110 kJ mol^{-1} have been determined for bidentate coordination (Table 4.15), which translates to stability constants log β_1* (2.5-4.6) (Table 4.16). Stability constants of uranyl-humate corresponding to 1:1 stoichiometry were determined to 2.5-6.7[279–282] and for 1:2 stoichiometry, the stability constant is reported between 5.5-11.5[277–280,283] using different experimental techniques under variable conditions and for different sources of humic acids. Computationally determined stability constants of uranyl-carboxylate model complexes, are within the range of log β*, evaluated for uranyl-humate systems for 1:1 complexation. From the literature,[277–283] one finds that different complexation reactions postulated for the interpretation of experimental data that lead to different results. Since uranyl-humate complexes are not well defined, different methods lead to different evaluation schemes as well as varying results. Additionally, the formation of $UO_2(HA)_2$ complexes are often considered. The charge neutralization model developed by Kim *et al*.[145,284] allows the determination of an effective stability constant that is independent of pH, metal ion concentration and the origin of the humic acid. For the pH range 3-6, this models results in log β values ranging from 6.08±0.21 to 6.41±0.70. Stability constants determined for the same pH range show a large variation from 4.17±0.26 to 5.85±0.23, depending on pH, uranyl concentration, and the origin of the humic acid. Comparison of computationally determined stability constants to experimental values of log β* independent of conditions would be more appropriate. Larger values of log β* compared to calculated results for carboxyl groups may well point towards more stable complexation sites of different type, although these larger values are well within the range of experimental and computational uncertainty.

The interval of substitution free energies estimated above will be even wider when one accounts for chelate conformations and for monodentate configurations as possible meta stable intermediates of the complexation process. Thus, this study supports strategies where the complexation of metal ions by humic substances is described by an ensemble of sites that represent a continuum of interaction energies.[251]

4.2.2.6 Conclusion

In summary, as the previously studied aliphatic uranyl monocarboxylates,[62,219] complexes with aromatic carboxylates may serve as models of corresponding sites of humic substances. Density functional modeling of uranyl benzoate complexes were carried out and the study was extended to various groups differing in nature and positions with respect to acid group. Substitution on the benzene ring affects the complexes only slightly. In contrast to common interpretations of EXAFS results, the coordination mode

was determined to have no effect on the average distance U-O_{eq} from uranyl to carboxylate and aqua ligands in the equatorial plane. U=O_t uranyl terminal bonds and U-C distances to the carbon center of the carboxyl moiety were calculated in good agreement with experimental results for benzoate and p-hydroxyl benzoate complexes; this agreement corroborates the assignment of carboxylate coordination as bidentate. Calculated energies for the exchange of aqua ligands of solvated uranyl by one carboxylate ligand yielded a propensity of monodentate rather than bidentate coordination of the benzoate ligand. However, entropy effects lead to a preference of bidentate coordination at the level of Gibbs free energies. Interestingly, chelate coordination of salicylate to uranyl results in a complex of rather low stability compared to mono- or bidentate coordination. Aromatic acids bind slightly weaker than their aliphatic congeners. The present results support also the earlier suggestion that U-O_{eq} is not sensitive to the coordination mode of carboxylate ligands, but reflects mainly the coordination number.

4.3 Ternary complexes: uranyl-hydroxo-acetate

Uranyl complexation with humic substances at about neutral pH is of pertinent interest for the environmental chemistry of uranium (see Section 2.2.2). However, only the complexation of uranyl with humic substances is commonly studied at low pH,[61,121,132,143] because at elevated pH other competing phenomena, such as hydrolysis, precipitation etc., complicate the experimental situation. As discussed in Section 4.1, hydrolysis of uranyl(VI) leads to the formation of both monomeric and polymeric species. With increasing pH, one expects two competing phenomena: on the one hand, hydrolysis of uranyl-humate complexes, on the other hand, complexation of uranyl-hydroxide species with humic acids. Both processes may result in the formation of ternary complexes of uranyl(VI) with humic acid and hydroxide ligands.

As a simple model system, ternary uranyl complexes with carboxyl, hydroxide and aqua ligands have been examined in this thesis. In extension of the model approach applied in the previous section to investigate uranyl complexation by humic substances, uranyl-monoacetate-monohydroxide complexes were studied here. Limited results on C_s symmetric bidentate complexes have been obtained earlier.[62]

As just mentioned, experimental results on ternary actinide-humate complexes are scarce, only some information about stability constants of ternary complexes is available. In a laser-induced fluorescence spectroscopy study Sachs *et al.*[159] reported the formation

of the complex $UO_2(OH)HA(I)$, starting from $[UO_2OH]^+$ and HA at pH 7. The fluorescence signal corresponding to the proposed ternary complex was not observed and the concentration of the ternary complex was determined indirectly as the difference between the total uranyl concentration and the concentration of uranyl not bound to humic acid $[UO_2(OH)HA(I)] = [U(VI)]_{tot} - [U(VI)]_{non\text{-}HA}$. The stability constant

$$\beta = [UO_2(OH)HA(II)] / [UO_2OH(I)][HA(I)] \quad (4.14)$$

was determined at 6.58 ± 0.24 in logarithmic unit. Speciation calculations using that value suggest an equilibrium between binary and ternary uranyl-humate complexes with hydroxide already at pH ~ 4. Pashalidis *et al.*[158] studied the formation of ternary uranyl-humate complex at pH from 7.5 to 7.9 by the solubility enhancement method. The stability constant for the formation of the ternary complex $UO_2(OH)HA(I)$, $\log \beta = 6.94$, is slightly higher than the one for uranyl-humate $UO_2HA(II)$ complex, $\log \beta = 6.2$. Zeh *et al.*[157] examined the sorption of UO_2^{2+} ions onto humic colloids between pH 1 to 10 by ultrafiltration and anion exchange. They reported the stability constant of the complex $UO_2(OH)HA(I)$ at $\log \beta = 6.2$. Thus, stability constants of uranyl-humate and ternary uranyl-hydroxo-humate complexes seem to be comparable.[157–159] However, as a first approach one would expect complexation constants for the complexation of uranyl monohydroxide by humates to be lower than those of the non-hydrolyzed uranyl ion, since the charge of the ion $[UO_2OH]^+$ is lower. From the experimental work mentioned above, it is clear that the formation of ternary uranyl-humate complexes is not well defined. The few experimental studies done in the corresponding pH range do not provide direct evidence of the formation of such complexes. Also, no direct data on the speciation or structures of ternary uranyl-hydroxo-humate complexes are available in the literature.

The primary aim of this study is the determination of the structure of ternary uranyl-hydroxo-carboxylate complexes with major emphasis on the coordination mode. Energetic aspects and the stability of the ternary complexes with respect to uranyl-carboxylate complexes will be considered in the light of available experimental evidence.

4.3.1 Models

Acetic acid is used again to model carboxyl groups of humic substances. The monohydroxide of uranyl $[UO_2OH]^+$ is considered as reference species, to have a simple model system, excluding higher-order hydrolysis products. Ternary complexes with a single hydroxide group may also result from polynuclear hydrolytic species present in solution, but the propensity to form complexes with humic substances will be strongest

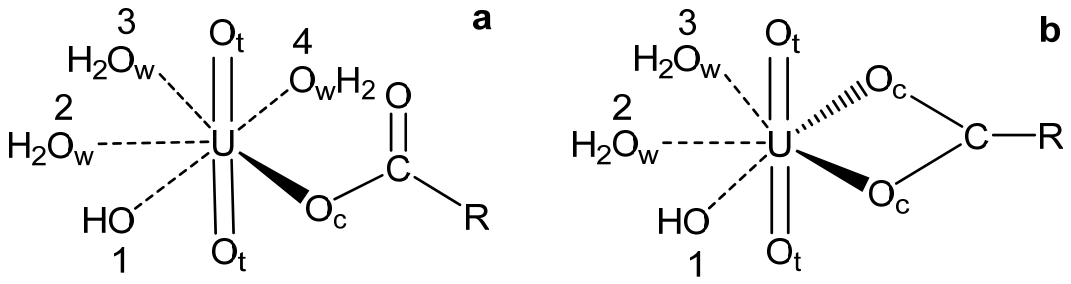

Figure 4.22. Schematic representation of (a) monodentate and (b) bidentate uranyl-hydroxo-carboxylate complexes. Additionally, three or two aqua ligands are coordinated in the equatorial plane to yield pentagonal coordination of the uranium center. Numbers are used to specify the position of the hydroxide relative to the carboxylate group in various isomers.

for the positively charged species $[UO_2OH]^+$. For uranyl-hydroxo-carboxylate complexes, initially assigned as penta-coordinated, this study compares two coordination modes: monodentate $[UO_2(OH)CH_3COO(H_2O)_3]$ and bidentate $[UO_2(OH)CH_3COO(H_2O)_2]$. Note, however, that for some isomers, aqua ligands were found to be displaced to the second coordination shell during geometry optimization (see below). The monodentate complex yields four and the bidentate complex two isomers, depending on the position of the hydroxide group with respect to carboxyl group. Numbers are used to specify the position of the hydroxide ligand relative to the carboxylate group (Fig. 4.22). Isomers with the hydroxide group oriented away from the carboxyl are designated as *trans,* otherwise the configuration is labeled as *cis*. In this regard, isomers 1 and 4 of the monodentate complex are classified as *cis*, whereas isomers 2 and 3 are *trans*. The *cis* isomers 1 and 3 of the bidentate complexes are similar due to their (local) symmetry of the ligand arrangement around uranyl; therefore, only isomer 1 has been studied. As for the monodentate complex, isomer 2 of the bidentate exhibits a *trans* configuration.

4.3.2 Geometry

Table 4.17 compares geometry parameters of the complexes $[UO_2(OH)CH_3COO(H_2O)_n]$, n = 3 for monodentate and n = 2 for bidentate coordination of the acetate ligand, to those of the uranyl-monoacetate. The strong ligation of the hydroxide group to uranyl weakens the uranyl bonds to aqua and acetate ligands in uranyl-hydroxo-acetate complexes, irrespective of the coordination mode. In contrast to uranyl-acetate complexes (Fig. 4.17) this results in a hydrogen-bonding network between the ligands of the first coordination shell (Figs. 4.23, 4.24). The position of the hydroxide group determines the structural

parameters, irrespective of the coordination mode. In the gas phase as well as in solution, the uranyl bond U=O_t is slightly elongated, by about 1–2 pm. This is reflected in the corresponding stretching frequencies, ν_{sym}, which decrease by ~45 cm^{-1} in the gas phase and ~30 cm^{-1} in solution compared to uranyl-acetate. Overall, the uranyl-carboxyl bond U-O_c is elongated due to the coordination of hydroxide. This effect is stronger for *trans* isomers (13–17 pm) than *cis* isomers (2–12 pm). The distance U-C follows the same trend. Many of the aqua ligands are involved in hydrogen bonding. For the ternary complexes, the average distance U-O_w is calculated slightly longer, at most by 8 pm, than for binary complexes (see Section 4.2.1).

In the gas phase, isomer 1 of the monodentate complex is a four-coordinated complex (Fig. 4.23 a) with one aqua ligand in the second coordination shell, hydrogen-bonded to the OH group, an adjacent aqua ligand as well as to terminal oxygen. All other isomers are five-coordinated.

Table 4.17. Calculated structural parameters for isomers (LDA, distances in pm) of monodentate (mono) and bidentate (bi) uranyl-acetate and uranyl-hydroxo-acetate complexes [$UO_2OH(OOCCH_3)$]. The symmetric uranyl stretching frequency ν_{sym} (in cm^{-1}) is also shown. Given are the results from gas phase (GP) and solvation (PCM) calculations.

	Complex		isomer	U=O_t	U-O_c	U-C	U-O_w	U-O_h	U-O_{eq}	ν_{sym}
GP	bi	UO_2		177.8	233	274	242		239	881
		$UO_2(OH)$	1	179.0	240	278	250	219	240	829
			2	179.6	250	289	247	210	241	839
	mono	UO_2		178.0	229	333	241		239	860
		$UO_2(OH)$	1	179.8	234	336	244	209	233	816
			2	179.3	245	340	244	219	239	825
			3	179.9	246	344	248	210	240	818
			4	179.7	231	333	249	218	239	816
PCM	bi	UO_2		178.6	237	277	236		237	854
		$UO_2(OH)$	1	180.7	241	280	245	213	237	
			2	180.6	244	284	244	212	238	820
	mono	UO_2		178.9	229	340	238		236	822
		$UO_2(OH)$	1	180.8	235	335	246	215	238	
			2	180.8	242	341	243	214	237	796
			3	180.9	242	342	245	212	238	793
			4	180.9	241	341	244	214	237	

Among the monodentate complexes, structural parameters vary notably with the position of the hydroxide group. The geometry of *cis* isomers differs significantly from that of *trans* isomers; in the former, the uranyl-acetate bond is more than 10 pm shorter. The hydroxide bond to uranyl U-O_h varies among penta-coordinated monodentate complexes, depending on the hydrogen bonding involving the OH group. In isomers 2 and 4 the strong hydrogen bonding to the OH group (O···H ≈ 170 pm) renders the distance U-O_h (8 pm) considerably longer than in isomer 1 and 3. Also, isomer 1 shows a hydrogen bond at the OH group, but this isomer reveals relatively short ligand bonds since it is four-coordinated. Similarly, U-O_c was calculated relatively long for isomer 2 and 3 which features a short distance O_c···H ≈ 170 pm (Fig. 4.23 b, c). In isomer 4 there is no hydrogen bond to the center O_c, hence the U-O_c bond, 231 pm, is shorter than in isomers 2 and 3 where U-O_c ≈ 245 pm). The terminal uranyl bonds vary only slightly

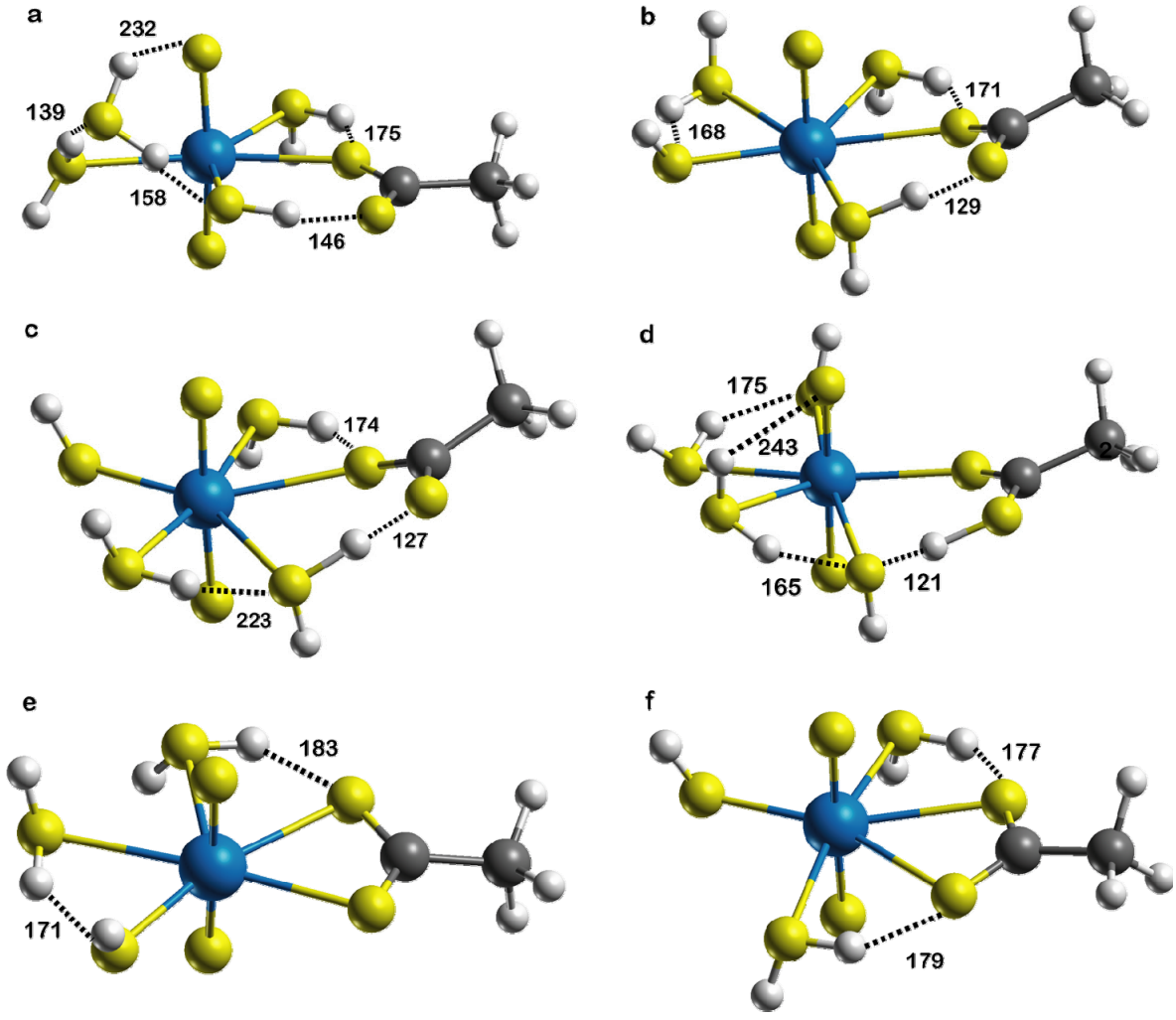

Figure 4.23. Optimized structures of monodentate and bidentate uranyl-hydroxo-acetate [$UO_2OH(OOCCH_3)$] complexes in the gas phase. Monodentate complexes: a) isomer 1, b) isomer 2, c) isomer 3, and d) isomer 4. Bidentate complexes e) isomer 1 and f) isomer

among the monodentate isomers, by about 0.6 pm, which is confirmed by the trend in the symmetric uranyl stretching frequency ν_{sym} (Table 4.17). With the exception of isomer 1 in the gas phase, the average U-O bond to equatorial ligands varies only slightly among the various isomers (Table 4.17). This confirms again that this parameter is sensitive essentially only to the coordination number. Thus, a deviation is only calculated for isomer 1, which exhibits a shorter value of U-O_{eq} due to four-coordination; see also the discussion on uranyl monohydroxide in Section 4.1.2.

Also for bidentate complexes in the gas phase, the position of the hydroxide group and the structure of the shell of aqua ligands also significantly affect the overall geometry. In isomer 1, the electrostatic repulsion between the hydroxide and the acetate groups, as well as a hydrogen bond between the OH and H_2O ligands result in a large angle O_h-U-O_c, 112° (Fig. 4.23 e); this is to be compared to the average O_w-U-O_c angle, 72°, in the

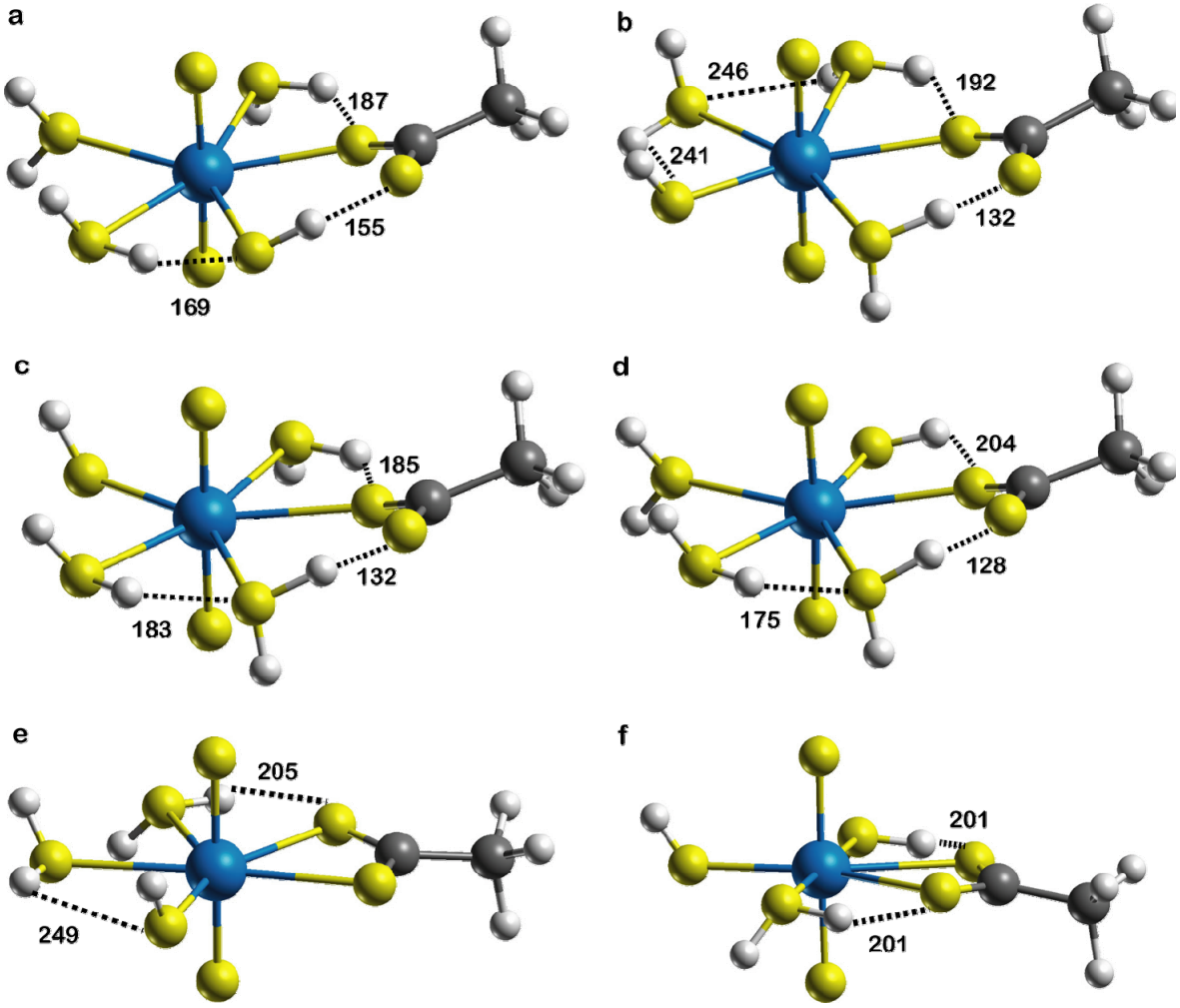

Figure 4.24. Optimized structures of monodentate and bidentate uranyl-hydroxo-acetate complexes [UO_2(OH)OOCCH_3] in solution. Monodentate complexes: a) isomer 1, b) isomer 2, c) isomer 3 and d) isomer 4. Bidentate complexes e) isomer 1 and f) isomer 2.

non-hydrolyzed uranyl-acetate complex studied earlier (Section 4.2.1).[62] This hydrogen bond to the OH group in isomer 1 considerably elongates the U-O_h bond, by about 8 pm compared to isomer 2. In the latter isomer, two short hydrogen bonds ($O_c \cdots H$ = ~178 pm) to the carboxyl oxygen centers lead to elongated U-O_c bonds; also, the distance U-O_h, 210 pm, is relatively short due to the lack of hydrogen bonds (Fig. 4.23 f).

Table 4.17 also summarizes the results for mono- and bidentate complexes $[UO_2(OH)OOCCH_3(H_2O)_{3/2}]$ in solution. The change in the structural parameters due to solvent effects is similar for all isomers, except for isomer 1 in monodentate coordination, where the coordination number changes. Long-range solvent effects reduce the uranium-oxygen distances to the aqua ligands, by 6 pm at most. This translates into a reduction of the average U-O bond length of uranyl to its ligands, U-O_{eq}, by 2–3 pm (Table 4.17). In consequence, the uranyl bonds U=O_t are slightly activated, by ~1 pm, for both coordination modes. Polar bonds are expected to become elongated due to solvent interaction, as observed for uranyl-carboxylate complexes (Section 4.2.2.2). However, in uranyl-hydroxo-acetate complexes, the trend from gas phase to solvation models is not consistent for such polar bonds as U-O_c and U-O_h. It highly depends on the local environment of the ligand shell and the hydrogen bonds therein. Solvent effects generally elongate hydrogen bonds. For *cis* isomers, the U-O_c bond is elongated due to solvation, but shortens for *trans* isomers. In most cases (except the monodentate isomers 1 and 2) an opposite solvation effect is calculated for U-O_c and U-O_h. The polar bond U-O_h shortens when U-O_c elongates due to solvation and vice versa. This may point to a direct bonding competition of OH and acetate ligands.

For bidentate complexes, the uranyl bond U=O_t was calculated marginally shorter ~0.20 pm, than for the monodentate complexes, in line with a red shift of the symmetric uranyl stretching frequency of about 20 cm^{-1}. This indicates a slightly stronger ligand interaction for the monodentate complexes. The uranyl-ligand bond U-O_c exhibits a clear trend: in monodentate complexes, it is shorter (235–242 pm) than in bidentate complexes (241–244 pm) when corresponding isomers are compared (*cis* or *trans*; Table 4.17). U-C distances, which commonly are used in experiment to identify the complexation mode,[285–287] are calculated at 335–342 pm in monodentate and 280-284 pm in the bidentate complexes. Average bond lengths U-O_w to aqua ligands increase slightly when the interaction of uranyl with the hydroxide strengthens, as inferred from the discussion above. Distances U-O_w were calculated at 234 pm for bidentate and 235–238 pm for monodentate complexation. Nevertheless, bonding competition ensures that the average bond distance U-O_{eq} to equatorial ligands remains at about 237 pm, independent of the coordination mode (Table 4.17). The insensitivity of U-O_{eq} to the coordination mode of

the carboxylate noted earlier[62] for uranyl-acetate (see Section 4.2.2) is nicely corroborated by the present results. In addition to that, U-O_{eq} is not affected by the presence of strongly binding ligands like hydroxide. Overall, geometry variations between various isomers are smaller in solution than in the gas phase (Table 4.17).

All parameters discussed and collected in Table 4.17 are rather similar for monodentate isomers 2 to 4. Only the monodentate isomer 1 shows a U-O_c bond of 235 pm which is about 7 pm shorter than that of the other isomers. Concomitantly, also the distance U-C is shorter for isomer 1 (335 pm) than for isomers 2 to 4 (243–245 pm). This deviation of isomer 1 from the others may be related to the presence of an accepting hydrogen bond from the OH ligand to the non-coordinated oxygen of the carboxyl group. For *trans* isomers the geometry parameters are comparable: among them, U-C varies by 1 pm, U-O_h and the average U-O_w by 2 pm, and distances U-O_c are calculated the same (242 pm) for both isomers. Terminal uranyl bonds remain almost constant for different positions of the hydroxide group with respect to the carboxyl group.

For bidentate complexes, terminal uranyl bonds are similar, as observed for monodentate complexes. The variation of U-O_c and U-C is about 4 pm between both isomers; however, U-O_w and U-O_h are rather similar, differing by 1 pm. Also the average distance U-O_{eq} is almost same (~1 pm) for both the isomers, just as for the monodentate counter parts, in line with the by now well-established insensitivity of U-O_{eq} to the coordination mode of the ligands.[62] The long U-O_c bond in isomer 2 compared to isomer 1 (Table 4.17) may be rationalized by the presence of two hydrogen bonds, instead of one, of aqua ligands to the hydroxide group (Fig. 4.24 f). As a side, it may be worthwhile to examine hexa-coordinate species for these ternary complexes since for some isomers large angles between ligands have been calculated. The largest angles between ligands calculated are 89° for the bidentate isomer 2 (Fig. 4.24 f) and 82° for the monodentate isomer 3 (Fig. 4.24 c). Both considerably exceed the average, 72°, expected for five-coordinate species from earlier results; see Section 4.1.

4.3.3 Energetics

The complexation of carboxylate ligands to uranyl at weakly acidic to neutral pH was examined via the formal substitution of aqua ligands of the uranyl monohydroxide ion $[UO_2(H_2O)_4OH]^{1+}$ by a carboxylate ligand. The corresponding energy ΔE_{sub} is defined by the reaction

$$[UO_2(H_2O)_4OH]^{1+} + RCOO^- \rightarrow [UO_2OH(OOCR)(H_2O)_n] + (4–n)H_2O \quad (4.15)$$

Here n = 3 corresponds to monodentate and n = 2 to bidentate coordination modes. As a reference, isomer 1 of uranyl monohydroxide is used with 4 aqua ligands. Calculated reaction energies E_{sub} and Gibbs free energies ΔG_{sub} in the gas phase and in solution are listed in Table 4.18, along with results for non-hydrolyzed uranyl-acetate complexes. For all complexes considered, the formation of bi- and monodentate species by substituting acetate for aqua ligands is exothermic, both in the gas phase and in solution. In the gas phase, substitution energies E_{sub} are smaller (by absolute value) for bidentate complexes (-485 kJ mol^{-1}) than for monodentate complexes (-515 to -557 kJ mol^{-1}). Substitution is strongly exothermic because oppositely charged moieties are combined. In aqueous solution, the reactants are strongly stabilized. Hence, the reaction energies are significantly smaller, about -65 kJ mol^{-1} for bi- and -63 to -97 kJ mol^{-1} for monodentate complexes. Compared to uranyl-acetate, substitution energies are by 30–70 kJ mol^{-1} smaller in absolute terms (Table 4.18). This is easily rationalized by the higher charge for non-hydrolyzed uranyl UO_2^{2+} compared to $[UO_2OH]^+$. Thus, hydrolysis competes with complexation. Again, the preference for monodentate coordination, calculated for the gas phase, remains in solution.

Comparing E_{sub} among the isomers of monodentate complexes, *trans* isomers are found to be more stable than *cis* species, due to the reduction of the electrostatic repulsion between acetate and hydroxide group in the latter case. A similar trend in energy should

Table 4.18. Ligand substitution energy E_{sub} and Gibbs free energy ΔG_{sub} in the gas phase (GP) and in solution (PCM) (Eq. 4.15, in kJ mol^{-1}) for monodentate (mono) and bidentate (bi) uranyl-hydroxo-acetate complexes $[UO_2(OH)CH_3COO(H_2O)_{3/2}]$. Also shown are Gibbs free energy values ΔG_{aq}^{corr} in solution where standard state corrections have been applied. The corresponding energies for uranyl-acetate complexes are provided for comparison (Eq. 4.9, Section 4.2.2.2).

Complex		isomer	GP		PCM		
			ΔE_{sub}	ΔG_{sub}	ΔE_{sub}	ΔG_{sub}	ΔG_{sub}^{corr}
bi	UO_2		-861	-902	-95	-137	-109
	UO_2OH	1	-485	-511	-65	-92	-64
		2	-486	-519	-65	-97	-69
mono	UO_2		-926	-916	-129	-120	-110
	UO_2OH	1	-515	-491	-63	-39	-29
		2	-555	-532	-96	-73	-63
		3	-557	-535	-97	-76	-66
		4	-547	-528	-73	-54	-44

be expected for bidentate coordination. However, isomer 1 is stabilized in view of the hydrogen bond between the OH group and its neighboring aqua ligand, which leads to a large angle O_c-U-O_h of 109° (Figs. 4.23 and 4.24). Thus, E_{sub} is similar for both isomers of bidentate coordination. With inclusion of thermodynamic corrections, monodentate coordination is preferred in the gas phase by only ~15 kJ mol^{-1}; bidentate coordination is favorable in solution by about 20 kJ mol^{-1}. Similar effects were calculated for uranyl-acetate complexes as discussed previously; see Section 4.2.2.3. Thus, bidentate coordination is substantially preferred as an effect of entropy as well by solvation.

Carboxylate complexation including the deprotonation of the carboxylic group was considered in the model reaction

$$[UO_2(H_2O)_4OH]^{1+} + HOOCR \rightarrow [UO_2OH(OOCR)(H_2O)_n] + (2\text{-}n)H_2O + H_5O_2^+ \quad (4.16)$$

As already discussed in Section 4.2.2.4, the solvated proton is better described by the species $H_5O_2^+$. Thus, $H_5O_2^+$ is used in Eq. 4.16. Energies and Gibbs free energies including standard state corrections are collected in Table 4.19 for various isomers. Among the bidentate complexes, *trans* isomer 2 is slightly preferred in energy, by (~5 kJ mol^{-1}). *Trans* isomers in monodentate and bidentate coordination have comparable binding strength. As judged by the calculated Gibbs free energies, both coordination

Table 4.19. Reaction Gibbs free energy ΔG* (Eq. 4.16, in kJ mol^{-1}) and the corresponding stability constants log β* as well as quantities ΔG' and log β' modified for pK_a of acetic acid of monodentate (mono) and bidentate (bi) ternary uranyl-hydroxo-acetate complexes $[UO_2(OH)CH_3COO(H_2O)_{3/2}]$ in solution. Also provided are experimental stability constants for ternary complex of uranyl-hydoxo-humate.

Complex		isomer	ΔG*	logβ*	ΔG'	logβ'[a]
bi	UO_2		-15	2.5	-40	7
	$UO_2(OH)$	1	31	-5.4	4	-0.6
		2	26	-4.5	-2	0.3
mono	UO_2		-15	2.6	-46	8
	$UO_2(OH)$	1	66	-11.5	35	-6
		2	32	-5.6	5	-0.8
		3	30	-5.2	2	-0.4
		4	51	-8.9	23	-4
Exp.	$UO_2(OH)HA$		-38±1 -40±1	6.58±0.24[b] 6.94±0.03[c]		

[a] Determined as log β' = log β* + pK_a of acetic acid (exp. 4.76, Ref. 128).

[b]) Ref. 159 [c]) Ref. 158

Table 4.20. Reaction energy ΔE_{hyd} and Gibbs free energy ΔG_{hyd} for the hydrolysis of bidentate (bi) and monodentate (mono) uranyl-acetate complexes (Eq. 4.17, in kJ mol^{-1}) and the corresponding stability constants log β* for the formation of uranyl-hydroxo-acetate complexes $[UO_2(OH)CH_3COO(H_2O)_{2/3}]$.

Complex	isomer	ΔE_{hyd}	ΔG_{hyd}	log β*
bi	1	30	39	-6.9
	2	30	34	-5.9
mono	1	67	74	-12.9
	2	33	39	-6.8
	3	34	39	-6.8
	4	57	59	-10.3

modes are in equilibrium (Table 4.19). In contrast to Eq. 4.15, which describes the complexation process with a deprotonated carboxylic acid, the energies are determined endothermic in Eq. 4.16. This difference reflects the fact that in reaction 4.16 a neutral ligand attaches to a positively charged species in contrast to the binding of oppositely charged species in Eq. 4.15. However, both formal reactions yield similar trends among the various isomers of monodentate and bidentate complexes.

Alternatively, the complexation process followed by hydrolysis is modeled by the formal reaction where the uranyl-acetate complexes undergo hydrolysis:

$$[UO_2OOCCH_3(H_2O)_n]^{1+} + (H_2O)_2 \rightarrow [UO_2(OH)OOCR(H_2O)_n] + H_5O_2^+ \quad (4.17)$$

Table 4.20 collects the energies E_{hyd} of hydrolysis of uranyl-acetate complexes and the corresponding (corrected) Gibbs free energies ΔG_{hyd}. Both energy quantities show that the hydrolysis of the uranyl-carboxylate complex forming a ternary complex with hydroxide is an endothermic process. *Cis* isomers of monodentate complexes (~65 kJ mol^{-1}) show a higher endothermicity in the Gibbs free energy than *trans* isomers as well as bidentate complexes (~30 kJ mol^{-1}). The endothermicity of reaction 4.17 reflects the suppression of hydrolysis by carboxylate complexation.[83]

4.3.4 Stability constants

For the ternary complexes of uranyl with acetate and hydroxide, the stability constant log β* was determined according to Eq. 4.16. The results are summarized in Table 4.19. Due to the known inaccuracy of the solvation energy determined for anions (Section 4.2.2.4), log β' is determined as log β* + pK_a where the experimental pK_a of acetic acid of 4.76 is

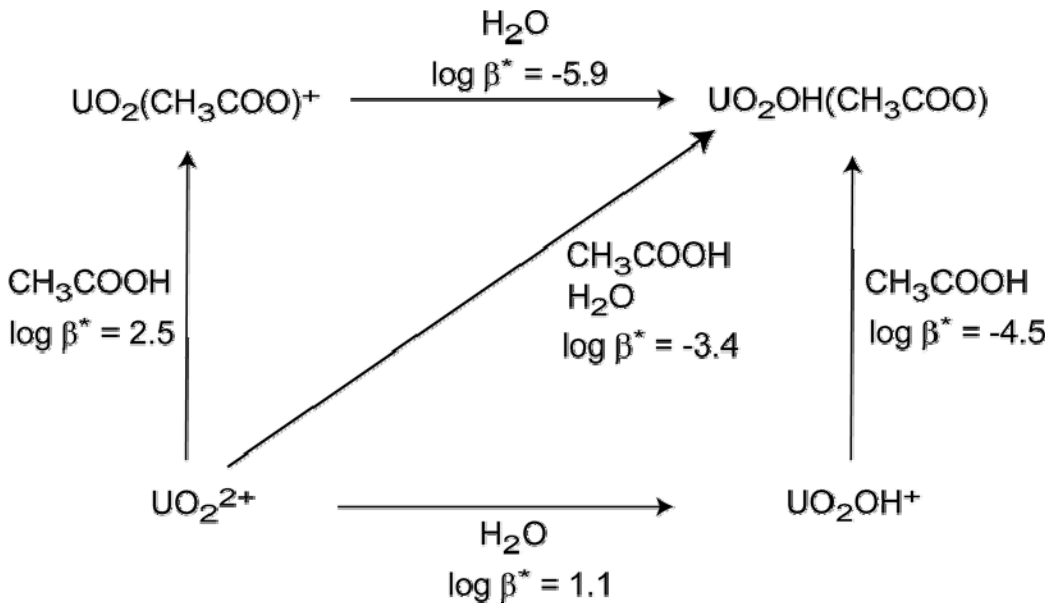

Figure 4.25. Schematic diagram of complexation and hydrolysis processes possible in aqueous solution along with the corresponding stability constants (log β*).

used.[128] The free energy of formation of the ternary uranyl-hydroxo-acetate complex is endothermic if one considers the complexation of uranyl monohydroxide with carboxylic acid in solution (Eq. 4.16). However, the reaction free energy is exothermic for acetate (Eq. 4.15).

Fig. 4.25 presents an overview of the complexation processes along with the corresponding stability constants log β*. Accordingly, the free energy corresponding to the hydrolysis of uranyl (Eq. 4.2, Section 4.1) is calculated as -6 kJ mol^{-1} using $H_5O_2^+$ on the product side as model of the solvated proton, which translates to log β* = 1.1. The hydrolysis of the uranyl-acetate complex (Eq. 4.17) is accompanied by a free energy change of 34 kJ mol^{-1} for the most stable isomer in bidentate coordination. The stability constant related to this free energy is log β* = -5.9. The hydrolysis of the uranyl-acetate complex is notably endothermic, in contrast to the hydrolysis of uranyl, and the energy difference is reflected by a difference of 7 units in log β*. This shows that complexation suppresses hydrolysis,[83] which is in line with the general intuition that the presence of one ligand hinders the complexation by a second one.

The free energy change for complexation of non-hydrolyzed uranyl with acetate is determined to -15 kJ mol^{-1} which leads to a stability constant log β* of 2.5 for bidentate coordination (Section 4.2.2.4). Alternatively, the complexation of acetate with hydrolyzed uranyl exhibits a free energy change of 26 kJ mol^{-1}, thus, log β* = -4.5. Hence, the formation of ternary uranyl-hydroxo-acetate from uranyl monohydroxide is calculated

much weaker than the formation of uranyl-acetate from the uranyl ion, in line with the different charge of the ions involved. Again a difference of 7 units in log β* is obtained between both processes described above. Thus, also hydrolysis hinders complexation.

4.3.5 Comparison to experiment

In experimental investigations of structures of uranyl-humate complexes by means of EXAFS, only $U{=}O_t$ and $U\text{-}O_{eq}$ are commonly measured.[61,131,132] Until now, such an experiment at about neutral pH is missing. Comparison of calculated results for uranyl-monoacetate and uranyl-monoacetate-monohydroxide reveals that these parameters are rather insensitive to the presence of the OH group (Table 4.17). While going from binary to ternary uranyl-acetate complexes, $U{=}O_t$ elongates by about 1.5 pm and $U\text{-}O_{eq}$ may elongate by at most 2 pm, since it is essentially determined by the coordination number – 5 in all models studied here. These geometry changes due to hydrolysis are well within (or close to) the experimental uncertainty. Thus, differentiation of binary and ternary uranyl-humate complexes is hardly possible on the basis of $U{=}O_t$ and $U\text{-}O_{eq}$ measurements alone. A discussion on geometric parameters of ternary complexes in comparison to experimental finding for uranyl-carboxylate species can be found in Ref. 62.

Few experimental studies are done on uranyl-humate complexation at environmental conditions. Sachs *et al*.[159] examined the complexation of U(VI) with humic

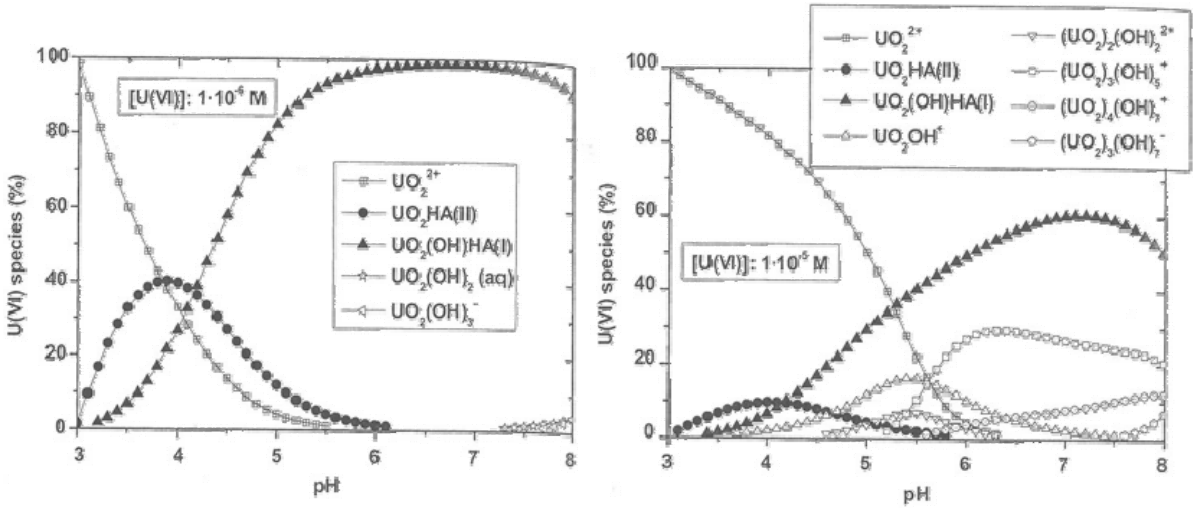

Figure 4.26. Speciation of U(VI) in presence of humic acid as a function of the pH calculated using charge neutralization model at [U(VI)]: 1x 10^{-6} and 1x10^{-5} mol/L, [HA]: 2 mg/L, I: 0.1 M $NaClO_4$, 0% CO_2). Adapted from Ref. 159.

acid at pH 7, using TRLFS spectroscopy. They proposed the exclusive formation of a ternary uranyl-monohydroxo-humate complex via complexation of $[UO_2OH]^+$ and humic acid. Fig. 4.26 gives the results of a speciation analysis of uranyl-humate and ternary uranyl-monohydroxo-humate complexes at about pH 6 to 8. Sachs *et al*. obtained the stability constant log β = 6.58±0.24.[159] The stability constant evaluated for $UO_2HA(II)$ is 6.20±0.56 based on the charge neutralization model.[284] From these values, marginally stronger complexation of hydrolyzed uranyl compared to non-hydrolyzed may be suggested. For comparison, note that Am(III) shows a slightly smaller complexation constant (log β = 5.78) for ternary than for binary complexation with humic acids (log β = 6.23).[288] However, Cm(III) exhibits a behavior similar to that of U(VI), with log β = 6.37 for ternary humate complexes,[288,289] while log β is 6.23 for binary humate complexes.

A solubility study between pH 7.5 and 7.9 yielded comparable results.[158] The log β value of 6.94±0.03 is a little larger than the stability constant of non-hydrolyzed uranyl-humate, 6.2.[145,284] Both these results are at variance with the simple expectation that the low charge of $[UO_2OH]^+$ should lead to weaker complexation compared to UO_2^{2+}. The reason for this effect is not clear as pointed out by the authors; they suggested that some unknown stabilization effect might be responsible for this result.[158]

The stability constant

$$\beta = [UO_2(OH)RCOO)] / [(UO_2^{2+}][OH^-][RCOO^-] \qquad (4.18)$$

for the formation of ternary uranyl-hydroxo-acetate from uranyl has been computationally determined. The dissociation constant of water (14)[128] and acetic acid (4.8)[128] was added to the corresponding log β* = -3.4 value. The agreement of log β = 15.4 is rather good compared to the experimentally determined values, 14.7[157] and 15.3.[158]

The free energies of hydrolysis of uranyl ion, calculated at -6 kJ mol^{-1}, and of hydrolysis of uranyl-monoacetate, calculated at 34 kJ mol^{-1} (corresponding to the most stable coordination mode of carboxyl ligand i.e. bidentate) differ by 40 kJ mol^{-1}. Thus, the present results imply a difference of 7 units in the stability constants for the complexation of uranyl and uranyl monohydroxide. As stated earlier, hydrolysis of uranyl begins at about pH 3. Thus, the present study predicts the formation of ternary complex to begin above neutral pH.

As already noted in Section 4.2.2.4, there is considerable uncertainty in the calculated complexation constants. On the other hand, the clear difference between experimental and computational results needs an explanation. One possibility is that UO_2HA complexes are not well represented by monocarboxylates complexes. An assignment of these complexes to involve two carboxylate groups indeed would lead to a

slightly increased complexation constant for uranyl complexation. In a consequence, the difference between the complexation constants for binary and ternary complexes will decrease, but most probably not vanish.

4.3.6 Conclusion

In summary, for ternary uranyl-monohydroxo-monocarboxylate complexes, the position of the hydroxide group determines the stability. *Cis* isomers are more stable than *trans* isomers for monodentate coordinated carboxylate, but for bidentate coordination both *cis* and *trans* isomers have comparable stability. The introduction of the hydroxide ligand into the first coordination shell of uranyl-monoacetate has a strong impact on characteristic structural parameters. The binding strength of the carboxylate ligand to hydrolyzed uranyl is weaker compared to the binding to non-hydrolyzed uranyl, contrary to the experimental suggestions for the corresponding uranyl-humate binary and ternary complexes. Experimental complexation constants suggest a comparable or larger propensity for the formation of ternary complexes of uranyl-humate from hydrolyzed uranyl(VI) than for the formation of uranyl-humate from non-hydrolyzed uranyl(VI). An equilibrium between binary and ternary uranyl-humate complexes has been claimed already at pH 4.[159] In contrast, a notably weaker complexation propensity of $[UO_2OH]^+$ compared to UO_2^{2+} with acetate as model ligand was calculated in this study, in line with basic electrostatic considerations. Consequently, the hydrolysis of uranyl-humate complexes is suggested to start above neutral pH. Finally, a cautionary remark on the interpretation of experimental data is appropriate since direct evidence for the formation of the proposed ternary uranyl-hydroxo-humate complexes is still missing.

5 Summary and outlook

Understanding the chemistry of actinides in solution is an essential aspect of environmental issues. Knowledge of physical and chemical processes responsible for the speciation of actinides in the environment enables also the prediction of migration of actinides, thus helps to advance new remediation strategies for contaminated sites and to analyze the safety of long-term repositories. Two aspects of that chemistry have been treated in this thesis for the example of uranyl: hydrolysis and the complexation by carboxylate ligands, which are used as models for humic substances. Actinides provide many challenges to chemical research especially due to their large number of oxidation states yielding fascinating structural and electronic behavior in solution. Applying quantum chemical methods to obtain information on the physical and chemical behavior of actinides is an alternative approach to elaborate experimental investigations that have to face a complicated chemistry in solution as well as the radioactivity and the toxicity of actinides. However, electron correlation, relativistic effects and numerous, easily accessible electronic states make actinide compounds a thorny problem for a theoretical treatment.

In this work, the complexation of uranium in its most stable oxidation state VI in aqueous solution was studied computationally, within the framework of density functional (DF) theory. All complexes in this thesis were calculated with an all-electron scalar-relativistic DF method based on the Douglas-Kroll approach as implemented in the program PARAGAUSS. Most of the geometry optimizations were carried out at the LDA level while energetic parameters were determined with a GGA functional. Structures were also optimized at the GGA level for a better description of weak interactions in uranyl monohydroxide complexes. Short-range solvent effects were considered explicitly via coordinated aqua ligands of the first hydration shell and long-range electrostatic interactions were described self-consistently by treating the remaining solvent via a

polarizable continuum model (PCM).

In the beginning, structure, energetics, and the hydrolysis energy of $[UO_2OH]^+$, the mononuclear hydrolysis product of uranyl, was discussed and compared with available experimental results (Section 4.1). The second part dealt with actinide complexation by carboxylate ligands. First of all the coordination number of uranyl-monoacetate was discussed with various model approaches. To supplement previous work on aliphatic carboxylates, a model study on uranyl complexation to various aromatic acids was carried out. These complexes may serve as simple models of complexating sites of humic acid with uranyl (Section 4.2). In the end, results for ternary uranyl-hydroxo-carboxylate complexes were discussed, which model uranyl-humate complexation at ambient conditions (Section 4.3).

Uranyl monohydroxide is the smallest hydrolysis product occurring in dilute solutions. Previous theoretical studies revealed different structures for that species; the computational determination of the formation energy of uranyl monohydroxide was also under debate. Thus, structure and energetics of uranyl monohydroxide was studied using different exchange-correlation functionals and considering four to six coordination of uranyl. Seven isomers were optimized for uranyl monohydroxide; six of them are penta-coordinated and one is four-coordinated. The isomers mainly differ with respect to the orientations of the aqua ligands in the first coordinating shell of uranyl. The structures obtained with the generalized gradient approach agree with that from the local density approach, except for the four-coordinated isomer with an aqua ligand in the second shell. That four-coordinated isomer was found to be the most stable species. The five-coordinated isomers, which had also been suggested in earlier studies, form a set of nearly degenerate isomers, which are 10–20 kJ mol^{-1} less stable than the four-coordinated isomer. Modeling the solvated proton as H_3O^+, the free energy of hydrolysis of the uranyl-aqua complex agreed well with experiment; this agreement was traced back to, in part, favorable error cancellation.

Monocarboxylate complexes $[UO_2(OOCR)]^{1+}$ of U(VI) with various aromatic carboxylic ligands were studied in this work to extend an earlier investigation on uranyl complexation with aliphatic acids. Here, the relative stability of penta- and hexa-coordinated uranyl-monoacetate was examined using various model approaches. The addition of an aqua ligand in the first coordination shell of uranyl-acetate was calculated to be endothermic. For hexa-coordination the bidentate uranyl-acetate complex was determined to be preferred over the monodentate complex. From the results of various model approaches applied, one can conclude that five-coordination of uranyl monoacetate is more stable than six-coordination, in line with experimental evidence.

The investigation of uranyl monocarboxylate complexes with aromatic carboxylate ligands focused on a comparison and characterization of different coordination modes of the carboxylic group: bidentate, monodentate, or chelate via an adjacent hydroxyl group. Small substituent effects on the geometry were obtained only for monodentate species. In contrast to common interpretations of EXAFS results, no effect of the coordination mode on the average distance U-O_{eq} from uranyl to the carboxylate and the aqua ligands in the equatorial plane was determined. U=O_t uranyl terminal bonds and U-C distances to the carbon center of the carboxyl moiety were calculated in good agreement with experimental results for benzoate and p-hydroxy benzoate complexes; this agreement corroborates the assignment of carboxylate coordination as bidentate. The discrepancy of calculated and experimental (~5 pm longer) values of U-O_{eq} for species interpreted as bidentate is tentatively ascribed to different coordination numbers.

Calculated energies for the exchange of aqua ligands of solvated uranyl by a carboxylate ligand yield a preference for monodentate over bidentate coordination of the aromatic carboxylates. However, entropy as well as solvent effects lead to a preference of bidentate coordination at the level of Gibbs free energies. Interestingly, chelate coordination of salicylate to uranyl results in a complex of rather low stability compared to mono- or bidentate coordination. Overall, the propensity of uranyl to form complexes with aromatic acids was estimated to be slightly weaker than with aliphatic carboxylates. Stability constants were determined for various uranyl-carboxylate complexes, and a rather good agreement was achieved for acetate and benzoate ligands.

The present work on uranyl-carboxylate complexes may be used as models of uranyl-humate species, recalling the view that humic substances offer an ensemble of mainly carboxylic functional groups as active sites. According to present and previous results on uranyl aliphatic acids, that ensemble leads to the formation of uranyl complexes with rather similar pertinent structural characteristics, despite notable variations in the interaction (free) energies. The computationally determined stability constants of monocarboxylate complexes are well within the range of experimental log β values; they allow an interpretation of the data for uranyl-humate systems as 1:1 complexation.

The results of this thesis corroborate the earlier suggestion that the average equatorial distance U-O_{eq} is not sensitive to the coordination mode, here comprising also carboxylate ligands, but mainly reflects the coordination number. Consequently, measured U-O_{eq} values of ~238 pm for uranyl-humate complexes cannot unequivocally be interpreted as indicative of monodentate carboxylate coordination. The present work corroborates the interpretation that penta-coordinate uranyl complexes with bidentate coordination

dominate, in line with the calculated energetic trends and the common preference of carboxylate ligands for this coordination mode.

Ternary complexes of uranyl-humate are expected to play an important role at environmental conditions. They were studied here, considering carboxylate model ligands in both monodentate and bidentate coordination modes. The introduction of the hydroxide ligand to the first coordination shell of uranyl-acetate tends to have a strong impact on characteristic structural parameters. Again, no effect of the coordination mode on the average distance U-O_{eq} was determined as long as the coordination number is preserved. According to the present results, an experimental discrimination of binary and ternary complexes will be hardly possible if only data on the distances U=O_t and U-O_{eq} are available.

The relative positions of the hydroxide and the carboxylate groups was calculated to determine the stability of the ternary complexes, irrespective of the coordination mode. Isomers with monodentate t*rans* coordination of acetate were found to be more stable than *cis* isomers. *Cis* and *trans* bidentate complexes are of comparable stability. The carboxylate ligand binds weaker to hydrolyzed than to non-hydrolyzed uranyl as is easily rationalized by the different charges of UO_2^{2+} and UO_2OH^+. In contrast, experiments yielded quite similar complexation constants for uranyl-humate and uranyl-hydroxo-humate. The present study predicts the difference in the complexation constants to be 7 units in log β*. Thus, the hydrolysis of uranyl-humate complexes should begin above neutral pH.

This detailed study on uranyl complexation with various ligands provided adequate and valuable information, which can be very useful for understanding the chemical behavior of systems under different chemical and environmental conditions. Also, a new view on the complexity of uranyl monohydroxide species was provided. Structures and energies of uranyl carboxylate complexes will be helpful for the empirical modeling of the uranyl-humic acid interaction. The results on structure and stability of the ternary uranyl-hydroxo-humate complexes may be helpful to design and interpret further experimental attempts in directly identifying ternary complexes of this type.

The present study also provides a reliable basis of computational methods and models which can be fruitfully applied also to study the complexation chemistry of other actinide ions.

Appendix – Basis Sets

This appendix summarizes all atomic basis sets used in this thesis. The program PARAGAUSS employs products of primitive Gaussian functions of the form $\exp(-\alpha_i r^2)$ and real spherical harmonic functions Y_l^m for the representation of the molecular orbitals. In the following tables the exponents α_i will be listed for the atoms hydrogen, carbon, oxygen, fluorine and uranium. The size of the basis sets and the corresponding size of the contracted basis sets are given in the notation introduced in Section 3.3, i.e. (n_0s, n_1p, n_2d, n_3f) and [N_0s, N_1p, N_2d, N_3f], respectively.

In addition, the size of the auxiliary basis sets to represent the charge density is given by (n_0s, n_1r^2, m_1p, m_2d, m_3f). The exponents of the corresponding *s*- and r^2-type "fitting functions" are generated from the orbital basis (see Section 3.3). The exponents for higher angular momenta *p*, *d*, and *f* are added each as a geometric series with a progression of 2.5, starting with 0.1, 0.2, and 0.3 au, respectively; typically, five "polarization exponents" are used for each angular momentum. The corresponding exponents are given in the following table.

Exponents for polarization fitting functions

	p	**d**	**f**
α_1	0.10000000	0.20000000	0.30000000
α_2	0.25000000	0.50000000	0.75000000
α_3	0.62500000	1.25000000	1.87500000
α_4	1.56250000	3.12500000	4.68750000
α_5	3.90625000	7.81250000	11.71875000

Hydrogen (Z = 1): (6s, 1p) basis set

Ref.229c,e

Contraction(6s, 1p) → [4s, 1p]

Fitbasis(6s, $1r^2$, 5p)

	s	**p**
α_1	0.08989100	1.00000000
α_2	0.25805300	
α_3	0.79767000	
α_4	2.82385400	
α_5	12.40955800	
α_6	82.63637400	

Carbon (Z = 6): (9s, 5p, 1d) basis set

Ref.229c,d

Contraction(9s, 5p, 1d) → [5s, 4p, 1d]

Fitbasis(9s, $5r^2$, 5p, 5d)

	s	**p**	**d**
α_1	0.15659000	0.12194000	0.60000000
α_2	0.51190000	0.38554000	
α_3	2.41804900	1.20671000	
α_4	6.17577600	4.15924000	
α_5	16.82356200	18.84180000	
α_6	50.81594200		
α_7	178.35083000		
α_8	782.20479500		
α_9	5240.63525800		

Oxygen (Z = 8): (9s, 5p, 1d) basis set

Ref.229c,d

Contraction(9s, 5p, 1d) → [5s, 4p, 1d]

Fitbasis(9s, $5r^2$, 5p, 5d)

	s	**p**	**d**
α_1	0.30068600	0.21488200	1.15000000
α_2	1.00427100	0.72316400	
α_3	4.75680300	2.30869000	
α_4	12.28746900	7.84313100	
α_5	33.90580900	34.85646300	
α_6	103.65179300		
α_7	364.72525700		
α_8	1599.70968900		
α_9	10662.28494000		

Fluorine (Z = 9): (9s, 5p, 1d) basis set

Ref.229a, b

Contraction(9s, 5p, 1d) → [5s, 4p, 1d]

Fitbasis(9s, $5r^2$, 5p, 5d)

	s	**p**	**d**
α_1	0.38886900	0.26640000	1.49600000
α_2	1.30721500	0.91859700	
α_3	6.03223200	2.95324600	
α_4	15.57144000	9.99342600	
α_5	42.97453100	44.14730300	
α_6	131.37366000		
α_7	462.37392000		
α_8	2028.69160000		
α_9	13521.52300000		

Uranium (Z = 92): (24s, 19p, 16d, 11f) basis set

Ref.228

Contraction(24s, 19p, 16d, 11f) → [10s, 7p, 7d, 4f]

Fitbasis(24s, $9r^2$, 5p, 5d, 5f)

	s	**p**	**d**	**f**
α_1	0.02058815	0.15790660	0.03447413	0.11032550
α_2	0.04313320	0.40899790	0.08774074	0.30254220
α_3	0.08254175	0.90591220	0.21542030	0.73748150
α_4	0.31243190	2.29137600	0.51211640	1.69235400
α_5	0.65236340	4.64911000	1.20507700	3.75266500
α_6	1.85772200	11.13758000	2.55673600	8.17341700
α_7	3.33603700	22.85757000	5.22965900	17.51736000
α_8	8.81990900	52.73747000	10.89752000	38.22365000
α_9	15.37485000	113.71170000	22.23856000	86.84438000
α_{10}	37.71001000	270.72840000	45.78370000	219.08110000
α_{11}	69.22380000	649.75080000	94.63173000	703.26150000
α_{12}	172.98510000	1673.81000000	205.18560000	
α_{13}	370.13750000	4676.74500000	474.04020000	
α_{24}	849.55400000	14437.84000000	1215.79900000	
α_{15}	1981.83800000	50135.61000000	3707.24200000	
α_{16}	4869.81100000	200185.00000000	16079.47000000	
α_{17}	12511.46000000	948314.40000000		
α_{18}	33651.45000000	5589055.00000000		
α_{19}	95179.62000000	30062560.00000000		
α_{20}	285123.90000000			
α_{21}	912190.10000000			
α_{22}	3147013.00000000			
α_{23}	12113820.00000000			
α_{24}	48171220.00000000			

Bibliography

[1] Bequerel, H. *C. R. Acad. Sci. Paris* **1896**, *122*, 501.

[2] Nash, K. L.; Cleveland, J. M.; Rees, T. F. *J. Environ. Radioact.* **1988**, *7*, 131.

[3] Choppin, G. R. *Radiochim. Acta* **1988**, *44/45*, 23.

[4] Choppin, G. R. *J. Rad. Nucl. Chem.* **1991**, *147*, 117.

[5] Dozol, M.; Hagemann, R. *Pure. Appl. Chem.* **1993**, *65*, 1081.

[6] Silva, R. J.; Nitsche, H. *Radiochim. Acta* **1995**, *70/71*, 377.

[7] Lieser, K. H. *Radiochim. Acta* **1995**, *70/71*, 355.

[8] Clark, D. L.; Hobart, D. E.; Neu, M. P. *Chem. Rev.* **1995**, *95*, 25.

[9] Choppin, G. R.; Wong, P. J. *Aqu. Geochem.* **1998**, *4*, 77.

[10] Morss, L. R.; Edelstein, N. M.; Fuger, J.; Katz, J. J. *The Chemistry of the Actinide and Transactinide Elements*, Vol. 1; Springer: **2006**.

[11] Choppin, G. R.; Allard, B. in: *Handbook of the Physics and Chemistry of the Actinides*; Vol. 3, A. J. Freeman, C. Keller, Eds.; Elsevier: Amsterdam, **1985**, p. 407-429.

[12] Pompe, S.; Brachmann, A.; Bubner, M.; Geipel, G.; Heise, K. H.; Bernhard, G.; Nitsche, H. *Radiochim. Acta* **1998**, *82*, 89.

[13] Belling, T.; Grauschopf, T.; Krüger, S.; Mayer, M.; Nörtemann, F.; Staufer, M.; Zenger, C.; Rösch N. in: *High Performance Scientific and Engineering Computing*, Bungartz, H.-J.; Durst, F.; Zenger, C., Eds.; Lecture Notes in Computational Science and Engineering, Vol. 8, Springer: Heidelberg, **1999**, p. 439-453.

[14] Belling, T.; Grauschopf, T.; Krüger, S.; Nörtemann, F.; Staufer, M.; Mayer, M.; Nasluzov, V. A.; Birkenheuer, U.; Shor, A.; Matveev, A. V.; Hu, A.; Fuchs-Rohr, M. S. K.; Neyman, K. M.; Ganyushin, D. I.; Kerdcharoen, T.; Woiterski, A.; Gordienko, A.; Majumder, S.; Rösch, N. PARAGAUSS Version 3.1, Technische Universität München, **2004**. Previous versions of the code have also been used.

[15] Pepper, M.; Bursten, B. E. *Chem. Rev.* **1991**, *91*, 719.

[16] Rösch, N.; Krüger, S.; Mayer, M.; Nasluzov, V. A. in: *Recent Developments and Applications of Modern Density Functional Theory*, Seminario, J., Ed.; Theoretical and Computational Chemistry Series, Vol. 4, Elsevier: Amsterdam, **1996**, p. 497-566.

[17] Rösch, N.; Matveev, A. V.; Nasluzov, V. A.; Neyman, K. M.; Moskaleva, L.; Krüger, S. in: *Relativistic Electronic Structure Theory-Applications*, Schwerdtfeger, P., Ed.; Theoretical and Computational Chemistry Series, Vol. 14, Elsevier: Amsterdam, **2004**, p. 676-722.

[18] Schreckenbach, G.; Hay, P. J.; Martin, R. L. *J. Comp. Chem.* **1999**, *20*, 70.

[19] Vallet, V.; Wahlgren, U.; Schimmelpfennig, B.; Moll, H.; Szabó, Z.; Grenthe, I. *Inorg. Chem.* **2001**, *40*, 3516.

[20] Privalov, T.; Schimmelpfennig, B.; Wahlgren, U.; Grenthe, I. *J. Phys. Chem. A* **2003**, *107*, 587.

[21] Spencer, S.; Gagliardi, L.; Handy, N. C.; Ioannou, A. G.; Skylaris, C.-K.; Willets, A.; Simper, A. M. *J. Phys. Chem. A* **1999**, *103*, 1831.

[22] Tsushima, S.; Yang, T.; Suzuki, A. *Chem. Phys. Lett.* **2001**, *334*, 365.

[23] Nakajima, T.; Hirao, K. *J. Chem. Phys.* **2003**, *119*, 4105.

[24] Gagliardi, L.; Roos, B. O. *Nature*, **2005**, *433*, 848.

[25] Kaldor, U.; Eliav, E.; Landau, A. in: *Relativistic Coupled Cluster Calculations for Heavy and Superheavy Elements*, Sen, K. D. Ed.; Reviews of Modern Quantum Chemistry, World Scientific: Singapore, **2002**, p. 260-292.

[26] Eichler, R.; Brüchle, W.; Buda, R.; Bürger, S.; Dressler, R.; Düllmann, Ch. E; Dvorak, J.; Eberhardt, K.; Eichler, B.; Folden III, C. M.; Gäggeler, H. W.; Gregorich, K.E.; Haenssler, F.; Hoffman, D. C.; Hummrich, H.; Jäger, E.; Kratz, J. V.; Kuczewski, B.; Liebe, D.; Nayak, D.; Nitsche, H.; Piguet, D.; Qin, Z.; Rieth, U.; Schädel, M.; Schausten, B.; Schimpf, E.; Semchenkov, E.; Soverna, S.; Sudowe, R.; Trautmann, N.; Thörle, N.; Türler, A.; Wierczinski, B.; Wiehl, N.; Wilk, P. A.; Wirth, G.; Yakushev A. B. *Radiochim. Acta* **2006**, *94*, 181.

[27] Pyykkö, P. *Chem. Rev.* **1988**, *88*, 563.

[28] Kaltsoyannis, N.; Hay, P. J.; Li, J.; Blaudeau, J. P.; Bursten, B. E. in *The Chemistry of the Actinide and Transactinide Elements*, L. R. Morss, N. Edelstein, and J. Fuger Ed.; Ch. 17, 3rd ed., Springer: Heidelberg, **2006**.

[29] Balasubramanian, K. in: *Handbook on the Physics and Chemistry of Rare Earths*, Lanthanide/Actinide Chemistry, Ch. 119, Vol. 18, Elsevier: Amsterdam, **1994**.

[30] Baerends, E. J.; Ellis, D. E.; Ros, P. *Chem. Phys.* **1973**, *2*, 41.

[31] Baerends, E. J.; Ros, P. *Chem. Phys.* **1973**, *2*, 52.

[32] Hay, P. J. *J. Chem. Phys.* **1983**, *79*, 5469.

[33] Küchle, W.; Dolg, M.; Stoll, H.; Preuss, H. *J. Chem. Phys.* **1994**, *100*, 7535.

[34] Häberlen, O. D.; Rösch, N. *Chem. Phys. Lett.* **1992**, *199*, 491.

[35] Buenker, R. J.; Chandra, P.; Hess, B. A. *Chem. Phys.* **1984**, *84*, 1.

[36] van Lenthe, E.; Baerends, E. J.; Snijders J. G. *J. Chem. Phys.* **1993**, *99*, 4597.

[37] van Lenthe, E.; Baerends, E. J.; Snijders J. G. *J. Chem. Phys.* **1994**, *101*, 9783.

[38] van Lenthe, E.; Ehlers, A.; Baerends, E. J. *J. Chem. Phys.* **1999**, *110*, 8943.

[39] Ramana, M. V.; Rajagopal, A. K. *Adv. Chem. Phys.* **1983**, *54*, 231.

[40] Tomasi, J.; Mennucci, B.; Cammi, R. *Chem. Rev.* **2005**, *105*, 2999.

[41] Tsushima, S.; Suzuki, A. *J. Mol. Struct. Theochem* **1999**, *487*, 33.

[42] Kongsted, J.; Mennucci, B. *J. Phys. Chem. A* **2007**, *111*, 9890.

[43] Hemmingsen, L.; Amara, P.; Ansoborlo, E.; Field, M. J. *J. Phys. Chem. A* **2001**, *104*, 4095.

[44] Farkas, I.; Bányai, I.; Szabó, Z.; Wahlgren, U.; Grenthe, I. *Inorg. Chem.* **2000**, *39*, 799.

[45] Hay, P. J.; Martin, R. L.; Schreckenbach, G. *J. Phys. Chem. A* **2001**, *104*, 6259.

[46] Tsushima, S.; Suzuki, A. *J. Mol. Struct. Theochem* **2000**, *529*, 21.

[47] Fuchs, M. S. K.; Shor, A.; Rösch, N. *Int. J. Quant. Chem.* **2002**, *86*, 487.

[48] Wahlgren, U.; Moll, H.; Grenthe, I.; Schimmelpfennig, B.; Maron, L.; Vallet, V.; Gropen, O. *J. Phys. Chem. A* **1999**, *103*, 8257.

[49] Moskaleva, L.; Krüger, S.; Spörl, A.; Rösch, N. *Inorg. Chem.* **2004**, *43*, 4080.

[50] Bolvin, H.; Wahlgren, U.; Moll, H.; Reich, T.; Geipel, G.; Fanghänel, Th.; Grenthe, I. *J. Phys. Chem. A*, **2001**, *105*, 11441.

[51] Tsushima, S.; Yang, T.; Mochizuki, Y.; Okamoto, Y. *Chem. Phys. Lett.* **2003**, *375*, 204.

[52] Schreckenbach, G.; Hay, P. J.; Martin, R. L. *Inorg. Chem.* **1998**, *37*, 4442.

[53] Vallet, V.; Moll, H.; Wahlgren, U.; Szabó, Z.; Grenthe, I. *Inorg. Chem.* **2003**, *42*, 1982.

[54] Vallet, V.; Wahlgren, U.; Schimmelpfennig, B.; Szabó, Z.; Grenthe, I. *J. Am. Chem. Soc.* **2001**, *123*, 11999.

[55] Meinrath, G. Freibrug On-line Geoscience Vol.1, **1998**.

[56] Sawant, R. M.; Sharma, R. S.; Chaudhuri, N. K.; Ramakumar, K. L. *J. Radioanal. Nucl. Chem.* **2002**, *256*, 263.

[57] Fuger, J.; Khodakovsky, I. J.; Sergeyeva, E. I.; Medvedev, V. A.; Navratil, J. D. in: *The Chemical Thermodynamics of Actinide Elements and Compounds*, Part 12, The Actinide Inorganic Complexes, Oetting, F. L. Ed., IAEA, Vienna, **1992**.

[58] Ray, R. S.; Krüger, S.; Rösch, N. *in preparation*.

[59] Pompe, S.; Schmeide, K.; Bubner, M.; Geipel, G.; Heise, K. H.; Bernhard, G.; Nitsche, H. *Radiochim. Acta* **2000**, *88*, 553.

[60] Stevenson, F. J.: *Humus Chemistry, Genesis, Compositions, Reactions*, 2nd ed.; Wiley: New York, **1994.**

[61] Denecke, M. A.; Pompe, S.; Reich, T.; Moll, H.; Bubner, M.; Heise, K. H.; Nicolai, R.; Nitsche, H. *Radiochim. Acta* **1997**, *79*, 151.

[62] Schlosser, F. "*A Relativistic Density Functional study of actinide complexation in aqueous solution*" Ph.D. Thesis, Technical University Munich, **2006**.

[63] Hatcher, P. G.; Schnitzer, M.; Dennis, L. W.; Maciel, G. E. *Soil Sci. Soc. Am. J.* **1981**, *45*, 1089.

[64] Hobart, D. E. *Proc. Robert A. Welch Found. Conf. Chem. Res.* **1990**, *34*, 379.

[65] Katz, J. J.; Seaborg, G. T.; Morss, L. R. *The Chemistry of the Actinide Elements*, 2nd ed., Vol. 2; Chapman and Hall: New York, **1986**. p. 1133-1146.

[66] Hollemann, A. F.; Wiberg, N.: *Lehrbuch der Anorganischen Chemie*, 101. Auflage; de Gruyter, Berlin **1995**, p. 1793-1821.

[67] Fischer, R.; Werner G. D.; Lehmann, T.; Hoffmann, G.; Weigel, F. *J. Less-Common Met.* **1981**, *80*, 121.

[68] Wadt, W. R. *J. Am. Chem. Soc.* **1981**, *103*, 6053.

[69] Dyall, K. G. *Mol. Phys.* **1999**, *96*, 511.

[70] Cotton, F. A.; Wilkinson, G. *Advanced Inorganic Chemistry*, 5th ed.; Wiley: New York, **1988**, p. 980.

[71] Cornehl, H. H.; Heinemann, C.; Marcalo, J.; Pires de Matos, A.; Schwarz, H. *Angew. Chem. Int. Ed. Engl.* **1996**, *35*, 891.

[72] Allen, P. G.; Bucher, J. J.; Shuh, D. K.; Edelstein, N. M.; Reich, T. *Inorg. Chem.* **1997**, *36*, 4676.

[73] Åberg, M.; Ferri, D.; Glaser, J.; Grenthe, I. *Inorg. Chem.* **1983**, *22*, 3986.

[74] Thompson, H. A.; Brown Jr., G. E.; Parks, G. A. *Am. Mineral* **1997**, *82*, 483.

[75] Cotton, S. *Lanthanide and actinide Chemistry*, John Wiley & Sons: England, **2006**, p. 174.

[76] Bühl, M.; Diss, R.; Wipff, G. *J. Am. Chem. Soc.* **2005**, *127*, 13506.

[77] Lieser, K. H.; Hill, R.; Mühlenweg, U.; Singh, R. N.; Steinkopff, Th. *J. Radioanal. Nucl. Chem.* **1991**, *147*, 117.

[78] Moll, H.; Reich, T.; Szabó, Z. *Radiochim. Acta* **2000,** *88*, 411.

[79] Brown, P. L. *Radiochim. Acta* **2002**, *90*, 589.

[80] Kitamura, A.; Yamamura, T.; Hase, H.; Yamamoto, T.; Moriyama, H. *Radiochim. Acta* **1998**, *82*, 147.

[81] Eliet, V.; Bidoglio, G.; Omenetto, N.; Parma, L.; Grenthe, I. *J.Chem. Soc. Faraday Trans* **1995**, *91*, 2275.

[82] Stefano, C. D.; Gianguzza, A.; Leggio, T.; Sammartano, S. *J. Chem. Eng. Data* **2002**, *47*, 533.

[83] Morss, L. R.; Edelstein, N. M.; Fuger, J.; Katz, J. J. *The Chemistry of the Actinide and Transactinide Elements* Vol. 4; Springer, **2006**.

[84] Choppin, G. R.; Jensen, M. P. *The Chemistry of the Actinide and Transactinide Elements;* Vol 4, **2006**, page 2545.

[85] Baes Jr., C. F.; Mesmer, R. E.: *The Hydrolysis of Cations*; Wiley: New York, **1976**, p. 174.

[86] Nguyen-Trung, C.; Palmer, D. A.; Begun, G. M.; Peiffert, C.; Mesmer, R. E. *J. Soln. Chem.* **2000,** *101*, 29.

[87] Zanonato, P.; Di Bernardo, P.; Bismondo, A.; Liu, G.; Chen, X.; Rao, L. *J. Am. Chem. Soc.* **2004**, *126*, 5515.

[88] Rush, R. M.; Johnson, J. S.; Kraus, K. A. *Inorg. Chem.* **1962**, *1*, 378.

[89] Dongarra, G.; Langmuir, D. *Geochim. Cosmochim. Acta.* **1980**, *44*, 1747.

[90] Bartusek, M.; Sommer, L. *Z. Phys. Chem. Leipzig.* **1964**, *226*, 306.

[91] Caceci, M. S.; Choppin, G. R. *Radiochim. Acta* **1983**, *33*, 207.

[92] Korotkin, Yu. S. *Radiokhimiya*. **1973**, *15*, 671.

[93] Gayer, K. H.; Leider, H. *J. Amer. Chem. Soc.* **1955**, *77*, 1448.

[94] Nikitin, A. A.; Sergeyeva, Z. I.; Khodakovskiy, I. L.; Naumov, G. B. *Geokhimiya.* **1972**, *3*, 297.

[95] Palmer, D. A.; Nguyen-Trung, C. *J. Sol. Chem. Soc., Faraday Trans.* **1995**, *91*, 2275.

[96] Clark, D. L.; Conradson, S. D.; Donohoe, R. J.; Keogh, D. W.; Morris, D. E.; Palmer, P. D.; Rogers, R. D.; Tait, C. D. *Inorg. Chem.* **1999**, *38*, 1456.

[97] Yamamura, T.; Kitamura, A.; Fukui, A.; Nishikawa, S.; Yamamoto, T.; Moriyama, H. *Radiochim. Acta* **1998**, *83*, 139.

[98] Åberg, M. *Acta Chem. Scand.* **1969**, *23*, 791.

[99] Åberg, M. *Acta Chem. Scand. A* **1978**, *32*, 101.

[100] Navaza, A.; Villain, F.; Charpin, P. *Polyhedron* **1984**, *3*, 143.

[101] Åberg, M. *Acta Chem. Scand. A* **1976**, *30*, 507.

[102] Åberg, M. *Acta Chem. Scand.* **1970**, *24*, 2901.

[103] Gschneidner, K. A.; Eyring, L.; Choppin, G. R.; Lander, G. H. *Handbook on the Physics and Chemistry of Rare Earths,* Vol. 18 *Lanthanides / Actinides: Chemistry*; North-Holland, Amsterdam **1994**, p. 529.

[104] Schlosser, F.; Krüger, S.; Fuchs-Rohr, M. S. K.; Rösch, N. *in preparation.*

[105] Grenthe, I.; Fuger, J.; Konigs, R. J. M.; Lemire, R. J.; Muller, A. B.; Nguyen-Trung, C.; Wanner, H. *Chemical Thermodynamics of Uranium*, Vol. 1; Elsevier: Amsterdam, **1992**.

[106] Kurta. K. A.; Nelson, F.; Johnson, L. J. *J. Am. Chem. Soc.* **1949**, *71*, 2510.

[107] Sullivan, J. C.; Hindman, J. C. *J. Phys. Chem.* **1959**, *63*, 1332.

[108] Sullivan, J. C.; Choppin, G. R.; Rao, L. F. *Radiochim. Acta* **1991**, *54*, 17.

[109] Neck, V.; Kim, J. I.; Kanellakopulos, B. *Radiochim. Acta* **1992**, *56*, 25.

[110] Madic, C.; Begun, G. M.; Hobart, D.´E.; Hahn, R. L. *Inorg. Chem.* **1994**, *23*, 1914.

[111] Cassol, A.; Magon, L.; Tomat, G.; Portanova, R. *Radiochim. Acta* **1972**, *17*, 28.

[112] Kirishima, A.; Kimura, T.; Tochiyama, O.; Yoshida, Z. *J. Alloy Comp.* **2004**, *374*, 277.

[113] Plyasunov, A. V.; Grenthe, I. *Geochim. Cosmochim. Acta* **1994**, *58*, 3561.

[114] Druchok, M; Bryk, T; Holovko, M. *J. Mol. Liquid* **2005**, *120*, 11.

[115] Choppin, G. R.; Mathur, J. N. *Radiochim. Acta,* **1991**, *52/53*, 25.

[116] McCarthy, P. *Adv. Chem. Ser. 219, Am.Chem. Soc.* Washington D.C., **1989**, pp. xvii.

[117] Kim, J. I. in: *Handbook of the Physics and Chemistry of the Actinides*; A. J. Freeman, C. Keller, Eds.; Ch. 8, Elsevier: Amsterdam, **1986**.

[118] Griffith, S. M.; Schnitzer, M. *Soil. Sci. Soc. Amer. Proc.* **1975**, *39*, 861.

[119] Oritz de Serra, M. I.; Schnitzer, M. *Soil. Biol.Biochem.* **1973**, *5*, 281.

[120] Schnitzer, M. I.; Vendette, E. *Can. J. Soil. Sci.* **1975**, *55*, 93.

[121] Schmeide, K.; Sachs, S.; Bubner, M.; Reich, T.; Heise, K. H.; Bernhard, G. *Inorg. Chim. Acta* **2003**, *351*, 133.

[122] Sachs, S.; Bubner, M.; Schmeide, K.; Choppin, G. R.; Heise, K. H.; Bernhard, G. *Talanta* **2002**, *57*, 999.

[123] Sachs, S.; Schmeide, K.; Reich, T.; Brendler, V.; Heise, K. H.; Bernhard, G. *Radiochim. Acta* **2005**, *93*,17.

[124] Sachs, S.; Bernhard, G. *Radiochim. Acta* **2005**, *93*, 141.

[125] Kremleva, A.; Krüger, S.; Rösch, N. *in press*.

[126] Halbach, P.; von Borstel, D.; Gundermann, K. D. *Chem. Geol.* **1980**, *29*, 177.

[127] Choppin, G. R.; Kullberg, L. *J. Inorg. Chem.* **1978**, *40*, 651.

[128] CRC *Handbook On Chemistry and Physics*, Ed. Lide, D. R. CRC Press: Boca Raton, 85th edn., **2004-2005**, p. 8-47.

[129] Leciejewicz, J.; Alcock, N. W.; Kemp, T. J. *Struct. Bonding* **1996**, *82*, 43.

[130] Templeton, D. H.; Zalkin, A.; Ruben, H.; Templeton, L. L. *Acta Cryst.* **1985**, *C41*, 1439.

[131] Denecke, M. A.; Reich, T.; Pompe, S.; Bubner, M.; Heise, K. H.; Nitsche, H.; Allen, P. G.; Bucher, J. J.; Edelstein, N. M.; Shuh, D. K. *J. Phys. IV 7* **1997**, *C2*, 637.

[132] Denecke, M. A.; Reich, T.; Bubner, M.; Pompe, S.; Heise, K. H.; Nitsche, H.; Allen, P. G.; Bucher, J. J.; Edelstein, N. M.; Shuh, D. K. *J. All. Comp.* **1998**, *271/273*, 123.

[133] Jiang, J.; Rao, L.; Di Bernardo, P.; Zanonato, P. L.; Bismondo, A. *J. Chem. Soc., Dalton Trans.* **2002**, *8*, 1832.

[134] Hudson, E. A.; Allen, P. G.; Terminello, L. J.; Denecke, M. A.; Reich, T. *Phys. Rev. B* **1996**, *54*, 156.

[135] Cousson, A.; Proust, J.; Pagès, M. *Acta Cryst.* **1990**, *C46*, 2316.

[136] Howatson, J.; Grev, D. M.; Morosin, B. *J. Inorg. Nucl. Chem.* **1975**, *37*, 1933.

[137] Moll, H.; Geipel, G.; Reich, T.; Bernhard, G.; Fanghänel, T.; Grenthe, I. *Radiochim. Acta* **2003**, *91*, 11.

[138] Nitsche, H.; Silva, R. J.; Brendler, V.; Geipel, G.; Reich, T.; Teterin, Y. A.; Thieme, M.; Baraniak, L.; Bernhard, G. in: *Actinide Speciation in High Ionic Strength Media*; Reed, D. T.; Clark, S. B.; Rao, L., Eds.; Kluwer Academic/Plenum Publishers: New York, **1999**, p. 11.

[139] Mentzen, B. F.; Sautereau, H. *Acta Cryst.* **1980**, *B36*, 2051.

[140] Denecke, M. A.; Pompe, S.; Moll, H.; Heise, K. H.; Reich, T.; Bernhard, G.; Nitsche, H. Forschungszentrum Rossendorf, Institute of Radiochemistry, Annual Report, FZR-123, **1995**, p. 87.

[141] Carrell, C. J.; Carrell, H. L.; Erlebacher, J.; Glusker, J. P. *J. Am. Chem. Soc.* **1988**, *110*, 8651.

[142] Ciavatta, L.; Ferri, D.; Grenthe, I.; Salvatore, F. *Inorg. Chem.* **1981**, *20*, 463.

[143] Denecke, M. A.; Reich, T.; Pompe, S.; Bubner, M.; Heise, K. H.; Nitsche, H.; Allen, P. G.; Bucher, J. J.; Edelstein, N. M.; Shuh, D. K.; Czerwinski, K. R. *Radiochim. Acta* **1998**, *82*, 103.

[144] Tipping, E.; Hurley, M. A. *Geochem. Cosmochim . Acta.* **1992**, *56*, 3627.

[145] Kim, J. I.; Czerwinski, K. R. *Radiochim. Acta* **1996**, *73*, 5.

[146] Mathur, J. N. *Solven. Extr. Ion. Exch.* **1983**, *1*, 349.

[147] Vitorge, P. *Radiochim. Acta*, **1992**, *58/59*, 105.

[148] Runde, W.; Meinrath, G.; Kim, J. I. *Radiochim. Acta*, **1992**, *58/59*, 93.

[149] Fairhurst, A. J.; Warwick, P.; Richardson, S. *Colloids Surf. A: Physicochem. Eng. Aspects* **1995**, *99*, 187.

[150] Th. Rabung, Geckeis, H.; Kim, J. I.; Beck, H. P. *Radiochim. Acta* **1998**, *82*, 243.

[151] Vandijk, H. *Geoderma* **1971**, *5*, 53.

[152] Szabó, Z.; Aas, W.; Grenthe, I. *Inorg. Chem.* **1997**, *36*, 5369.

[153] Szabó, Z.; Grenthe, I. *Inorg. Chem.* **2000**, *39*, 5036.

[154] Szabó, Z.; Moll, H.; Grenthe, I. *J. Chem. Soc. Dalton Trans.* **2000**, *18*, 3158.

[155] Crea, S.; Robertis, D. A.; Sammartano, S. *Annali. Di Chimica* **2003**, *93*, 1027.

[156] Kumar, R.; Singh, U. P. *J. Rare Earths* **2005**, *23*, 389.

[157] Zeh, P.; Czerwinski, K. R.; Kim, J. I. *Radiochim. Acta* **1997**, *76*, 37.

[158] Pashalidis, I.; Buckau, G. *J. Radio. Anal. Nucl. Chem.* **2007**, *273*, 315.

[159] Sachs, S.; Brendler, V.; Geipel, G. *Radiochim. Acta.* **2007**, 95, 103.

[160] Glaus, M. A.; Hummel, W.; Van loon, L. R. *Environ. Sci. Technol.* **1995**, *20*, 2150.

[161] Martell, A. E.; Motekaitis, R. J. *Determination and use of stability constants,* Wiley-VCH, **1992**.

[162] Quilès, F.; Burneau, A. *Vibr. Spectros.* **1998**, *18*, 61.

[163] Maya, L.; Begun, G. M. *J. Inorg. Nucl. Chem.* **1981**, *43*, 2827.

[164] Nitsche, H. *J. Alloy. Comp.* **1995**, *223*, 274.

[165] Denecke, M. A. *Coor. Chem. Rev.* **2006**, *250*, 730.

[166] Giepel, G.; Acker, M.; Vulpius, D.; Bernhard, G.; Nitsche, H.; Fanghänel, Th. *Spectrochim. Acta A* **2004**, *60*, 417.

[167] Reich, T. private communications.

[168] Keller, C.: *The Chemistry of the Transuranium Elements*; Verlag Chemie Weihnheim, Germany, **1971**, p. 94-115.

[169] DenAuwer, C.; Simoni, E.; Conradson, S.; Madic, C. *Eur. J. Inorg. Chem.* **2003**, *21*, 3843.

[170] Allen, G. C.; Baerends, E. J.; Vernooijs, P.; Dyke, J. M.; Ellis, M. F.; Morris, A. *J. Chem. Phys.* **1988**, *89*, 9.

[171] Beatham, N.; Orchard, A. F.; Thornton, G. *J. Elec. Spec.***1980**, *19*, 205.

[172] Cox, L. E. *J. Elec. Spec.* **1982**, *26*, 167.

[173] Dunlap, B. I.; Rösch, N. *Adv. Quantum Chem.* **1990**, *21*, 317.

[174] Kerdcharoen, T.; Birkenheuer, U.; Krüger, S.; Woiterski, A.; Rösch, N. *Theor. Chem. Acc.* **2003**, *109*, 285.

[175] Nasluzov, V. A.; Rivanenkov, V. V.; Gordienko, A. B.; Neyman, K. M.; Birkenheuer, U.; Rösch, N. *J. Chem. Phys.* **2001**, *115*, 8157.

[176] Nasluzov, V. A.; Ivanova, E. A.; Shor, A. M.; Vayssilov, G. N.; Birkenheuer, U.; Rösch, N. *Phys. Chem. B* **2003**, *107*, 2228.

[177] Matveev, A. V.; Mayer, M.; Rösch, N. *Comp. Phys. Commun.* **2004**, *160*, 91.

[178] Wadt, W. R.; Hay, P. J. *J. Am. Chem. Soc.* **1979**, *101*, 5198.

[179] Pyykkö, P.; Zhao, Y. *Inorg. Chem.* **1991**, *30*, 3787.

[180] Pyykkö, P.; Li, J.; Runeberg, N. *J. Phys. Chem.* **1994**, *98*, 4809.

[181] Bratlett, R. J. *Annu. Rev. Phys. Chem*. **1981**, *32*, 359.

[182] Bratlett, R. J. *J. Chem. Ph*ys. **1982**, *76*, 1910.

[183] Koch, W.; Holthausen, M. C. *A Chemist's Guide to Density Functional Theory*; Wiley: Weinheim, **2000**.

[184] Parr, R. G.; Yang, W.: *Density Functional Theory of Atoms and Molecules*; Oxford University Press, New York, **1989**.

[185] Hohenberg, K.; Kohn, W. *Phys. Rev. B* **1964**, *136*, 864.

[186] Kohn, W.; Sham, L. J. *Phys. Rev. A* **1965**, *140*, 1133.

[187] Kohanoff, J. *Electronic Structure Calculations for Solids and Molecules: Theory and Computational Methods*, Ch. 5, Cambridge University Press: Cambridge, **2006.**

[188] Furche, F.; Perdew, J. P. *J. Chem. Phys*. **2006**, *124*, 044103.

[189] Vosko, S. H.; Wilk, L.; Nusair, M. *Can. J. Phys.* **1980**, *58*, 1200.

[190] Becke, A. D. *Phys. Rev. A* **1988**, *38*, 3098.

[191] Perdew, J. P. *Phys. Rev. B* **1986**, *33,* 8822; *ibid*. **1986**, *34*, 7406.

[192] Hammer, B.; Hansen, L. B.; Nørskov, J. K. *Phys. Rev. B* **1999**, *59*, 7413.

[193] Ziegler, T. *Chem. Rev.* **1991**, *91*, 651.

[194] Görling, A.; Trickey, S. B.; Gisdakis, P.; Rösch, N. in: *Topics in Organometallic Chemistry*, Vol. 4, Brown, J.; Hoffmann, P., Eds.; Springer: Heidelberg, **1999**, p. 109-165.

[195] García-Hernández, M.; Lauterbach, C.; Krüger, S.; Matveev, A.; Rösch, N. *J. Comp. Chem.* **2002**, *23*, 834.

[196] Dyke, T. R.; Mack, K. M.; Muenter, J. S. *J. Chem. Phys*. **1977**, *66*, 498

[197] Becke, A. D. *J. Chem. Phys.* **1988**, *88*, 2547.

[198] Pyykkö, P.; Desclaux, J. P. *Acc. Chem. Res.* **1979**, *12*, 276.

[199] Batrakov, Y. F.; Krivitsky, A. G.; Pospelov, O. V.; Puchkova, E. V. *Radiochim. Acta* **2004**, *92*, 73.

[200] Douglas, M.; Kroll, N. M. *Ann. Phys.* **1974**, *82*, 89.

[201] Visscher, L.; van Lenthe, E. *Chem. Phys. Lett.* **1999**, *306*, 357.

[202] Dolg, M. in: *Relativistic Electronic Structure Theory, Part 1: Fundamentals*, P. Schwerdtfeger, Ed.; Theoretical and Computational Chemistry, Vol. 11, Ch. 14, Elsevier: Amsterdam, **2002,** p. 793 -862.

[203] Dolg, M. in: *Modern Methods and Algorithms of Quantum Chemistry*, J. Grotendorst, Ed.; John Neumann Institute for Computing, NIC Series, Vol. 1, Jülich **, 2000**, p. 479-508, Vol.3, Jülich **, 2000,** p.507-540.

[204] Cao, X.; Dolg, M. *Coor. Chem. Rev.* **2006**, *250*, 900.

[205] Tomasi, J.; Persico, M. *Chem. Rev.* **1994**, *94*, 2027.

[206] Cramer, C. J.; Truhlar, D. G. *Chem. Rev.* **1999**, *99*, 2161.

[207] Bonaccorsi, R.; Scrocco, E.; Tomasi, J. *J. Chem. Phys.* **1970**, *52*, 5270.

[208] Huron, M. J.; Claverie, P. *J. Phys. Chem.* **1972**, *76*, 2123.

[209] Rinaldi, D.; Rivail, J. L. *Theor. Chim. Acta* **1973**, *32*, 57.

[210] Tapia, O.; Goscinski, O. *Mol. Phys.* **1975**, *29*, 1653.

[211] Miertus, S.; Scrocco, E.; Tomasi, J. *J. Chem. Phys.* **1981**, *55*, 117.

[212] Klamt, A.; Schüürmann, G. J. *J. Chem. Soc. Perkin Trans.* **1993**, *2*, 799.

[213] Andzelm, J.; Kölmel, C.; Klamt, A. *J. Chem. Phys.* **1995**, *103*, 9312.

[214] Baldrige, K.; Klamt, A. *J. Chem. Phys.* **1997**, *106*, 6622.

[215] Barone, V.; Cossi, M.; Tomasi, J. *J. Chem. Phys.* **1997**, *107*, 3210.

[216] Warshel, A.; Levitt, M. *J. Mol. Biol.* **1976**, *103*, 227.

[217] Singh, U. C.; Kollman, P. A. *J. Comput. Chem.* **1986**, *7*, 718.

[218] Field, M. J.; Bash, P. A.; Karplus, M. *J. Comput. Chem.* **1990**, *11*,700.

[219] Schlosser, F.; Krüger, S.; Rösch, N. *Inorg. Chem* **2006**, *45*, 1480.

[220] Szabó, Z.; Toraishi, T.; Vallet, V.; Grenthe, I. *Coor. Chem. Rev.* **2006**, *250*, 784.

[221] Cossi, M.; Mennucci, B.; Cammi, R. *J. Comput. Chem.* **1996**, *17*, 57.

[222] Cossi, M.; Barone, V.; Cammi, R.; Tomasi, J. *Chem. Phys. Lett.* **1996**, *255*, 327.

[223] Bondi, A. *J. Phys. Chem.*, **1964**, *68*, 441.

[224] Pasqual-Ahuir, J. L.; Silla, E.; Tuñón, I. *J. Comput. Chem.* **1994**, *15*, 1127.

[225] Aguilar, M. A.; Olivares del Valle, F. J. *Chem. Phys.* **1989**, *129*, 439.

[226] Stefanovich, E. V.; Truong, T. N. *Chem. Phys. Lett.* **1996**, *225*, 327.

[227] Barone, V.; Cossi, M.; Tomasi, J. *J. Comput. Chem.* **1998**, *19*, 404.

[228] Minami, T.; Matsuoka, O. *Theo. Chim. Acta* **1995**, *90*, 27.

[229] [a]R. Poirier, R. Kari, I. G. Csizimadia, Handbook of Gaussian Basis Sets, Elsevier, Amsterdam, 1985.[b]Van Duijneveldt, F. B. *IBM Res. Rep.* **1971**, RJ 945.[c]Huzinaga, S.; Andzelm, J.; Klobukowski, M.; Radzio-Andzelm, E.; Sakai, Y.; Tatewaki, H. *Gaussian Basis Sets for Molecular Calculations*; Elsevier: Amsterdam, 1984 [O: d exponent 1.15; C: d exponent 0.60]. [d]Frisch, M. J.; Pople, J. A.; Binkley, J. S. *J. Chem. Phys.* **1984**, *80*, 3265 [H: p exponent 1.0].

[230] García-Hernández, M.; Willnauer, C.; Krüger, S.; Moskaleva, L. V.; Rösch, N. *Inorg. Chem.* **2006**, *45*, 1356.

[231] Schlick, T. in *Optimization Methods in Computational Chemistry*, Lipkowitz, K. B.; Boydvol, D. B. Eds.; Reviews in computational chemistry; John Wiley & Sons, Inc., Vol. 3, **2007**, p. 1-72.

[232] Schlosser, F., Diplomarbeit, Technische Universität München, **2001**.

[233] Basile, L. J.; Sullivan, J. C.; Ferraro, J. R.; LaBonville, P. *Appl. Spectrosc.* **1974**, *28*, 142.

[234] Toth, L. M.; Begun, G. M. *J. Phys. Chem.* **1981**, *85*, 547.

[235] Matveev, A. M.; Nasluzov, V. A.; Rösch, N. *Int. J. Quant. Chem.* **2007**, *107*, 3236.

[236] Druchok, M; Bryk, T; Holovko, M. *J. Mol. Liquid* **2005**, *120*, 11.

[237] Bühl, M; Kabrede, H. *ChemPhysChem*. **2006**, *7*, 2290.

[238] Ingram, K. I. M; Haller, L.J.L; Kaltsoyannis, N. *Dalton Transac.* **2006**, *20*, 2403.

[239] Oda, Y.; Aoshima A. *J. Nucl. Sci. Techno.* **2002**, *39*, 647.

[240] Privalov, T.; Schimmelpfennig, B.; Wahlgren, U.; Grenthe, I. *J. Phys. Chem. A* **2002**, *106*, 11277.

[241] Bursten, B. E.; Casarin, M.; Ellis, D. E.; Fragala, I.; Marks, T. J. *Inorg. Chem.* **1986**, *25*, 1257.

[242] Sonnenberg, J. L.; Hay, P. J.; Martin, R. L.; Bursten, B. E. *Inorg. Chem.* **2005**, *44*, 2255.

[243] Tuttle, T. R.; Malaxos, S.; Coe, J. V. *J. Phys. Chem. A* **2002**, *106*, 925.

[244] Cornehl, H. H.; Heinemann, C.; Marcalo, J.; de Matos, A. P.; Schwarz, H. *Angew. Chem. Int. Ed. Engl.* **1996**, *35*, 891.

[245] Gutowski, K. E.; Dixon, D. A. *J. Phys. Chem. A*. **2006**, *110*, 8840.

[246] Balasubramanian, K.; Cao, Z. *Chem. Phys. Lett.* **2007**, *433*, 259.

[247] Shamov, G. A.; Schrecken bach, G. *J. Phys. Chem.* A **2005**, *109*, 10961.

[248] Bailey, E. H.; Mosselmans, J. F. W.; Schofield, P. F. *Geochim. Cosmochim. Acta* **2004**, *68*, 1711.

[249] Jeffrey, G. A.: *An Introduction to Hydrogen Bonding*; Oxford University Press: New York, **1997**, p. 12.

[250] Siboulet, B.; Marsden, C. J.; Vitorge, P. *Chem. Phys*. **2006**, *326*, 289.

[251] Dudal, Y.; Gerard, F. *Earth-Science Reviews*, **2004**, *66*, 199.

[252] Wiberg, K. B. *J. Org. Chem.* **2002**, *67*, 4787.

[253] Fiedler, P.; Bohm, S.; Kulhanek, J.; Exner, O. *Org. Biomol. Chem.* **2006**, *4*, 2003.

[254] Otyepkova, E.; Nevecna, T.; Kulhanek, J, Exner O. *J. Phy. Org. Chem.* **2003**, *16*, 721.

[255] Natario, R. *J. Mol. Struct.* **2000**, *556*, 245.

[256] Böhm, S.; Fiedler, P.; Exner, O. *New. J. Chem.* **2004**, *28*, 67.

[257] McMahon, T. B.; Kebarle, P. *J. Am. Chem. Soc.* **1977**, *99*, 2222.

[258] Shapley, W. A.; Bacskay, G. B.; Warr, G. G. *J. Phys. Chem. B*. **1998**, *102*, 1938.

[259] Nagy, P. I.; Dunn, III. W. G.; Alagona, G.; Ghio, G. *J. Phys. Chem*. **1993**, *97*, 4628.

[260] Namazian, M.; Halvani, S. *J. Chem. Thermodyn*. **2006**, *38*, 1495

[261] Martinez, J. M.; Pappalardo, R. R.; Marcos, E. S.; Mennucci, B.; Tomasi, J. *J. Phys. Chem.B,* **2002**, *106*, 1118.

[262] Lajunen, L. J.; Portauova, R.; Piispanen, J.; Tolazzi, M. *Pure Appl. Chem.* **1997**, *69*, Vol. 2, p. 329.

[263] Wang, Z. M.; Burgt, L. J.; Choppin, G. R. *Inorg. Chim. Acta.* **2000**, *310*, 248.

[264] Anca, R.; Martinez, S.; Graciabl, S. *Acta Crystallogr. A: Found. Crystallogr.* **1967**, *23*, 1010

[265] Benghiat, V.; Leiserow, L. *J. Chem. Soc., Perkin Trans*. **1972**, *2*, 1778.

[266] D. Vulpius, G. Geipel, L. Baraniak, A. Rossberg, G. Bernhard, *J. Radioanal. Nuc. Chem.* **2006**, *270*, 661.

[267] Wiebke, J; Moritz, A.; Glorious, M.; Moll, H.; Bernhard, G.; Dolg, M. *Inorg. Chem.* **2008***, 47*, 3150.

[268] Alcock, N. W.; Kemp, T. J.; Leciejewicz, J.; Pennington, M. *Acta Crystallogr., Sect. C: Cryst. Struct. Commun.* **1989**, *45*, 719.

[269] Rossotti, F. J. C.; Rossotti, H. in: *The Determination of Stability Constants and Other Equilibrium Constants in Solution*. McGraw-Hill: New York, **1961**.

[270] Berto, S.; Crea, S.; Daniele, P. G. Stefano, C., Prenesti, E.; Sammartano, S. *Annali. Di Chimica* **2006**, *96*, 399.

[271] Ahrland, S. *Acta chem. scand.* **1949**, *3*, 783, *Acta chem. scand.* **1951**, *5*, 199.

[272] Rao, L.; Zanonato, P.; Bernardo, P. *J. Nucl. Radiochem. Sci*. **2005**, *6*, 31.

[273] Marx, D.; Tuckerman, M. E.; Hutter, J.; Parrinello, M. *Nature* **1999**, *397*, 601.

[274] Asthagiri, D.; Pratt, L. R.; Kress, J. D. *Proc. Nat. Acd. Sci*. **2005**, *102*, 6704.

[275] Ray, R. S.; Krüger, S.; Rösch, N. *Article in press*.

[276] Cramer, C. J.; Truhlar, D. G. *J. Am. Chem. Soc.* **1991**, *113*, 8305.

[277] Glorius, M.; Moll, H.; Bernhard, G. *Radiochim. Acta* **2007**, *95*, 151.

[278] Vulpius, D. Dissertation, Technische Universität Dresden, **2005**.

[279] Shanbhag, P. M.; Choppin, G.R. *J. Inorg. Nucl. Chem.* **1981**, *43*, 3369.

[280] Munier-Lamy, C.; Adrian, Ph. Berthelin, J.; Rouiller, *J. Org. Geochem.* **1986**, *9*, 285.

[281] Lenhart, J. J.; Cabaniss, S. E.; MacCarthy, P.; Honeyman, B. D. *Radhochim. Acta* **2000**, *88*, 345.

[282] Lubal, P.; Fetsch, D.; Široký, D.; Lubalová, M.; Šenkýr, J.; Havel, J. *Talanta* **2000**, *51*, 977.

[283] Kříbek, B.; Podlaha, J. *Org. Geochem.* **1980**, *2*, 93.

[284] Czerwinski, C. R.; Buckau, G.; Scherbaum, F.; Kim, J. I. *Radiochim. Acta* **1994**, *65*, 111.

[285] E. A. Hudson, P. G. Allen, L. J. Terminello, M. A. Denecke and T. Reich, *Phys. Rev. B*, 1996, **54**, 156–165.

[286] J. Jiang, L. Rao, P. Di Bernardo, P. L. Zanonato and A. Bismondo, *J. Chem. Soc., Dalton Trans.*, 2002, **8**, 1832–1838.

[287] M. A. Denecke, S. Pompe, T. Reich, H. Moll, M. Bubner, K. H. Heise, R. Nicolai and H. Nitsche, *Radiochim. Acta*, 1997, **79**, 151–159.

[288] Panak, P.; Klenze, R.; Kim, J. I. Radiochimica Acta, 1996, 74, 141.

[289] Morgenstern, M.; Klenze, R. Kim, J. I. Radiochimica Acta, 1992, 56, 79.